

NOVEL CELL BASED *IN VITRO* MODELS TO STUDY
NANOPARTICLE INTERACTION WITH THE INFLAMED
INTESTINAL MUCOSA

Dissertation

Zur Erlangung des Grades des

Doktors der Naturwissenschaften

der Naturwissenschaftlich-Technischen Fakultät III

Chemie, Pharmazie, Bio- und Werkstoffwissenschaften

Der Universität des Saarlandes

Von

Fransisca Leonard

Saarbrücken 2012

Tag des Kolloquiums:	8. Februar 2013
Dekan:	Uni.-Prof. Dr. Volkhard Helms
Berichterstatter:	Prof. Dr. Claus-Michael Lehr
	Prof. Dr. Mauro Ferrari
Vorsitz:	Prof. Dr. rer. nat. Rolf W. Hatmann
Akad. Mitarbeiter:	Dr. Matthias Engel

Die vorliegende Dissertation entstand unter der Betreuung von

Prof. Dr. Claus-Michael Lehr
Dr. Eva-Maria Collnot

In der Fachrichtung Biopharmazie und Pharmazeutische Technologie
der Universität des Saarlandes

*Bei Herr Prof. Lehr und Frau Dr. Collnot möchte ich mich für die Überlassung des
Themas und die wertvollen Anregungen und Diskussionen herzlich bedanken*

Table of Contents

Summary.....	vi
Kurzzusammenfassung.....	viii
1. Introduction.....	1
1.1 Drug discovery and formulation.....	1
1.2 Epithelial cell culture.....	2
1.3 <i>In vitro</i> models of the intestinal mucosa.....	4
1.4 Advanced <i>in vitro</i> models techniques.....	6
1.4.1 Co-culture of multiple cell types.....	6
1.4.2 Disease relevant <i>in vitro</i> models.....	10
1.5 Inflammatory Bowel Disease.....	13
1.6 Nanocarrier system in drug delivery.....	15
1.7 Aim of the thesis.....	17
2. A 3-dimensional co-culture of enterocytes, macrophages and dendritic cells to model the inflamed intestinal mucosa <i>in vitro</i>	19
2.1 Abstract.....	20
2.2 Introduction.....	22
2.3 Material & Methods.....	26
2.3.1 Materials.....	26
2.3.2 Cell culture.....	27
2.3.3 Cell stimulation, isolation of RNA and reverse transcription.....	27
2.3.4 Quantification of pro-inflammatory gene expression with real-time PCR.....	28
2.3.5 Protein expression assessment with FACS-based CBA Flex kit.....	28
2.3.6 Transepithelial electrical resistance and paracellular permeability.....	29
2.3.7 Immunostaining of tight junctional protein.....	29
2.3.8 Permeability of fluorescein on the Caco-2 cell monolayer.....	30
2.3.9 Fluoresbrite polystyrene nanoparticles uptake in Caco-2 cell monolayer and co- culture.....	31
2.3.10 Caco-2 monolayer mucus staining with alcian blue.....	32
2.3.11 Mucus quantification by glycoprotein measurement.....	32
2.3.12 Macrophages and Dendritic cells cell culture.....	33

2.3.13	Three-dimensional triple cell culture	33
2.3.14	Sample preparation for histological staining	34
2.3.15	Statistical analysis	35
2.4	Results.....	36
2.4.1	Inflammatory marker in mRNA level in Caco-2 cells after stimulation with pro-inflammatory compounds	36
2.4.2	IL-8 protein release in response to pro-inflammatory compounds in Caco-2....	39
2.4.3	Pro-inflammatory compound-induced increase of Caco-2 monolayer permeability.....	40
2.4.4	Transport of fluorescein in inflamed Caco-2 cells	41
2.4.5	Immunostaining of tight junction protein ZO-1	42
2.4.6	Nanoparticles allocation in non-stimulated and stimulated Caco-2 monolayers ..	43
2.4.7	Three dimensional co-culture of Caco-2 cells with dendritic cells and monocytes	45
2.4.8	Release of IL-8 protein from the three-dimensional co-culture.....	46
2.4.9	Optical image of three-dimensional co-culture by histological cut and CLSM.	49
2.4.10	Disposition of polystyrene nanoparticle in the triple co-culture.....	50
2.5	Discussion	52
3.	Screening of budesonide nanoformulations for treatment of inflammatory bowel disease in an inflamed 3D cell-culture model	65
3.1	Abstract	66
3.2	Introduction	67
3.3	Materials and methods.....	73
3.3.1	Materials	73
3.3.2	Fabrication and characterization of budesonide loaded PLGA nanoparticles...	73
3.3.3	Liposome fabrication	75
3.3.4	Setting up of co-culture	76
3.3.5	Budesonide formulation testing.....	77
3.3.6	IL-8 cytokine measurement.....	77
3.3.7	Transepithelial Electrical Resistance (TEER) measurement.....	78
3.3.8	Confocal Laser Scanning Microscopy.....	78
3.3.9	Statistical analysis	78

3.4	Results.....	79
3.4.1	PLGA nanoparticle and liposome characterization.....	79
3.4.2	TEER value monitoring.....	80
3.4.3	IL-8 release rate.....	83
3.4.4	Deposition of drug carrier systems.....	85
3.5	Discussion.....	87
4.	SIMPLI-Well: A novel cell culture system based on ultrathin silicon nitride (Si ₃ N ₄) porous supports for transport and translocation studies.....	97
4.1	Abstract.....	98
4.2	Introduction.....	100
4.3	Material and Methods.....	104
4.3.1	Materials.....	104
4.3.2	Design and fabrication of the Silicon Microporous Permeable Insert (SIMPLI) - Well system.....	104
4.3.3	Pre-treatment and regeneration of silicon nitride porous supports.....	105
4.3.4	Cell culture.....	106
4.3.5	Permeability of fluorescein, propranolol and nanoparticles on blank and cell grown filter.....	107
4.3.6	Immunohistological staining and Confocal Laser Scanning Microscopy.....	108
4.3.7	Scanning Electron Microscopy.....	108
4.3.8	Transmission Electron Microscopy.....	108
4.3.9	Statistical analysis.....	109
4.4	Results.....	110
4.4.1	SIMPLI-Well.....	110
4.4.2	Silicon nitride chip.....	111
4.4.3	Epithelial cell growth and differentiation.....	112
4.4.4	Confocal and SEM analysis.....	113
4.4.5	Translocation of small molecules and polystyrene beads in the absence of cells	114
4.4.6	Translocation of small molecules and polystyrene beads in the presence of cells.	114
4.5	Discussion.....	117
5.	Summary.....	125

6. Outlook	129
7. References	131
8. Abbreviations	143
9. Curriculum vitae	147
10. Acknowledgement	151

ABSTRACT

Along with increasing research in the field of drug delivery and nanotechnology there is an urgent need to improve test tools for efficacy and safety of nanomedicines. In this thesis an *in vitro* model of the inflamed intestinal mucosa was developed which combined with a novel silicon nitride based cell culture support advances drug and formulation testing in the context of inflammatory bowel disease. The *in vitro* model consists of an epithelial cell line combined with primary macrophages and dendritic cells and stimulated via pro-inflammatory factors such as interleukin-1 β (IL-1 β). The model reflects pathophysiological changes observed *in vivo* e.g. decreased epithelial barrier function, increased production of pro-inflammatory cytokines, and increased mucus production.

The potential as a testing system for (nano)-formulations was demonstrated comparing anti-inflammatory activity of liposomal budesonide and polymeric nanospheres. Increased activity of budesonide nanoparticles which accumulate in the tight junctional region was observed.

In addition, hindered diffusion of particles and macromolecules that caused underestimation of transport across standard, polyester based cell culture supports was addressed. The silicon nitride based microporous membranes of only 500 nm thickness proposed in this thesis provided excellent growth properties while reducing the membrane influence, thus allowing the first study on nanoparticle translocation across the intestine *in vitro*.



KURZZUSAMMENFASSUNG

Um die Effizienz und Sicherheit von Nanomedikamenten zu bestimmen müssen *in vitro* Testsysteme angepasst und optimiert werden. In dieser Arbeit wurde ein *in vitro* Modell der entzündeten Darmmukosa und einem neuartigen Silikonitrid basiertem Zellkultursystem entwickelt, mit dem die Testung von Arzneistoffen und Formulierungen zur Therapie chronisch entzündlicher Darmerkrankungen erlaubt.

In einer Ko-Kultur von intestinalen Epithelzellen mit primären Makrophagen und dendritischen Zellen, wird über die Zugabe von IL-1 β eine Entzündung ausgelöst. Im Modell zeigen sich daraufhin pathophysiologische Veränderungen wie eine Verminderung der Barriereigenschaften und eine verstärkte Produktion von Mukus und Zytokinen.

Der Einsatz als Testsystem für verschiedene pharmazeutische (Nano)-Formulierungen wurde am Beispiel des Budesonid überprüft und wurden miteinander verglichen. Nur die Nanopartikel reicherten sich zwischen den Epithelzellen an und hatten die höchste antientzündliche Potenz.

Ein zusätzliches Problem in der *in vitro* Testung von Nanopartikeln stellen die herkömmlichen Zellkultursubstrate auf Basis von Polyestermembranen dar. Auf Grund des kleinen Porenradius und der relativen Membrandicke wird die freie Diffusion größerer Teilchen über den Filter eingeschränkt. Der Einsatz einer Silikonitridmembran mit einer Dicke von nur 500 nm beschleunigte den Transport der Partikel und erlaubte erstmals die Bestimmung relevanter Translokationsdaten über funktionelle Caco-2 Monolayer.



1. Introduction

1.1 Drug discovery and formulation

Modern drug development consists of a series of processes starting with the identification of lead compounds and their pharmacological effects, subsequent study in cell and animal models and ending with drug safety, pharmacokinetics and efficacy studies in patients. Although drug candidate developments have been optimized through rational drug design in recent years, adequate screening processes are needed to narrow down the number of potential active pharmaceutical compounds (API) and to refine the formulation through the pipeline.

A variety of obstacles may present in the translation from *in vitro* to *in vivo* (animal testing) and from animal testing to preclinical and clinical development which lead to the failure of a compound to reach the shelf. One of the main problems in transferring the compound and its formulation to *in vivo* systems is the reliability of the validated simplified *in vitro* techniques, which by design, lack the complexity of the whole tissue, organ or body.

However, the disadvantages do not overwhelm the advantages as *in vitro* systems are considered (1) more ethical, (2) cheaper, (3) and less time consuming than animal studies, and (4) allow testing under clearly defined conditions in a steady environment. This drives further developments in modern cell culture and tissue engineering techniques as well as progress in molecular biology to provide a wide panel of validated *in vitro* models with increasing complexity. The developed *in vitro* models mostly developed based on cells from human origin thus eliminating problems with species differences.

1.2 Epithelial cell culture

Cell culture based *in vitro* techniques are particularly important when studying drug pharmacokinetics i.e. the process of drug absorption, distribution, metabolism and excretion (ADME). Epithelia, the cellular coverings of internal and external body surfaces, can be considered as a rate limiting factor in all of these steps [1]. Historically, epithelial cell culture models have been proven to be powerful tools in predicting drug bioavailability at the place of action and provide mechanistic insight into the interaction between the API and the biological barrier. Mass screening of potential APIs and their formulation is thus possible due to small scaling and reproducible quality.

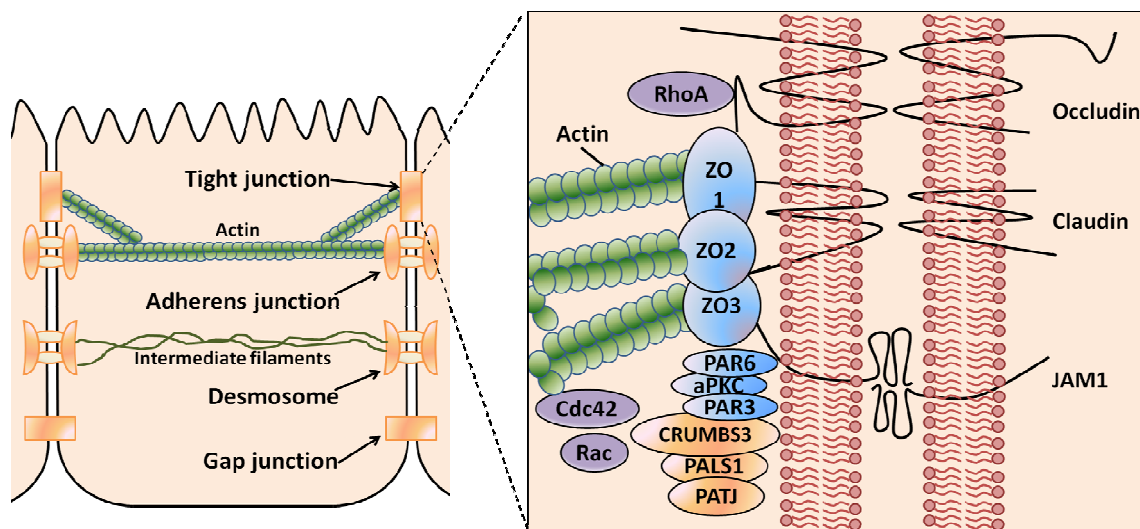


Figure 1. Tight junction assembly forming the main barrier in the epithelium. The assembly consists of transmembrane protein: occludin, claudins and junctional adhesion molecules (JAMs), and adaptor proteins such as zona occludens (ZO1, ZO2 and ZO3) as well as additional proteins. Illustration modified from Aktories, K., et al. [2]

Internal epithelia are polarized cells and are characterized by the expression of different cell contacts: desmosomes and hemi-desmosomes provide adhesion of epithelial cells to each other and to the basement membrane respectively and gap junctions are intercellular

connection channels. Composed by a strand of several pivotal proteins, with transmembrane proteins Claudin and Occludin linked to actin cytoskeleton via ZO-1 to form a beltlike network, the tight junctions surround the cells act as the primary gate of the epithelium (Fig. 1). They serve as a physical barrier to the environment, allowing transport of water and small molecules across epithelia but limiting bigger molecules. The assembly, maintenance, and disassembly of tight junction protein is regulated by various signaling molecules such as protein kinase C, mitogen-activated protein kinases, myosin light chain kinase, and Rho GTPases, and influenced by intestinal bacteria and dietary components [3].

The tightness of an epithelium can be quantified via the so called transepithelial resistance (TEER), i.e. the resistance that the epithelium provides to a current in an electric circuit. The higher this resistance value (given as $\Omega \cdot \text{cm}^2$ i.e. normalized to the surface area), the tighter the epithelium and the higher the diffusion barrier is.

Several transport routes are available depending on the physicochemical properties (size and hydrophobicity) of the respective compound. In principal, transcellular (through the cells) transport and paracellular (between the cells) transport can be distinguished. Passive paracellular transport is mainly limited to hydrophilic molecules sized <300 Da as diffusion takes place through the tight junction pores which size varies between 0.5 to 5 nm [4]. Moderately lipophilic compounds with $\log P < 5$, molecular weight of up to approximately 500 Da and up to 5 H-bond donors and 10 H-bond acceptors are transported through the cells i.e. they have to diffuse in and out of the phospholipid bilayer of the cell membrane [5]. Transcellular transport can either be passive process following a concentration gradient between apical and basolateral side of the epithelial barrier, or active transport which requires the work against a concentration gradient. Active transport may also enable uptake

of bigger or more lipophilic structures mediated by transport proteins embedded in the cell membrane.

In vivo, the basement membrane anchors down the epithelium to the loose connective tissue of the respective organ. *In vitro*, this growth support is simulated using porous polyester or polycarbonate membranes of ~10 μm thickness which are suspended by a plastic holder in standard multi-well cell culture plates. Thereby a two-compartmental system is formed which allows nutrient support to the cells from both sides, which gives better approach to *in vivo* condition than the one sided nutrient sustentation in conventional cell culture flasks. The epithelial cells can differentiate and polarize in this setup, as confirmed by a hindered lateral diffusion across the cell membrane and the distinct expression of microstructures and membrane proteins on the apical lumen site and on the basolateral tissue site. Transport processes of ions, nutrients and drug compounds can easily be studied in this setup as it is assumed that the epithelial layer provides the main barrier for diffusion of small molecular compounds while the resistance of the porous membrane is negligible. However, not in all cases the filter support is completely inert; highly lipophilic substances, proteins or particles could adsorb to the material and might clog the pores.

1.3 *In vitro* models of the intestinal mucosa

Out of all drug delivery strategies, oral application is the most frequently used with more than 40% of all APIs being applied as tablets [6]. Oral delivery of tablets is both price efficient in production and convenient for the patient with good compliance to therapy. Formulated to withstand the low pH of gastric tract, the drug absorption mostly takes place in the small intestine which is substructured by the formation of villi and microvilli greatly increasing the

surface area available for absorption. With a huge interface of approximately 250m², small intestinal mucosa offers a huge absorption surface area. They are mainly comprised of enterocytes covering most of the surface, but also consist of other cell types such as mucus-producing goblet cells or M-cells, specialized in the uptake of particulate structures and potentially harmful microorganism and subsequent presentation to the immune system. Thus to simulate simple absorption, enterocyte cell lines are used. A number of cell culture models for the intestinal epithelium are available, but only few develop functional tight junctions that are needed for pharmacokinetic studies (such as Caco-2 and T84) [7].

The *in vitro* model developed in our study is based on the most common model for epithelial barrier, Caco-2 cell line. Caco-2 cells were first isolated from human colon adenocarcinoma of a 77 year-old male Caucasian in the 1970s. When grown on permeable membrane supports, the proliferation stop after confluence and the cells differentiate to small intestinal enterocyte-like cells forming polarized, fully differentiated monolayers. Phenotypical characteristics include microvilli on the apical side, the formation of functional tight junctions, and the expression of a wide range of metabolic enzymes (e.g. small intestinal hydrolases, including sucrase-isomaltase, lactase, aminopeptidases) and of transport proteins on the apical (e.g. P-gp, MRP-2, BCRP) and basolateral (e.g. MRP-1, PepT1) surfaces [8]. A comparative study on 20 different intestinal cell lines, found Caco-2 to have the highest correlation to the *in vivo* enterocyte phenotype e.g. showing the highest enrichment factor of brush boarder-associated hydrolases enzyme activity [9].

Despite having higher TEER values compared to the *in vivo* small intestinal epithelium [10] and deficits in the expression of certain enzymes (e.g. CYP3A4) the permeability of a wide range of APIs across Caco-2 cell monolayers was found to correlate to *in vivo* permeability data. Thus Caco-2 is one of the chosen cell line to predict permeability and subsequently

bioavailability of drug candidates in the context of the Biopharmaceutical Classification System (BCS) and the biowaiver guideline of the Food and Drugs Administration (FDA) [11]. Additionally, Caco-2 is also a well established model to perform in-depth mechanistic and absorption studies, to study the role of transporters and potential transporter-mediated drug-drug interactions.

1.4 Advanced *in vitro* models techniques

Although the Caco-2 model can be considered the gold standard for epithelial *in vitro* models in the context of drug absorption and bioavailability studies, it faces some limitations if other questions are to be addressed, e.g. the prediction of drug toxicity and efficiency at an organ level. The interplay between different cell types such as epithelial cells and immune cells or between cells and the extracellular matrix is essential for these kinds of questions and is not mirrored in the simplified one dimensional monoculture models. Therefore, in recent years several approaches have tried to improve the predictive power by enhancing the geometrical and cellular complexity as well as the quality of cell culture techniques, relying less on cell lines of cancerous origin and trying to address specific pathophysiological conditions.

1.4.1 Co-culture of multiple cell types

Depending on the tissue to be mimicked, the cell types that are used vary from combination of epithelial cells and immune cells in the intestine and lung, or endothelial cells and immune cells in vascular models to co-cultures of endothelial cells with neuronal cells at the blood brain barrier.

At the intestinal barrier, several groups have tried to compensate for the low mucus production in Caco-2 cells by adding goblet like cells. Combining Caco-2 with HT-29 at the correct seeding rate, the system develops good barrier properties which cannot be achieved in HT-29 monocultures but shows significantly raised mucus levels. The benefit of these models for permeability studies is limited, as *in vitro-in vivo* correlation for small molecular compounds was not greatly improved compared to Caco-2 monoculture. However, they are highly relevant for drug formulation with specific mucoadhesive targeting (e.g. chitosan, eudragit analogues, etc.) [12, 13] or when studying transport of macromolecular structure and particles.

Other systems increase the immunocompetency of the intestinal cell culture model. In a pharmaceutical context, in particular M cell models have been investigated by co-culturing Caco-2 cells with Raji B cells. The early model by des Rieux et al. [14] has been improved over the years by changing the orientation of the epithelial cells within the compartmental setup, and was found to have 50-fold higher transport rate of nanoparticles compared with conventional monoculture or more than 15-fold of previous M-cell model. This model has been used widely in the research for permeability and antigen uptake by M-cells. However, a comparison study with *in vivo* condition is urgently needed to define the relevant model, as depending on the setup, the model gave high variation in permeability.

In a more medical context, Spottl et al. co-cultured HT-29, primary fibroblasts and primary monocytes and discovered the alternative differentiation of the co-cultured macrophages towards M2 phenotype [15], producing less CD14, CD11b, CD80, and CD86 expression, a condition similar to the intestinal macrophages. The model mostly focused on the interplay of the different cell types and the secretion factor driven differentiation of the immune cells and less for characterization in regards of intestinal barrier properties.

Table 1. List of advanced 3D *in vitro* models of biological barriers for specific characterization and disease study.

Organ	Cells	Studied system	Reference
Intestine	1. Caco-2 2. Raji B line	Human intestinal follicle-associated epithelium (FAE) and M-cells for nanoparticle transport study	[14]
	1. Exosomes harvested from high MHC class II expressing T-84 cells 2. HLA-DR4 (EBV-transformed human B-cell line) or DCs	Human epithelial exosomes in antigen presentation	[16]
	1. primary enteric neuronal tissue 2. HT-29	Model of innervated mucosal barrier (Hirschsprung's disease)	[17]
	1. Submucosa from colon cancer patients 2. HT-29- Cl.16E	Colon carcinoma model	[18]
	1. Apc+/+ or Apc+/- mouse colon epithelial cells 2. large intestine <i>intra-epithelial</i> lymph (LI-IEL) also from mouse	Mouse colon	[19]
	1. Caco-2 2. RAW264.7 cells	Assessment of anti-inflammatory effect from food factors in the intestine	[20]
	1. Caco-2 clone TC7 2. HT-29-MTX (goblet-like cells)	Model for internal absorption prediction in human intestine	[21]
	1. Caco-2 2. Leukocyte 3. E.coli, L.johnsonii, L. sakei	Study of bacterial response of IEC in regards of interaction with immunocompetent cells.	[22]

Organ	Cells	Studied system	Reference
Lung	1. A549 (epithelial cells) 2. airway macrophages (AM) from PBMC 3. dendritic cells (DC) derived from PBMC	Human airway barrier to study interaction with particles	[23]
Blood-brain-barrier	1. primary rat brain endothelial cells (RBEC) 2. primary astrocytes	Rat BBB model for molecular analysis of efflux transporters	[24]
	1. Brain capillaries from calf 2. astrocytes from newborn rats	<i>In vitro</i> model of BBB for physiological, pharmacological and pathophysiological study	[25]
Vascular endothelial	1. HUVEC (human umbilical vein endothelial cells) 2. U937 (monocyte cell line)	Arthrosclerosis model	[26]
Dental	1. HeLa 2. U937 differentiated to adherent macrophage-like cells	Chronic periodontal tissue destruction	[27]
Tyroid	1. Human thyrocytes 2. Monocytes	Thyroid epithelial barrier	[28]
Spheroids	3-d cell spheroids generation by RWV bioreactor.	Study of infectious diseases	[29]
Eyes	SV-40 immortalized human endothelial and epithelial cells and native stromal cells(fibroblasts)	Cornea <i>in vitro</i> model	[30]

The significance of dendritic cells in nanoparticle uptake has been shown in an *in vitro* model of at blood air barrier developed by the Rothen-Rutishauser group [23]. The model combines

A549 or primary lung epithelial cells co-cultured with blood derived macrophages on the apical side and dendritic cells on the basolateral side of the filter insert. Nanoparticles were found to be taken up by wandering alveolar macrophages and transferred to dendritic cells beneath the epithelial layer without disrupting the epithelial barrier, demonstrating direct interaction of different cell types in the recognition and presentation of particles and foreign objects to the immune system *in vivo*.

1.4.2 Disease relevant *in vitro* models

A certain level of complexity is also needed for mimicking pathophysiological conditions, in particular to mirror inflammatory or autoimmune conditions. While the inflammation process itself is quite straightforward and can be simulated by adding the source of inflammation to the model, the process in autoimmune diseases is more complex.

Their pathogenesis is based on signaling between different cell types i.e. tissue cells, adaptive and innate immune cells and leads to the immune system attacking the body's own tissues, subsequently resulting in increased inflammation.

Table 2 lists the infection models currently available in the research with a clear focus on autoimmune conditions can be observed with models for inflammatory bowel disease being most prominent. The models were utilized for specific aims either for observation of the effect of external stimuli on the inflamed model or to analyze the basic mechanism of the inflammation in this specific disease.

For inflammatory bowel disease, most *in vitro* models involved epithelial cells and immune cells. This can be developed by co-culturing of Caco-2 or primary colonic crypt cells and either primary monocytes from healthy or IBD patients or activated THP-1 cells (Table 2) [31]

[32]. The critic point for the model is the sample-to-sample variability for cells taken from IBD patients for screening process, although this may give a better approximation for a personalized drug therapy. In some cases intestinal microorganism are added to induce inflammation sometimes with addition of cytokine to enhance the inflammatory response. Phorbol 12-myristate 13-acetate (PMA)-activated THP-1 cells are widely used as alternative to primary macrophages due to its simplicity and morphological similarities. However, research findings showed relatively low correlation coefficient of transcribed genes in THP-1 and primary cell types. Therefore data generated from activated THP-1 cells should only be interpreted cautiously and better approach is needed to model immune cells in activated state.

Table 2. List of cocultures as *in vitro* models of inflammatory diseases

Disease	Cells	Studied system	Reference
Inflammatory bowel disease	1. Caco-2 or primary colonic crypts cells 2. PBMC and monocyte-depleted T cells from healthy and IBD patients	Cytokine analysis in IBD model	[31]
	1. Caco-2 2. activated THP-1 (monocyte cell line)	Co-culture system for epithelial cell survival study in IBD	[32]
	1. HT-29/MTX or Caco-2 (HTB 38) 2. PBMC from healthy donor or IBD patients 3. B. Vulgates or E.coli	Effect of non-pathogenic gram (-) bacteria to pro-inflammatory gene expression in IBD	[33]

Disease	Cells	Studied system	Reference
Inflammatory bowel disease	1. monocytes from PBMC 2. primary intestinal fibroblasts 3. HT-29	Cell-cell interaction in intestinal mucosa microenvironment	[15]
	1. T84 2. CCD-18Co (myofibroblast) 3. Lamina propria mononuclear cells (LPMC)	CD model	[34]
Asthma	1. BEAS-2B (bronchial epithel cell line) or primary bronchial epithelial cells (BEC) from asthmatic patients 2. monocyte-derived DCs (MDDCs)	Asthmatic bronchial epithelium activated by the an allergene	[35]
Arthritis	1. Fibroblast-like synoviocyte or dermal fibroblasts 2. U937 cells	Cytokine analysis in inflamed synovium	[36]
	1. bovine cartilage discs 2. human synovial fibroblast	Degradation of cartilage matrix components and synovial fibroblast activation	[37]
Tuberculosis	Human PBMC or J744	Invasion and intracellular replication of Mycobacterium tuberculosis	[38]
	1. NR8383 Cells 2. Mycobacterium tuberculosis	Chronic Infection of Mycobacterium Tuberculosis	[39]
Vascular endothelial	Human umbilical Veins	Leukocyte adhesion to inflammatory sites	[40]

1.5 Inflammatory Bowel Disease

Crohn's disease (CD) and ulcerative colitis (UC) are the most prevalent and commonly studied forms of inflammatory bowel disease (IBD), a group of chronic idiopathic inflammatory conditions of the gastrointestinal tract [41, 42]. In the US, more than 1.4 million people suffer from IBD and it is one of the highest causes of gastrointestinal morbidity. UC and CD differ in the intestinal areas and segments of the mucosa affected but present similar symptoms for example diarrhea, bloody stool, weight loss, abdominal pain, fatigue and fever. The pathogenesis of IBD is still not completely understood but an exaggerated immune response to the commensal intestinal microbial flora is assumed, leading to a weakening of the intestinal barrier function and further influx of pathogens. Genetic predisposition and environmental factor such as food intake and environmental pollutants also contribute to the disease. Still incurable, the current treatment schemes for IBD include non-specific anti-inflammatories and immunosuppressives to induce and maintain remission. Still, 60 to 80% of CD patients require surgery at one point in their life, while only 20% of UC patients need surgical intervention. In anti-inflammatory and immunosuppressive therapy both systemic and local colon targeted dosage forms are used. However, targeted drug delivery with conventional system has proven to be a challenge in IBD, as drug retention time in the gastrointestinal tract is significantly reduced due to diarrhea and the intravenous approach tends to have low bioavailability at the actual site of action combined with strong adverse effects and systemic toxicity.

Nanomedicines may enhance therapeutic options in IBD. Nanoparticles, by their size alone, were shown to accumulate in affected regions of the intestine in a TNBS induced rat model of colitis [43]. In the inflamed state, a reorganization of the tight junctions can be observed, leading to a leakier epithelium. Furthermore, immune cells such as neutrophils invade the

inflamed tissues in high numbers. Comparable to the Enhanced Permeation and Retention (EPR) effect observed at the leaky tumor vasculature, it is thus possible to passively target inflamed intestinal areas with nanomedicines, leading to a formation of local drug depots and reducing required doses as well as drug associated adverse effects.

Drug and formulation testing in IBD therapy so far has mostly been conducted in chemically induced rodent models of colitis. DSS (Dextran Sulfate Sodium) applied via the drinking water and TNBS (2,4,6-trinitrobenzenesulfonic acid) given intrarectally are commonly used to induce severe epithelial damage and inflammation with only low involvement of T cells and of the adaptive immune system. While in general the application of the chemical irritants induces an acute epithelial inflammation, repeated cycles of induction and recovery periods can also induce a chronic *in vivo* model. Although more relevant to the pathophysiology of the disease in humans, the chronic models are rarely used in drug or formulation testing as the length of the induction period as well as the loss of mice during that time make the test system more variable and unpredictable. Yet, the predictive power of the chemically induced colitis model is limited to a certain extent and can lead to failures to clinically translate experimental findings.

Recently, genetically modified mice such as IL-10 knockout mice have been established as IBD animal model and give better approach in chronic inflammatory disease. Species differences and differences in pathogenesis hinder drug and formulation testing in this regard. Recently, genetically modified mice s.a. IL-10 knockout mice have been established as IBD animal model as they develop a chronic enterocolitis due to an aberrant immune response to normal enteric antigens. Despite of giving a more relevant model, the genetically modified mice still lost its edge to the more popular and easy to maintain chemically induced animal model due to the high cost and sensitivity of the mice.

1.6 Nanocarrier systems in drug delivery

The medical application of nanomedicine has been gaining popularity in recent years. Defined as carrier systems in the nanosize range (preferably <100 nm), nanocarriers has been widely studied for drug or contrast agent loading vehicle. The size of carriers and its modification with PEG molecules has been also shown to increase the circulation time in the body, as they may escape the absorption and clearance by the mononuclear phagocyte system, therefore increasing the availability and potential accumulation in the targeted area. Some carriers can be also used as a trojan horse to shield the hydrophobicity of drug compounds and increased the bioavailability. Additionally, targeting moiety can be added to increase the active targeting of the drug to the site of action to enable specific targeting and sustained release of the loaded drugs and therefore reducing the side effects. The advantage of higher surface area is not only useful for moiety targeting but also for various imaging modalities. Some newer approaches in the development of imaging modalities targeted for theranostic (therapy and diagnostic) function. In this approach, drug and imaging probe loaded to nanoparticles are targeted to certain receptor to facilitate simultaneous targeted drug therapy and monitoring the therapy responses.

In inflammatory diseases, the vasculature and epithelial barriers seems to be leakier due to the reorganization of the tight junction, causing the Enhanced Permeation and Retention (EPR) effect similar to the tumor environment. This fact has been used previously for drug delivery in cancer therapeutics, as the leaky barrier may allow smaller nanovehicle to breach the barrier and accumulate in the cancer environment, letting them to release the therapeutic agents specifically in the area. In IBD, the targeting and prolonged circulation time results in the accumulation of the drugs at the inflamed sites in higher concentration than in the

healthy tissue. This may reduce the adverse effect and improve the strategy of optimized longer lasting medication with less side effects.

1.7 Aims of the thesis

With the *in vivo* models being ethically questionable, time consuming and of limited predictive power for drug and formulation testing, a disease relevant *in vitro* model can help overcome this bottleneck in the development pipeline of new IBD therapeutics. However, the available *in vitro* models so far are not suited for drug testing at the inflamed intestinal barrier as they either lack the pathophysiological background and complexity or were developed for a mechanistic study of disease origin failing to optimize the system for pharmacokinetic investigations. Thus, the aim of this thesis was to bridge this gap developing an *in vitro* model of the inflamed intestinal mucosa that in the healthy state demonstrates good epithelial barrier properties and then could be triggered to an inflamed state mirroring pathological symptoms of the inflamed intestine.

In the setting up of the system candidate epithelial cells and pro-inflammatory reagents were screened and a co-culture model incorporating primary blood derived immune cells was established. The model was characterized in the non-inflamed as well as in the inflamed state for epithelial barrier function and disease markers.

In the testing of the predictive potential of the model a liposomal and particulate formulation of the glucocorticoid budesonide were applied and recovery of epithelial barrier function and reduction of inflammation were monitored. Not only was it possible to treat the model but also mechanistic conclusions on the interaction of nanomedicines with the inflamed epithelial barrier could be drawn. In the context of nanomedicines it also became necessary to optimize cell culture tools for epithelial *in vitro* models to improve translocation studies. Using ultrathin porous silicon nitride membranes a novel cell culture system was established that can be combined with the inflamed co-culture model in future studies.

2. A 3-dimensional co-culture of enterocytes, macrophages and dendritic cells to model the inflamed intestinal mucosa *in vitro*

Parts of this chapter have been published in:

Fransisca Leonard, Eva-Maria Collnot, Claus-Michael Lehr. A 3-dimensional co-culture of enterocytes, macrophages and dendritic cells to model the inflamed intestinal mucosa *in vitro*, Mol Pharm 2010 Dec 6;7(6):2103-19. Epub 2010 Nov 1.

2.1 Abstract

While epithelial cell culture models (e.g. Caco-2 cell line) are widely used to assess the absorption of drug molecules across the healthy intestinal mucosa, there are no suitable *in vitro* models of the intestinal barrier in the state of inflammation. Thus development of novel drugs and formulations for the treatment of inflammatory bowel disease is largely bound to animal models. We here report on the development of a complex *in vitro* model of the inflamed intestinal mucosa, starting with the selection of suitable enterocyte cell line and pro-inflammatory stimulus and progressing to the setup and characterization of a three dimensional co-culture of human intestinal epithelial cells and immunocompetent macrophages and dendritic cells.

In the 3D setup, controlled inflammation can be induced allowing to mimicking pathophysiological changes occurring *in vivo* in the inflamed intestine. Different combinations of pro-inflammatory stimuli (lipopolysaccharides from *E. coli* and *S. typhimurium*, IL-1 β , IFN- γ) and intestinal epithelial cell lines (Caco-2, HT-29, T84) were evaluated and only Caco-2 cells were responsive to stimulation, with IL-1 β being the strongest stimulator. Caco-2 cells responded to the pro-inflammatory stimulus with a moderate up-regulation of pro-inflammatory markers and a slight, but significant decrease (20%) of transelectrical epithelial resistance (TEER) indicating changes in the epithelial barrier properties. Setting up the co-culture model, macrophages and dendritic cells derived from periphery blood monocytes were embedded in a collagen layer on Transwell filter insert and Caco-2 cells were seeded atop.

Even in the presence of immunocompetent cells Caco-2 cells formed a tight monolayer. Addition of IL-1 β increased inflammatory cytokine response more strongly compared to Caco-2 single culture and stimulated immunocompetent cells proved to be highly active in

sampling apically applied nanoparticles. Thus the 3D co-culture provides additional complexity and information compared to the stimulated single cell model. The co-culture system may serve as a valuable tool for developing drugs and formulations for the treatment of inflammatory bowel diseases, as well as for studying the interaction of xenobiotics and nanoparticles with the intestinal epithelial barrier in the state of inflammation.

2.2 Introduction

Inflammatory bowel diseases (IBD), such as Crohn's disease or colitis, have been postulated as being associated with both defects in the intestinal barrier and an impaired immune function. Genetic predispositions such as mutations in the NOD2 gene, as well as different environmental factors may also have contributed [44]. IBDs have been characterized by an exaggerated pro-inflammatory immune response to the commensal intestinal microbial flora. Studies have demonstrated also that this aberrant inflammation leads to an increased permeability of the intestinal epithelial barrier, allowing toxins and microbes to reach the underlying tissues [45]. Several studies reported for both affected and unaffected areas alterations in the mucosal architecture, such as transcellular bridge formation in epithelial cells and goblet cell hyperplasia or hypertrophy or both [46].

While most IBDs have so far been considered as incurable, therapeutic measures are directed to treat the symptoms by anti-inflammatory drugs and to prolong the remission by various immunomodulators especially corticosteroids [44]. Besides several approaches to optimize drug delivery by colon targeted dosage forms [47] efficient drug delivery in IBD is still hampered by diarrhea, a prominent symptom of the disease. Diarrhea decreases the drug carrier residence time thereby also shortening the time window for drug release and absorption [48]. Novel drug carriers have been designed to overcome this problem by decreasing the particle size. Several microparticulates have been shown to be successful in experimental treatment of IBD [49, 50]. In a rat model of IBD nanoparticles showed an even more pronounced retention effect in inflamed, mucus-rich areas of the intestine in comparison to microparticles, and prolonged anti-inflammatory action [43].

To further improve drug delivery in IBD a better understanding of the disposition of drugs and (nano)particulate delivery systems in the targeted tissue is essential. In conventional

ADME screening, cell lines such as Caco-2 are widely accepted as a model of the normal, healthy intestinal mucosa. However, models which consist only of enterocytes cannot mimic the complex interactions with other cells, in particular of the immune system. Such interactions however may be of utmost importance for the epithelial barrier function as well as for the uptake and translocation of (nano)particles in the state of inflammation.

In preclinical studies, animal models are mostly preferred. However, apart from its intrinsic complexity and ethical controversies, the main problems of animal model lies in the species differences compared to man, which often causes misleading results [51]. Chemically induced IBD by sulfonic acid derivatives TNBS and DSS in mice has been widely used in experiments. While these models show some characteristic histological and pathological changes, the reproducibility is difficult since the induced inflammatory effects depend on the dose, species and strain of the animal used. High dose of TNBS is needed to induce the colitis, which normally leads to high mortality rate of tested animals and impedes the pharmacological studies. Moreover, dimension differences of test animals here cannot be neglected as the length of small intestine in mice is less than 50 cm [52]. The induced colitis in mice may impact the whole intestine compared to only patches of inflamed regions in humans which have a small intestine length of about 3 to 4 m [53].

The crucial disadvantage of the chemically induced animal models is their limited relevance for human IBD as shown by the lack of responsiveness to corticosteroids and 5-ASA therapy [54]. Furthermore, these models simulate more an acute tissue injury of intestinal epithelial and are therefore less representative of an immune response-directed chronic inflammation. Other models such as transgenic or knock out genes based models have significantly increased in numbers recently. They are suitable to observe the pathological changes in

organism with disrupted genes, but their specificity makes their uses for common anti-inflammatory substances therapy testing in general inflammation of IBD questionable.

Intestinal epithelium plays the central role in inflammatory response and so far several enterocyte cells such as HT-29, T-84 and Caco-2 have been widely used to study intestinal epithelial barrier function [55]. These cells however, are cancer derived and not supposed to reflect the pathophysiological changes in the state of inflammation. Therefore, the objective of this study was to expand on the cell characteristic and establish a model of intestinal mucosa in the state of inflammation. This was achieved by stimulating intestinal epithelial cells with pro-inflammatory compounds such as LPS from intestinal micro flora and several chemokines or cytokines such as IL-1 β , TNF- α and IFN- γ .

Another point to be taken in consideration is the complexity of the tissue *in vivo*. Immune cells are particularly important in the pathogenesis of inflammatory bowel disease since they are highly dysregulated and mistakenly take up harmless non-pathogenic intestinal flora, processing them as an antigen [56]: Naïve dendritic cells are activated by inflammatory cytokines upon capturing antigen through pinocytosis and phagocytosis. They then carry the antigens and present them to naïve T-lymphocytes located in the lymph nodes, where the antibodies against the antigens are formed. Macrophages are able to eat up some microbes or infected/cancerous cells. After processing they also present the antigen to helper T-cells, thus activating adaptive immune response.

We herein describe the development of a new three-dimensional *in vitro* model from starting with the selection of an adequate enterocyte cell line and inducer of inflammation and progressing to the setup and characterization of a more complex co-culture model. The co-culture encompasses human intestinal epithelial cells and primary, blood derived

macrophages and dendritic cells and can be utilized as a stepping stone between the classical *in vitro* single cell culture testing and *in vivo* testing. The model was characterized with regards to release of pro-inflammatory marker IL-8, re-organization of tight junction proteins and recovery after removal of the pyrogenic compounds. The effects were evaluated by histology, immunohistochemistry and TEER measurement as well as by changes in expression and translation of key genes in the inflammatory cascade. Furthermore the barrier properties of the novel model for the transport of marker compound fluorescein sodium and the interaction with drug-free polymeric nanoparticles was evaluated.

2.3 Material & Methods

2.3.1 Materials

Human colon adenocarcinoma cell line Caco-2 clone C2Bbe1, HT-29 and T84 was obtained from American Type Culture Collection (Rockville, MD). Dulbecco's modified Eagle's medium (DMEM) was purchased from Gibco (Carlsbad, CA), Fetal calf serum and non-essential amino acids were purchased from PAA (Pasching, Austria). Trypsin/EDTA was obtained from Sigma (Steinheim, Germany). Plastic dishes, plates were obtained from Greiner Bio-One, Transwell inserts with pore size 0.4 μm were purchased from Corning Incorporated (Acton, MA, USA). IL-1 β , GM-CSF and IL-4 were purchased from R&D Systems (Minneapolis, USA) and Lipopolysaccharide(LPS) originated from both E.coli and S.typhimurium were obtained from Sigma (Steinheim, Germany). Ficoll Paque plus for PBMC isolation was obtained from GE Healthcare (Uppsala, Sweden) and human serum from Invitrogen (Wisconsin, USA). 4',6-Diamidino-2-phenylindol, Fluorescein sodium salt (FluNa) and organic solvents were acquired from Sigma (Steinheim, Germany). Rabbit anti-ZO-1 antibody, rabbit anti-Claudin-1 and mouse anti Occludin antibodies were obtained from Zymed Laboratories Inc (San Francisco, CA) and fluorescence coupled goat-anti rabbit and anti-mouse secondary antibody was purchased from BD Biosciences (Heidelberg, Germany). R-PE-coupled CD14 antibody for FACS analysis was purchased from Chemicon Internationals (Temecula, California 92590, USA) and FITC-coupled CD1a was purchased from BD Biosciences (Heidelberg, Germany). CBA human IL-8 Flex Set was also purchased from BD Biosciences (Heidelberg, Germany). RNeasy Mini Kit, QuantiTect Reverse Transcriptase and QuantiTect Probe Kit were from Qiagen (Hilden, Germany). Alcian blue was obtained from Sigma (Steinheim, Germany). Fluorescein- coupled Fluoresbrite carboxylate microspheres with size ranging from 50 to 500 nm were purchased from

Polysciences, Inc (Pennsylvania, USA). Purecol collagen was obtained from Advanced Biomatrix (Tucson, Arizona, USA). Veronal buffer (pH 8.5) for acid phosphatase staining was obtained from Morphisto (Frankfurt, Germany). All chemicals used in this study were of analytical grades.

2.3.2 Cell culture

Caco-2 clone C2Bbe1 (passage 65-78) were grown in a culture medium composed of DMEM, 10% FCS and 1% non-essential amino acid and maintained at 37°C in a 5% CO₂ and 95% humidity environment. HT-29 cells were grown in McCoy's medium with 10%FCS addition while T84 cells were grown in DMEM/F12 medium with 5% FCS supplement and maintained in similar condition as Caco-2. The medium was changed every other day and the cells were sub cultured every week at a split ratio of 1 to 20 by treatment with 0.1% trypsin and 0.02% EDTA.

2.3.3 Cell stimulation, isolation of RNA and reverse transcription

Caco-2 cells were cultivated in 6-well plate at a seeding density of 1.2×10^5 cells/cm². Total RNA was extracted from Caco-2 cells using Qiagen RNeasy Mini Kit after stimulation with varying concentration of LPS and IL-1 β and exposed for 2 to 24 hours. The double stranded cDNA was synthesized from 1 μ g mRNA using the Qiagen QuantiTect Reverse Transcriptase Kit and the product was used for further analysis with real-time PCR.

2.3.4 Quantification of pro-inflammatory gene expression with real-time PCR

PCR analysis was performed for 35 cycles (95°C for 12 seconds, 60°C for 45 seconds) with 75 ng of the synthesized cDNA, each 0,1 µl of 50 µM primers and 12,5 µM fluorescent probe using QuantiTect PCR Probe Kit. Sequences of primer pairs and probes are shown in table 3. An internal standard was included for each set of RNA samples analysed and standard curves were calculated for the quantification.

Table 3. Primer sequences for mRNA quantification by realtime PCR. All sequences were 5' ->3'. FAM= Fluorecein and BHQ1= Black Hole Quencher 1.

Gene	Sequences	Product (bp)
β-actin	Sense: TGC GTG ACA TTA AGG AGA AG A: GTC AGG CAG CTC GTA GCT CT Probe: FAM-CAC GGC TGC TTC CAG CTC CTC-BHQ1	107
TNFα	Sense: CTC CAC CCA TGT GCT CCT CA A: CTC TGG CAG GGG CTC TTG AT Probe: FAM-CAC CAT CAG CCG CAT CGC CGT CTC-BHQ1	99
IL-8	Sense: TGC CAG TGA AAC TTC AAG CA A: ATT GCA TCT GGC AAC CCT AC Probe: FAM-TCA ACA CTT CAT GTA TTG TGT GGG TCT G-BHQ1	78

2.3.5 Protein expression assessment with FACS-based CBA Flex kit

The initial study to compare the effect of various pro-inflammatory compounds on the IL-8 release was conducted with Caco-2. Caco-2 cells were cultured in 96-well plate at a seeding density of 2×10^4 cells/well. The assay was conducted after the cells formed a monolayer.

Cells were stimulated with various concentration of either LPS or IL-1 β . 50 μ l of the supernatant was used for IL-8 protein expression measurement.

IL-8 release was also measured in the established inflamed co-culture and compared with the release from stimulated and non-stimulated Caco-2 monoculture. For this purpose, Caco-2 cells with seeding density of 6×10^4 cells/filter were grown on collagen coated Transwell inserts, with macrophages and dendritic cells embedded in the collagen for the co-culture setup. The assay was conducted after 21 days of cultivation. 10 ng/ml IL-1 β were added to the apical side to induce the inflammation and 50 μ l of the apical and basolateral fluid were sampled after 24 h. IL-8 protein expression was measured by CBA Flex Set for IL-8 according to the manufacturer protocol.

2.3.6 Transepithelial electrical resistance and paracellular permeability

For Transepithelial electrical resistance (TEER) measurements, the cells were grown in Transwell inserts at a seeding density of 6×10^4 cells/cm². The cells formed fully differentiated monolayer after 21 days in culture. The integrity of cell monolayer was monitored by TEER measurement with Epithelial Voltohmmeter (World Precision Instruments, Sarasota, US). Monolayers with TEER value higher than 400 Ω *cm² were used for the experiments.

2.3.7 Immunostaining of tight junctional protein

Tight junction protein ZO-1, Occludin and Claudin-1 were stained with immunofluorescent antibodies. Caco-2 cells were seeded in Transwell filters as previously described. The cells were fixed with 100% ethanol at 4°C for 30 minutes and then incubated with either rabbit-

anti human ZO-1, mouse-anti human Occludin or rabbit-anti human Claudin-1 antibody (suspended in PBS + 1% BSA solution) for 1 hour followed by incubation with secondary antibody for 30 minutes and DAPI staining for 10 minutes. Fluorosafe was used to mount the filters onto cover slips. A Zeiss LSM 510 confocal microscope with the software LSM510 package was used for capturing fluorescent images of the immunostainings. Images were captured with z-stack to record three-dimensional dataset. This was done by random sampling to represents the general condition of the model. Volocity (Improvisions, Lexington, MA, USA) imaging software was used to reconstruct 3D images from stack datasets using Mackintosh computer.

2.3.8 Permeability of fluorescein on the Caco-2 cell monolayer

Tight Caco-2 monolayer obtained 21 days after seeding was used for fluorescein transport experiment. Transport was assessed in both absorptive (apical → basolateral) and secretory (basolateral → apical) directions. 1 μg/ml FluNa was dissolved in transport buffer consisting of DMEM without phenol red and 10% FCS. Cell monolayers on Transwell filters were rinsed gently twice and pre-incubated in transport buffer for one hour at 37°C and 5% CO₂. FluNa was added to the donor compartment and transport buffer was added to the acceptor compartment. Cell monolayers were agitated throughout the experiments with orbital shaker from IKA Werke GmbH & Co KG (Staufen, Germany). At different time points 50 μl samples were taken from the receiver compartment and the volume lost during sampling was replaced with fresh buffer. Fluorescein amount in the samples was measured using Tecan Infinite 200 Reader at the excitation wavelength of 488 nm and emission wavelength of 530 nm. Apparent permeability (P_{app}) was calculated according to:

$$P_{app} = (dQ/dt) \cdot (1/A) \cdot (1/C_0) \dots \dots \dots (eq1)$$

Where dQ/dt is the amount of drug transported per time, A is the surface area of the monolayer and C_0 is fluorescein concentration ($\mu\text{g/ml}$) at time 0.

Permeability of FluNa across non-stimulated Caco-2 monolayers was determined as control. TEER of all monolayers was monitored before and after the transport studies to ensure the integrity of monolayer.

2.3.9 Fluoresbrite polystyrene nanoparticles uptake in Caco-2 cell monolayer and co-culture

The experiments were conducted using Transwell-grown Caco-2 monolayers. 0.1% w/v Fluorescein-labeled polystyrene nanoparticles were added to the apical side and incubated at 37°C for 4 hours. The medium was removed and cells were washed three times with PBS to remove excessive non-adhered particles. For the single culture the cells were then stained with ZO-1 labeling antibody and DAPI. The co-cultures were stained with DAPI dye for Caco-2 nucleus localization and analysis was done by CLSM imaging. Immunocompetent cells in the model were detected by their auto fluorescence in red spectra region (Laser excitation : 543 nm, emission: 560-615 nm). , fluorescein-labeled particles were detected in the green spectra region (Laser excitation : 488 nm, emission: 500-550 nm). and DAPI in the blue spectra region (Laser excitation : 720 nm-multiphoton, emission: 390-465 nm).

All the particles were monitored for their size and polydispersity index by Dynamic Light Scattering measurement using Zetasizer Nano ZS (Malvern Instruments, Herrenberg, Germany). Nanoparticle adherence to Caco-2 cells was quantified using images taken from

randomly chosen areas of the monolayer. The analysis was conducted by fluorescence distribution analysis with ImageJ software.

2.3.10 Caco-2 monolayer mucus staining with alcian blue

Tight Caco-2 monolayers cultured on Transwell filter insert for 21 days were washed twice with PBS. Alcian blue dissolved in 3% acetic acid was added to the monolayer and incubated for 20 minutes at room temperature. The excessive alcian blue was removed by washing three times with PBS. Afterwards microscopic monolayer images were taken with digital camera C5050 (Olympus, Japan).

2.3.11 Mucus quantification by glycoprotein measurement

Content of the main mucus glycoprotein mucin in stimulated and non-stimulated Caco-2 cells was quantified using periodic acid/Schiff reagent method as described previously [57]. Briefly, Schiff reagent was prepared by dissolving fuchsin in 100 ml boiling water and letting the solution cool down to 50°C before adding 20 ml of 1M HCl. Directly before experiment 1.66 g sodium metabisulphite was added to the solution and incubate at 37°C until the solution is colorless or pale red.

The medium of Caco-2 cell monolayer was carefully removed and the cells were lysed with 100 µl PBS with 1% Triton-X addition. The samples were then incubated at 37°C for 2 hours with 10 µl periodic acid solution, which was prepared by adding 10 µl of 50% of periodic acid to 10 ml of 7% acetic acid. Afterwards, 10 µl Schiff reagent was added and samples were incubated at room temperature for 30 minutes before measuring adsorption at 555 nm using

Tecan Infinite 200 Reader spectral photometer. A calibration curve with a linear range of 10 – 600 µg/ml was generated using porcine mucin.

2.3.12 Macrophages and Dendritic cells cell culture

Macrophages and dendritic cells were differentiated from blood monocytes originated from buffy coats (Blood donation service, Saarbruecken, Germany). Buffy coats were processed by Ficoll density gradient centrifugation to obtain the peripheral blood mononuclear cells. These cells were plated with macrophages medium (RPMI medium supplemented with 10% human AB serum, 1% non-essential amino acid and 1% sodium pyruvate). Mature macrophages were obtained after seven days cultivation with macrophages medium while DCs were obtained after seven days cultivation with macrophages medium with addition of 25 ng/ml IL-4 and 50 ng/ml GM-CSF. The harvested DCs and macrophages were analysed for their marker CD1a and CD14 by FACS measurement.

2.3.13 Three-dimensional triple cell culture

100 µl of DCs and macrophages dispersed in a 80%(w/v) solution of type I bovine collagen pH 7.4 at a concentration of 10⁵ cells/ml were pipetted on top of 3460 Transwell filter inserts (1.12 cm² area) resulting in a seeding density of approximately 10⁴ cells/well. 1 hour later, 6x10⁴ Caco-2 cells were then seeded on top of the formed collagen gel layer. The co-culture was kept at 37°C in 5% CO₂ with Caco-2 medium at the apical side and macrophage medium in basolateral compartment as illustrated in figure 2. After 21 days the co-culture was utilized for the experiments. For the inflamed model 10 ng/ml IL-1β was added to the apical side and incubated for at least two days. Apical fluid was removed before experiment and

cells were washed three times with PBS to remove any IL-1 β leftovers. The TEER value was monitored before and after each experiment.

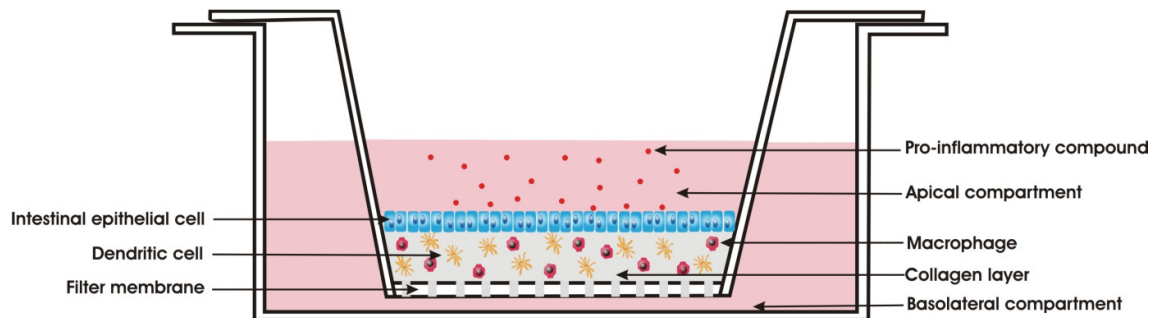


Figure 2. Experimental set up of the co-culture consisting intestinal epithelial cell line, macrophages and dendritic cells.

2.3.14 Sample preparation for histological staining

Transwell filter inserts were stained with acid phosphatase reagent for one hour and washed with water and treated with ethanol multiple times before fixing with paraffin overnight. Acid phosphatase reagent was obtained by mixing 0.4 ml pararosanilin-HCl solution, 0.4 ml sodium nitrit, 0.5 ml naphthol ASB1 phosphate buffer and 9 ml Veronal buffer. The paraffin block was cut into 4 μ m sections and mounted on glass slides. The histological cut was stained with Haemalaun solution for 5 minutes and washed with water before treatment with Eosin G for 30 seconds. The preparation was washed four times with 100% ethanol and xylol solution and later fixed with Roti-Histokitt.

2.3.15 Statistical analysis

Student's t-test and one way ANOVA was used to compare results from different treatments at different time points. The analysis was done with SigmaStat 3.0. Individual experiments were performed at least in triplicate and each experiment was repeated at least once.

2.4 Results

2.4.1 Inflammatory marker in mRNA level in Caco-2 cells after stimulation with pro-inflammatory compounds

First experiments for stimulation of inflammation were conducted by addition of LPS to the enterocyte cell lines T84, HT-29 and Caco-2. mRNA production from these cells was monitored at various time points from 0 to 24 h and the pro-inflammatory markers such as IL-8 and TNF- α were measured by real-time PCR. As can be seen in figure 3a & b T84 and HT-29 showed no response to the stimulation, while Caco-2 were the only responsive cells. Therefore the Caco-2 cell line was selected for all further experiments.

Caco-2 cells showed a time-dependent increase of pro-inflammatory cytokine mRNA in response to the stimulation with bacterial LPS from *S. typhimurium* and *E. coli*. LPS from *S. typhimurium* showed higher impact on Caco-2 cells than LPS from *E. coli* increasing the IL-8 expression by 40 to 70 and 2 to 20-fold respectively (Fig. 3a). IL-8 mRNA was upregulated in a concentration dependant way with the highest expression at the highest concentration of 10 $\mu\text{g/ml}$ of both bacterial LPS peaking immediately two and four hours after stimulation with a gradually decay afterwards.

The stimulation with bacterial LPS also increased the expression of TNF- α which gave a similar pattern as IL-8 expression by having the highest expression in the cells treated with 10 $\mu\text{g/ml}$ bacterial LPS. LPS from *E. coli* slightly upregulates TNF- α only about 2-3 fold while LPS from *S. typhimurium* achieved about 10 fold induction (Fig. 3b.)

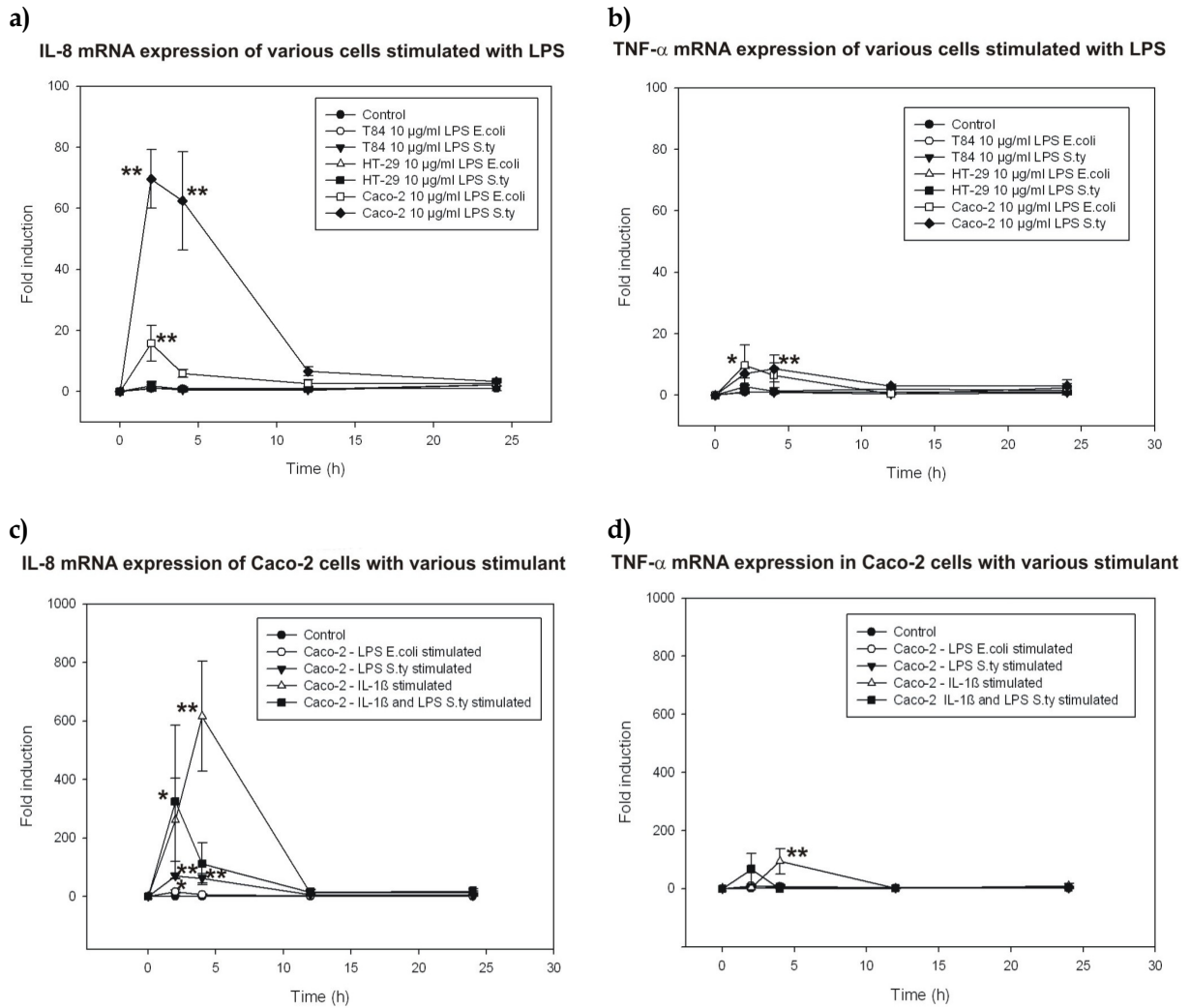


Figure 3. Expression of IL-8 (a) and TNF- α (b) mRNA in T84, HT-29 and Caco-2 intestinal epithelial cell lines in response to stimulation with *E. coli* or *S. typhimurium* LPS as determined by real time PCR. Effect of stimulation with IL-1 β alone or in combination with LPS on IL-8 (c) and TNF- α (d) mRNA expression in Caco-2 cells. (mean \pm SE, n=6, * indicates statistically significant differences compared to control, p<0.05; ** indicates statistically very significant differences compared to control, p<0.01).

In addition to LPS, pro-inflammatory cytokine IL-1 β was also evaluated as a stimulant, but in Caco-2 cells only. Cells responded slower to stimulation with IL-1 β but to higher extent in comparison to LPS stimulation both in their IL-8 and TNF- α expression (Fig. 3 c and d). The value for IL-8 reached about 600 fold induction compared to the control value four hours

after stimulation with IL-1 β . No concentration dependent effect was observed in a range from 1 to 10 ng/ml IL-1 β (data not shown). IL-1 β stimulation in Caco-2 cells also increased TNF- α expression up to 100 fold compared to the control (Fig. 3d).

Interestingly, co-stimulation of Caco-2 with both *S. typhimurium* LPS and IL-1 β yielded an increase of both IL-8 and TNF- α in similar level as stimulation with IL-1 β alone, but the response was faster: the cytokine release peaked already 2 hours after co-stimulation while the stimulation with IL-1 β alone resulted in a peak not before 4 hours (Fig. 3c and d).

2.4.2 IL-8 protein release in response to pro-inflammatory compounds in Caco-2

IL-8 protein release showed also an increase to the stimulation in both bacterial LPS in concentration-dependent manner. The non-stimulated control cells did not release a detectable amount of IL-8 protein while stimulation of 0.1-10 μ g/ml with LPS from both bacterial strains induced a release of 30 to 120 pg/ml IL-8 (Fig. 4).

In comparison, IL-1 β in concentrations as low as 1 ng/ml induced a release of more than 500 pg/ml IL-8; 10 ng/ml of IL-1 β induced more than 1500 pg/ml IL-8.

The co-stimulation by IL-1 β and LPS (10 μ g/ml) gave a similar IL-8 release as by stimulation with IL-1 β alone, but the maximal response was already reached at 5 ng/ml IL-1 β . No further increase was observed at 10 ng/ml IL-1 β .

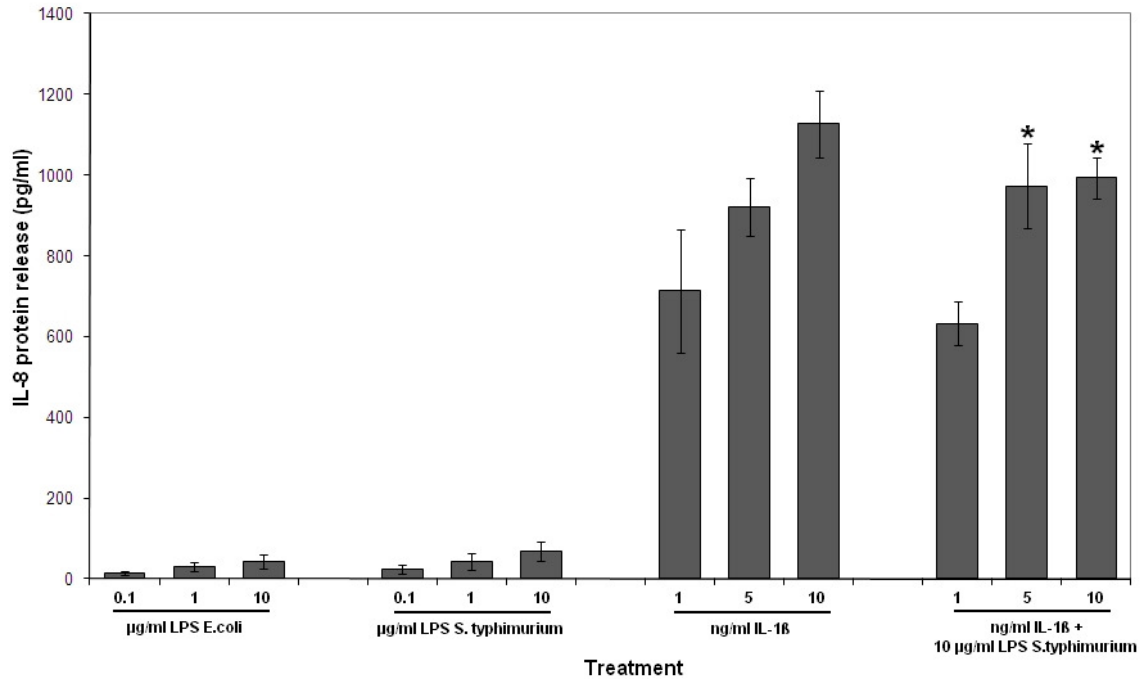


Figure 4. Modulation of IL-8 protein expression in Caco-2 cells after exposure to varying concentration of LPS from *E.coli*, *S.typhimurium*, IL-1 β and double stimulation with IL-1 β and LPS from *S.typhimurium*. (mean \pm SE, n=6, * indicates statistically significant differences compared to the lowest tested concentration of stimulant, p<0.05).

2.4.3 Pro-inflammatory compound-induced increase of Caco-2 monolayer permeability

Furthermore, the effect of inflammatory stimulation on Caco-2 cells barrier function was investigated via TEER measurement. TEER values of Caco-2 cells stimulated with both kinds of LPS resonated within limits of 90 - 110% of the unstimulated control value (data not shown). IL-1 β significantly decreased TEER to a nadir of 80% of the control value which was reached 72 h after stimulation as shown in figure 5a. Varying the concentration of IL-1 β within a range of 1 to 10 ng/ml had only marginal effect on TEER. Again, co-stimulation by IL-1 β and LPS from *S. typhimurium* resulted in a faster onset of the effect but did not further decrease the final TEER value (Fig. 5b).

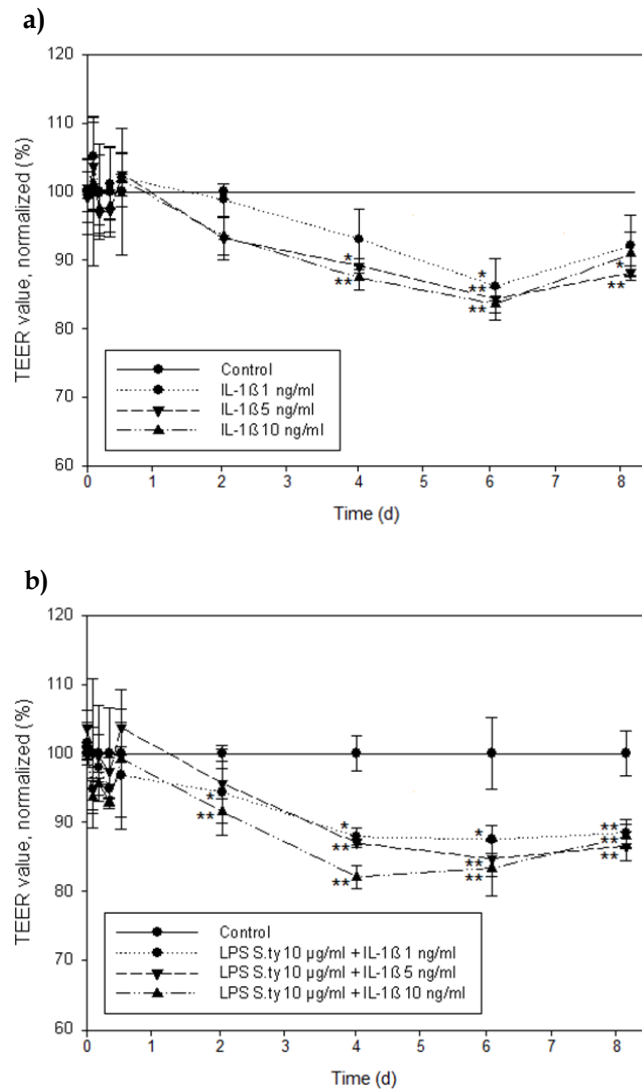


Figure 5. Effect of varying concentrations of IL-1 β (a.) or a co-stimulation with IL-1 β and 10 μ g/ml LPS from *S.typhimurium* (b.) on Caco-2 monolayer permeability measured by changes in Transepithelial Electrical Resistance (TEER) (mean \pm SE, n=6, * indicates statistically significant differences compared to control, p<0.05; ** indicates statistically very significant differences compared to control, p<0.01).

2.4.4 Transport of fluorescein in inflamed Caco-2 cells

Fig. 6 shows the fluorescein permeability in response to increasing concentrations of IL-1 β . The average Papp value in the control experiment with non-stimulated Caco-2 cells was the same for both apical-basolateral and basolateral-apical direction. After treatment with IL-1 β , TEER was decreased by up to 20% compared to control. Apical-basolateral transport was not affected by this relatively small change in TEER and only showed a marginal increase. However, basolateral-apical transport was increased by up to 84% when Caco-2 cells were stimulated with high doses of 500 ng/ml.

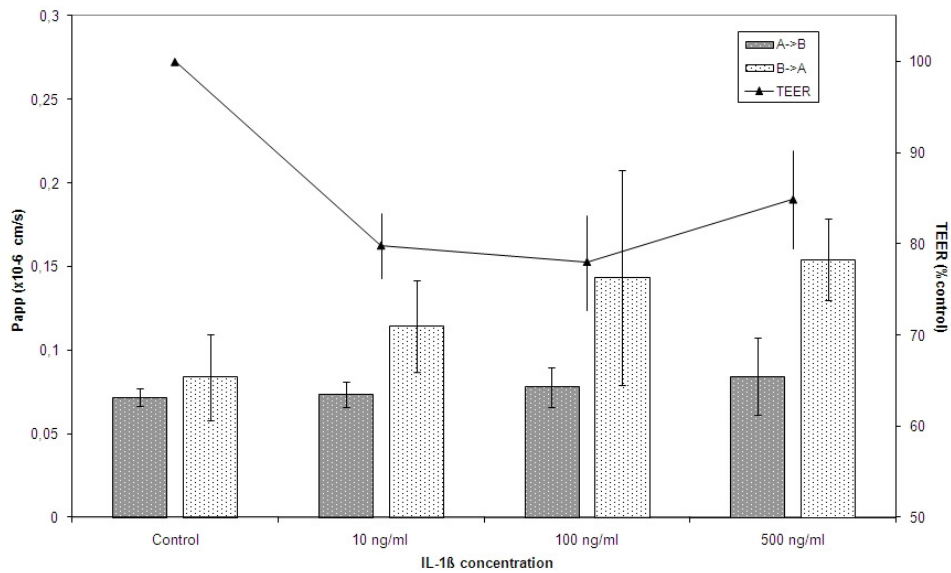


Figure 6. Apparent permeability values of fluorescein transport across Caco-2 monolayers pre-treated with IL-1 β and the respective TEER values. (mean \pm SE, n=6, * indicates statistically significant differences compared to control, $p < 0.05$; ** indicates statistically very significant differences compared to control, $p < 0.01$).

2.4.5 Immunostaining of tight junction protein ZO-1

As the monolayer permeability was increased in response to the stimulation, the ZO-1 tight junctional protein was tracked with fluorescent labeled antibody. ZO-1 as the essential pore forming part of the tight junctional complex is normally located towards the apical side of an epithelium as can be seen in figure 7a. In IL-1 β stimulated cells, the ZO-1 showed less intensity at the apical side but reached deeper down to the basolateral side indicative of an reorganization process of the tight junction proteins (Fig. 7b).

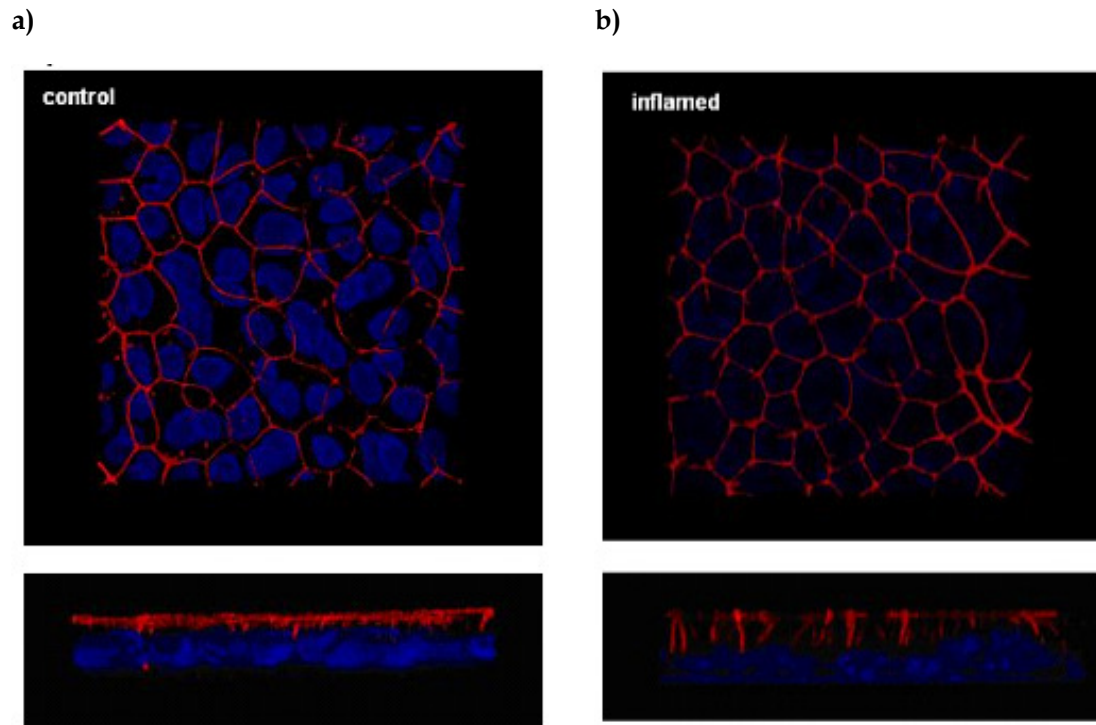


Figure 7. Immunofluorescence microscopy of Caco-2 cells, fixed and stained with antibodies specific for ZO-1 (red) and DAPI (blue) for nucleus dye, untreated control (a), IL-1 β 10 ng/ml treated cells (b).

2.4.6 Nanoparticles allocation in non-stimulated and stimulated Caco-2 monolayers

Nanoparticles of 100 nm size or larger were observed only on the apical side of Caco-2 monolayers, indicating adherence to the cells but no uptake. There was no difference between stimulated Caco-2 cells (Fig. 8b) and the non-stimulated control (Fig. 8a). In contrast to all larger particles, the fluorescence signal of 50 nm nanoparticles was also located clearly below the apical cell membrane. Moreover, there was an increased signal in stimulated cells compared to the control (Fig. 8a and b). The signal was not co-localized with the ZO-1 signal in either case. This indicates that 50 nm particles may penetrate into Caco-2 cells and that there is more adherence of these particles to cells in state of inflammation. Furthermore, it seems particles were not transported through the cell-cell junction.

Adherence of nanoparticles was quantified by calculating fluorescence distribution in the images taken randomly across the monolayer confirming the visual impression (Fig. 8). Only particles as small as 50 nm were significantly more accumulated in inflamed Caco-2 monolayers compared to the control (Fig. 9).

As can be seen from alcine blue staining and mucus quantification in figure 10a and b, inflammatory stimulation of Caco-2 cells was accompanied by an increased production of mucus of ~12%.

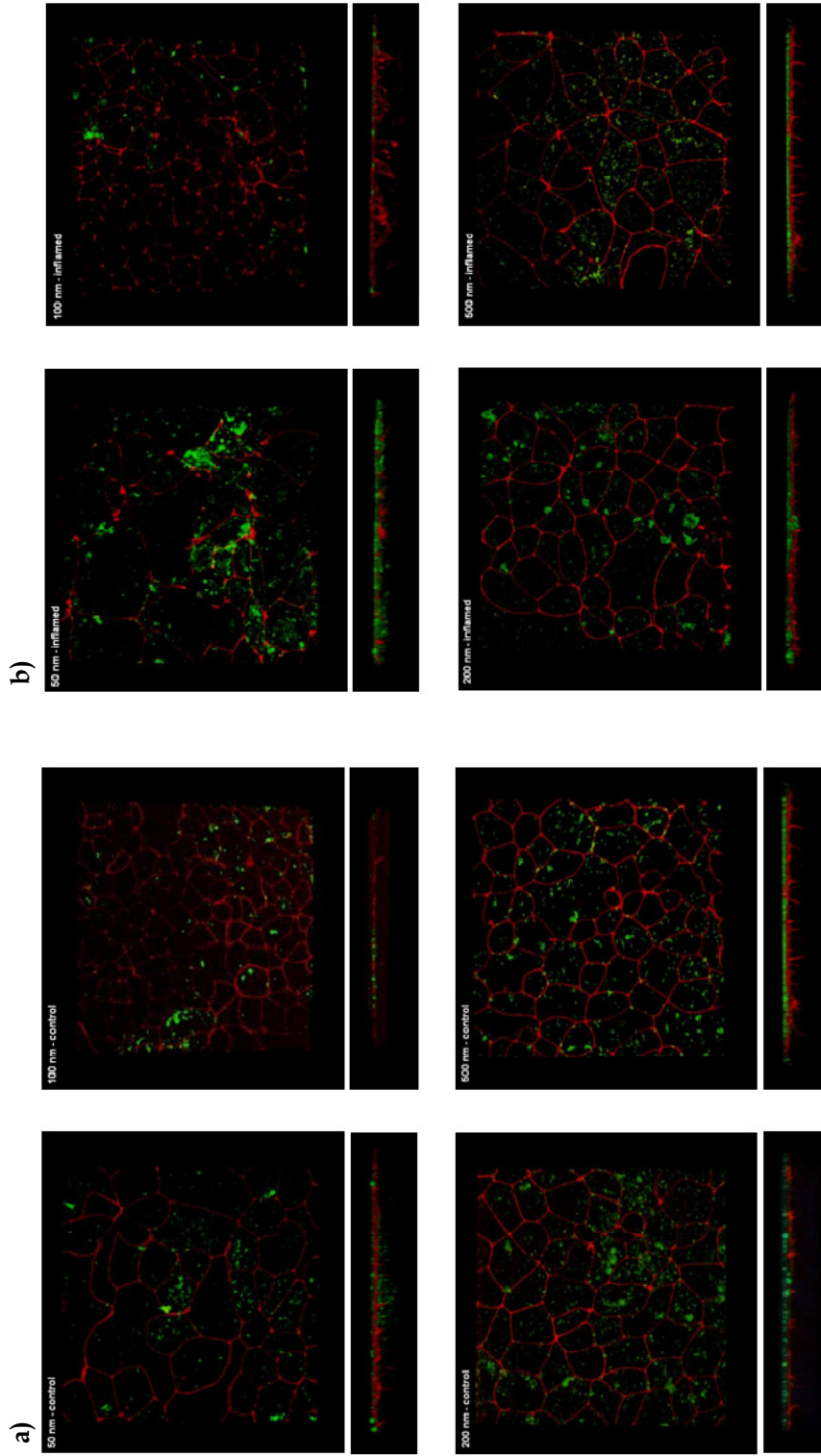


Figure 8. Disposition of 50 nm, 100 nm, 200 nm and 500 nm fluorescein-loaded polystyrene nanoparticles in control (a) and inflamed (b) Caco-2 cell monolayer. 3D images were reconstructed from z stack files with Velocity software and shown here in xy and yz-axis views.

2.4.7 Three dimensional co-culture of Caco-2 cells with dendritic cells and monocytes

As it is known for Caco-2 cells, monocultures form a tight monolayer when grown on a filter membrane, reaching a stable value of TEER after 21 days in culture (Fig. 11a.). In the presence of macrophages and dendritic cells, the time course of TEER was slightly delayed after seeding, but later increased similarly as for the Caco-2 single culture, also reaching the same plateau after 21 days.

Upon stimulation of the co-culture by adding IL-1 β to the apical compartment, TEER value of stimulated co-culture decreased to about 80% of the non-stimulated control values, similarly as previously observed with Caco-2 monoculture. There was no significant difference between the various combinations of the cells in co-culture (Fig. 11b).

After IL-1 β removal, the monolayer did not immediately recover from the inflammation as can be seen from figure 11c. TEER was stable after the inflammation, increased gradually and recovered after 7 days.

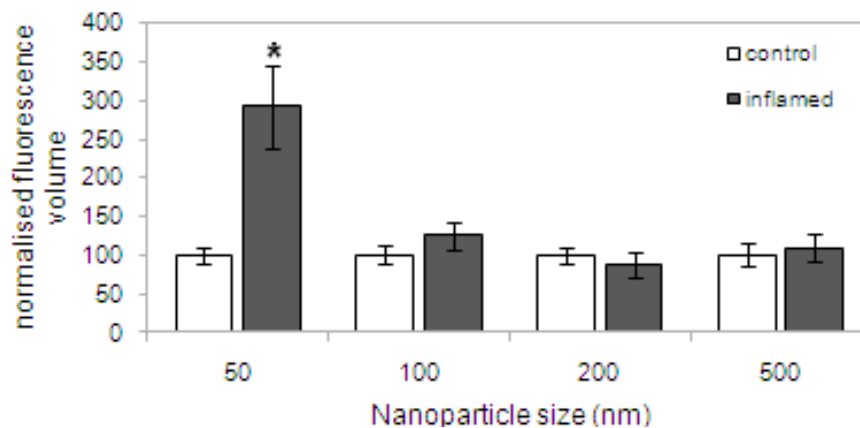
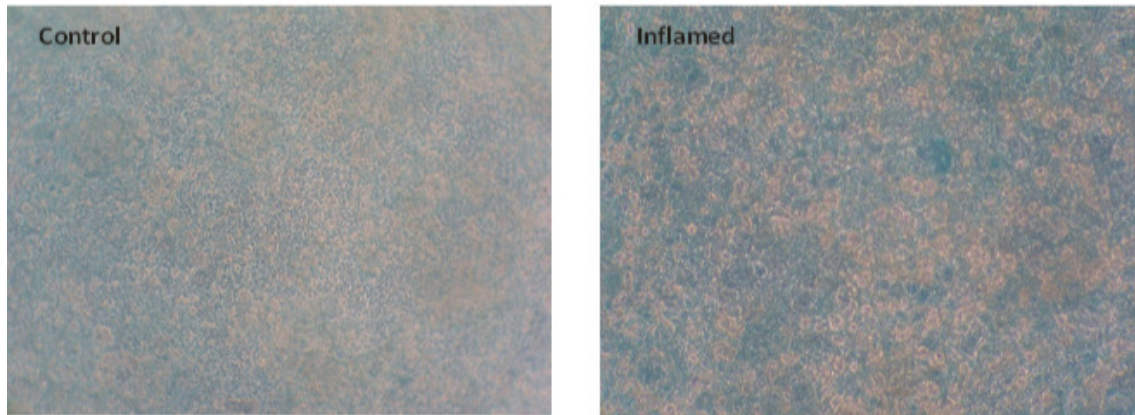


Figure 9. Quantification of adhered nanoparticles. Images of nanoparticles ranging in size from 50 to 500 nm adhered to Caco-2 cells were taken from random areas by CLSM and the images were analysed by pixel counter from ImageJ software (mean \pm SE, n=3, * indicates statistically significant differences compared to control, p<0.05).

a)



b)

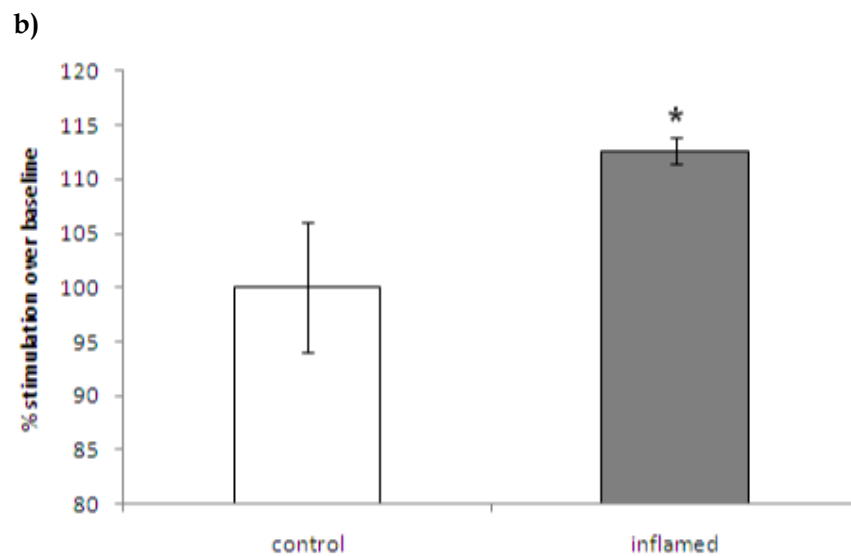


Figure 10. (a) Mucus layer in non-stimulated Caco-2 cells (left) and in cells stimulated with IL-1 β 10 ng/ml (right) all cultured on Transwell filter insert and dyed with Alcian blue. (b) Mucus quantification in Caco-2 cells with Periodic acid/Schiff stain colorimetric assay (mean \pm SE, n=3, * indicates statistically significant differences compared to control, p<0.05).

2.4.8 Release of IL-8 protein from the three-dimensional co-culture

IL-8 protein release into both the apical and basolateral compartment of the Transwell system was compared between the co-culture and similar single culture set-up of Caco-2 monolayer (Fig. 12). A marginal increase of IL-8 release in Caco-2 culture was obtained after

inflammation, both in apical and basolateral side. In contrast, co-culture seeded on Transwell filter insert released higher amount of IL-8 after stimulation with IL-1 β , reaching about 30-fold induction in the basolateral side. Interestingly, there were more IL-8 released to the basolateral side in a non-inflamed condition but significantly higher IL-8 amount was released to basolateral side in comparison to the apical side in inflamed condition. The effect of IL-1 β stimulation is found to be much stronger in co-culture compared to the single Caco-2 culture on Transwell filter.

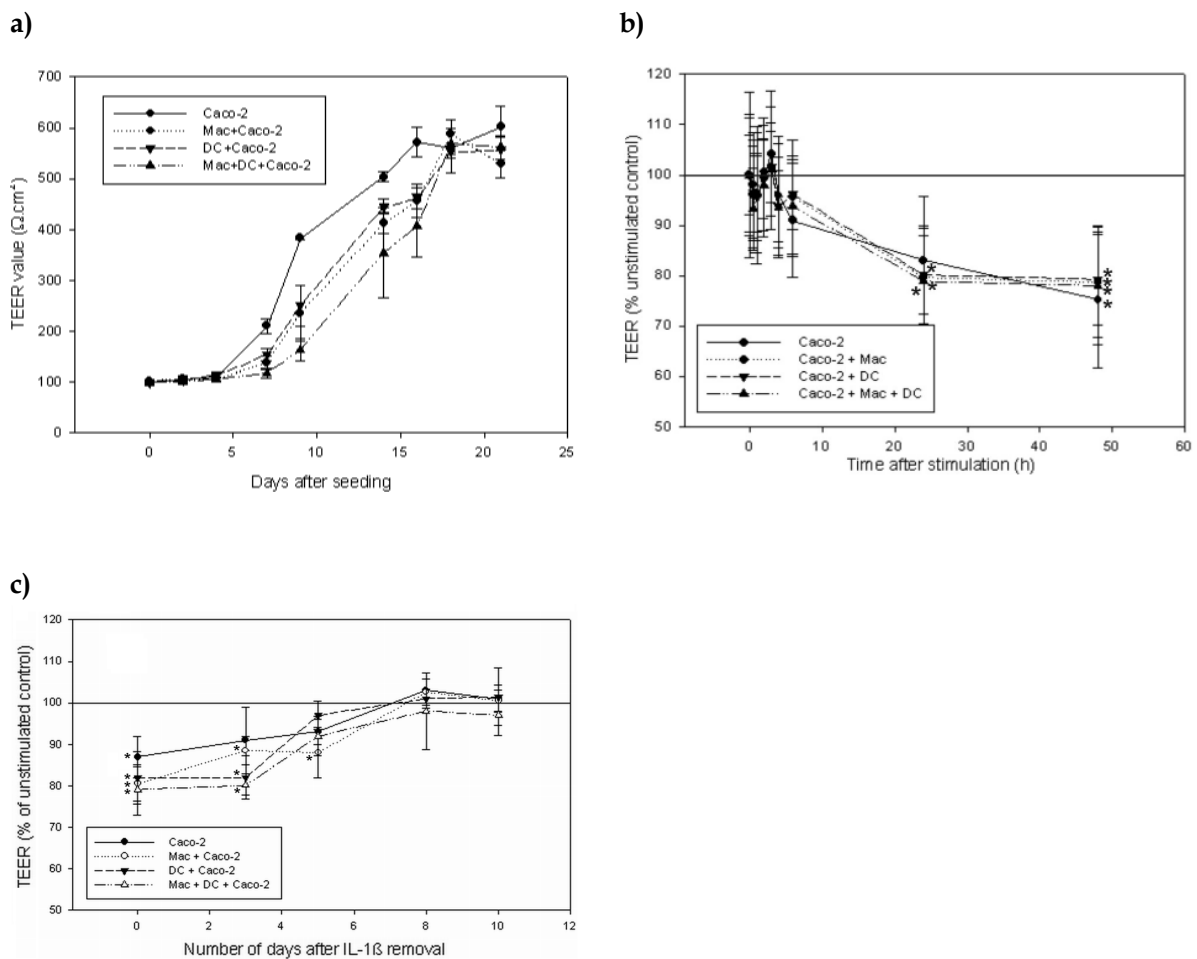


Figure 11. TEER development of Caco-2 cells in the presence of various combination of macrophages and dendritic cells (a), the influence of IL-1 β 10 ng/ml on the monolayer integrity (b), and recovery of TEER after removal of IL-1 β (c) (mean \pm SE, n=6, * indicates statistically significant differences compared to control, p<0.05).

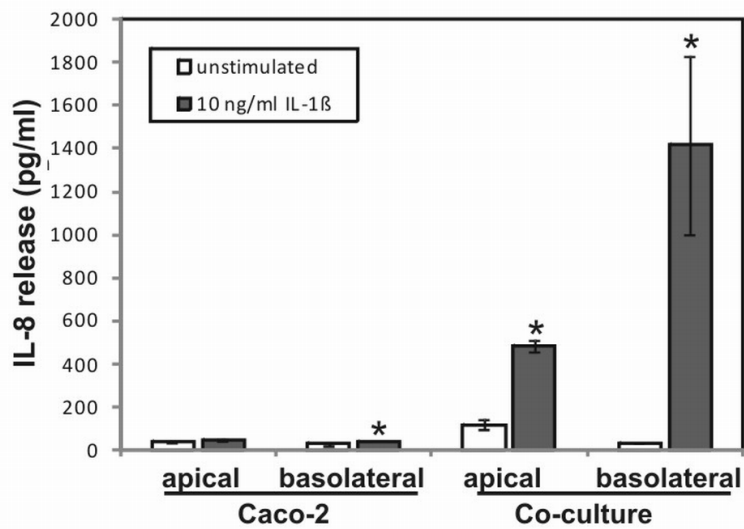


Figure 12. IL-8 protein release of Caco-2 cells in single culture or in co-culture with macrophages and dendritic cells cultivated in Transwell filter insert after stimulation of inflammation with IL-1 β 10ng/ml (mean \pm SE, n=3, * indicates statistically significant differences compared to control, p<0.05).

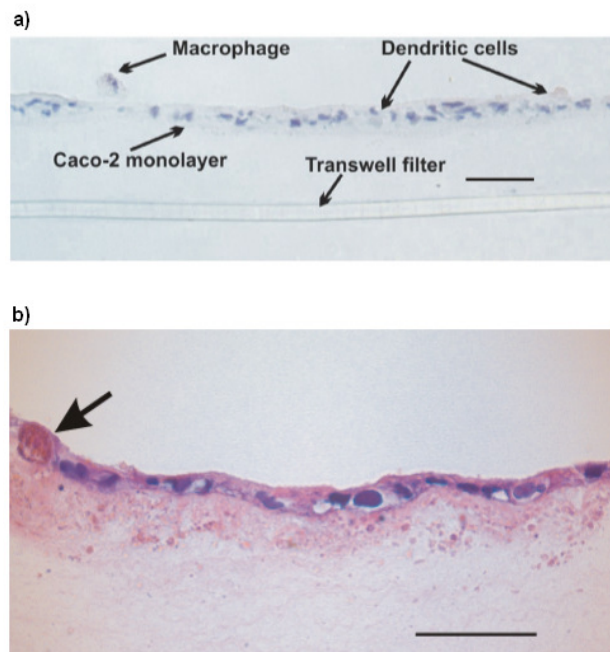


Figure 13. Histological image of the 3d triple co-culture with immune-competent cells and Caco-2 cells on Transwell filter inserts after hematoxylin staining (a) and with additional specific acid phosphatase staining for macrophages(b). The macrophage was pointed out with an arrow and scale bars indicate 100 μ m.

2.4.9 Optical image of three-dimensional co-culture by histological cut and CLSM

Light-microscopy of paraffin embedded sections of the triple co-culture showed an intact monolayer of Caco-2 cells on top of the collagen layer, as can be seen from their blue nucleus hematoxylin staining (Fig. 13a). The collagen contained macrophages and dendritic cells. As defined by acid phosphatase staining (immune cells colored red), immune-competent cells were also found to be integrated into the cell monolayer or on top of it. (Fig. 13b). Findings were confirmed in CLSM picture (Fig. 14), in which both immunocompetent cells, dendritic cells and macrophages, could only be detected from their auto fluorescence and not be distinguished. This observation is a hint for the vitality and mobility of the immune-competent cells which has been described to be able to migrate through the intestinal epithelium, reaching out for antigens present at the apical side, but still maintaining the overall tight junctional tightness and barrier function.

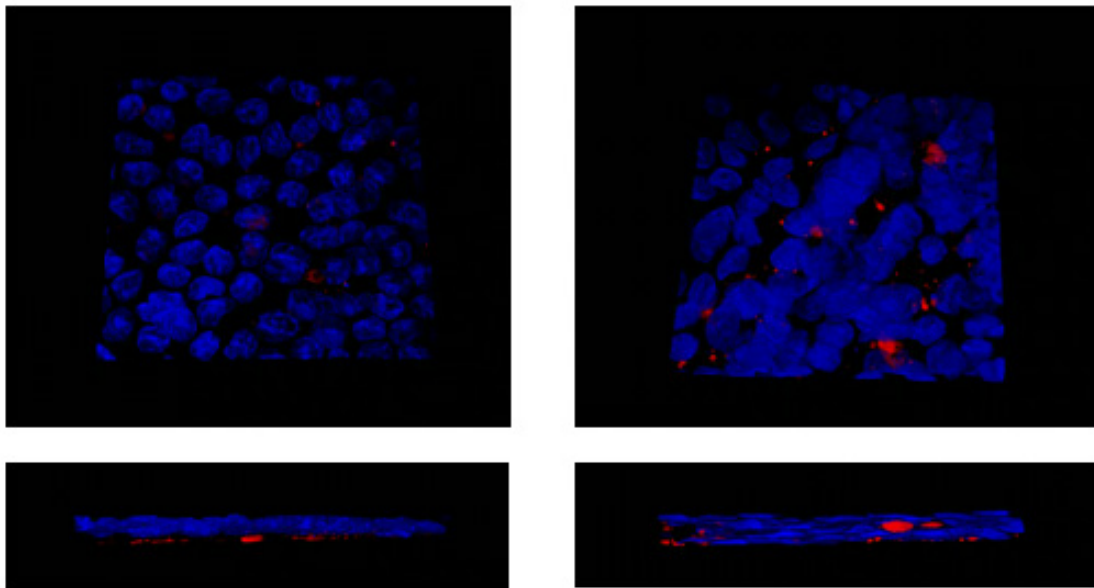


Figure 14. CLSM images of the 3D co-culture. Caco-2 cell nucleus was dyed with DAPI (blue) and the autofluorescence of the immune-competent cells (red) were used for their detection.

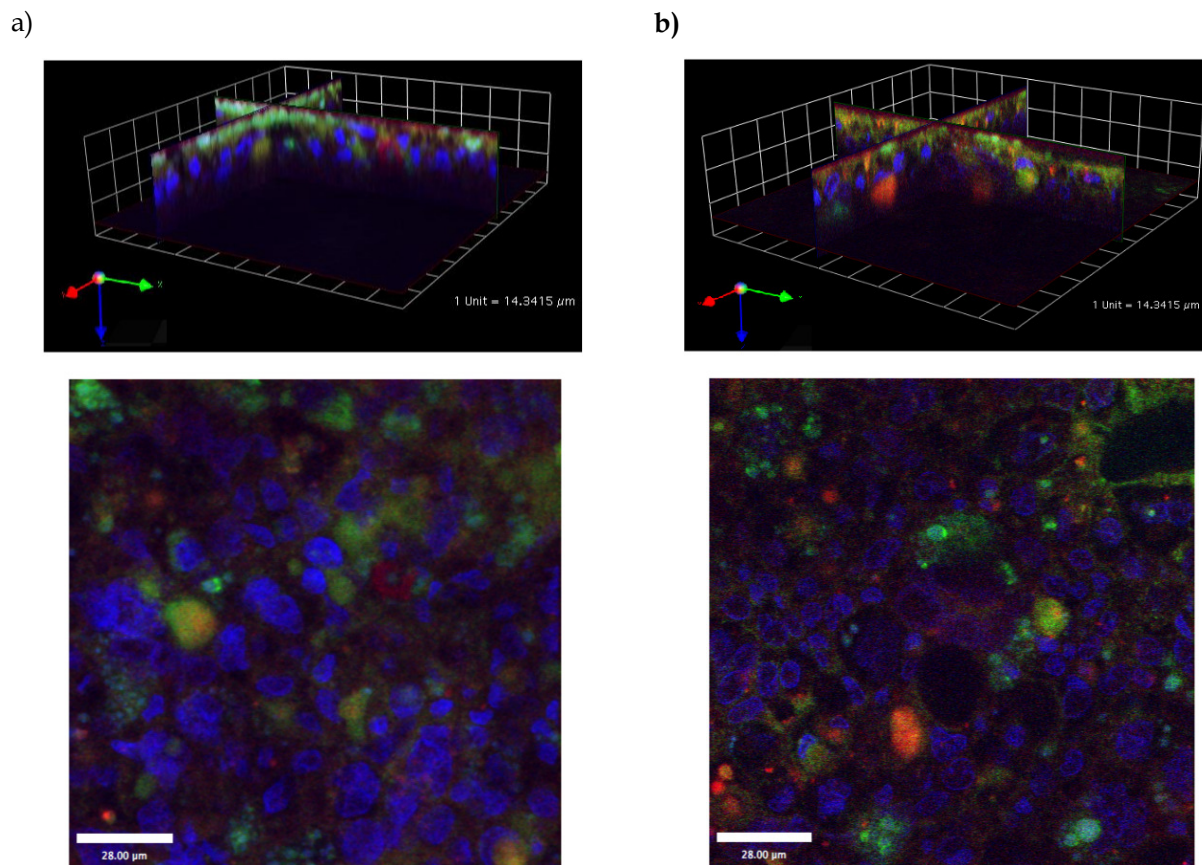


Figure 15. Confocal Laser Scanning Microscope image of a.) healthy and b.) inflamed intestinal mucosa model with 50 nm Fluoresbrite particles coupled with fluorescein (green) as model formulation. Nuclei were stained with DAPI dye (blue) while immunocompetent cells can be observed by their autoimmuno-fluorescence color (red). Uptake of nanoparticles by immunocompetent cells can be observed by colocalization signal in yellow. All images were captured in 630x magnification.

2.4.10 Disposition of polystyrene nanoparticle in the triple co-culture

Disposition of 50 nm polystyrene nanoparticles was investigated in the 3D co-culture stimulated with IL-1 β as well as in the non-stimulated control co-culture. In agreement with findings from the Caco-2 monoculture most of the nanoparticles adhered to the top of monolayer while some penetrated the Caco-2 cells (Fig. 15). However, also a strong uptake into the immunocompetent cells was observed. Uptake into immune-competent cells was

stronger in the inflamed model compared to the control as indicated by the stronger yellow co-localization signal of green nanoparticle fluorescence and red auto fluorescence of macrophages and dendritic cells. Furthermore, the immunocompetent cell population in non-stimulated control stayed mostly in basolateral side which represents the lamina propria side *in vivo*, while in the inflamed model there was an increased mobilization of immunocompetent cells to the apical side.

2.5 Discussion

The intestinal epithelium serves as essential cell barrier between the gut lumen and the lamina propria. It is known for its robustness against invasion of luminal bacteria which may be present at concentrations of more than 10^{14} CFU/ml. This barrier normally does not react to commensal bacteria, but activates the pro-inflammatory signaling pathway only in the presence of pathogenic bacteria. In IBD however, coupled with an increased permeability, the barrier fails to perform such initial recognition probably due to lack of defensin molecules, displaying no reaction before the bacteria invade the basolateral side [58]. The exact signaling processes however, still remain unclear.

Past *in vitro* studies of formulations targeting IBD have been conducted in conventional monoculture of cell lines. These cell lines represent the normal mucosa with intact tight junctions and strong barrier properties. However, such as test system does not reflect the pathophysiological changes happening in inflamed region of IBD. Moreover, a single cell line can never represent the complex interplay of different cell types during an inflammatory process.

Stimulation of inflammation in a single cell line model

One of the points to be taken into attention is that the loss of barrier in IBD is dependent on tight junctional intercellular permeability changes which is a function of cytokine production of immune cells instead of epithelial damage happening in tissue injury [59]. In the initial setting up of a more representative model of the intestinal barrier in the state of inflammation, we evaluated different intestinal epithelial cell lines (Caco-2, HT-29 and T84) in combination with several pro-inflammatory compounds (LPS from the commensal intestinal bacteria *Escherichia coli* and *Salmonella typhimurium* and the potent IL-1 β for

their ability to mimic the *in vivo* pathophysiology of the inflamed intestinal mucosa, i.e. the release of pro-inflammatory markers, structural re-organization of tight junction proteins and subsequent changes in barrier properties.

The problem in identifying a suitable cell line is that the most prominent epithelial cell lines are well known to be hyporesponsive to stimulation, which might be an advantage when the goal is to model an intact, non-inflamed intestinal mucosa. Several groups [60]^{8,19} found a general hyporesponsiveness of the polarized tight Caco-2 monolayer to various non-pathogenic bacteria except for increased level of human β -defensin-2 [61]. They also reported that stimulation of Caco-2 with IL-1 β or TNF- α from basolateral side induced strong increase of IL-8 and TNF- α but found no statistical significance [61]. This was confirmed in part in our experiments: as shown by real time PCR, HT-29 and T84 were unaffected by LPS stimulation and showed no increase in IL-8 and TNF- α expression. Only Caco-2 cells could be stimulated by LPS and were therefore chosen as the enterocyte cell line for all future experiments.

Inducing an inflammation, LPS acts via extracellular toll like receptor 4 (TLR4) and subsequent signaling cascades which activate the ubiquitination of I κ B leading to the translocation of NF- κ B into the nucleus and activation of the inflammation process [62]. Some of the molecules downstream of this inflammation signaling process are pro-inflammatory cytokines such as TNF- α and IL-8, which can be therefore used as markers to quantify the inflammatory reaction. TLR4 has been found in low level in healthy intestine but highly upregulated in IBD and has also been shown to be expressed in epithelial cells. Stimulation with LPS from both *E. coli* and *S. typhimurium* was sufficient to increase the IL-8 and TNF- α mRNA production in Caco-2 cells in our experiments in a time and concentration dependent manner, with highest mRNA levels being detected as early as 2h

after stimulation. LPS stimulation of inflammation in Caco-2 cells has already been observed in previous studies [63], although Abreu et al attributed the pro-inflammatory effect to a contamination of lipoprotein in the purified LPS and an activation of TLR2 [64]. A contrasting report showed a hyporesponsiveness of Caco-2 cells to LPS [65] which was ascribed to a lack of MD2 expression, a partner molecule for TLR4 in the signaling complex.

The up-regulation of IL-8 and TNF- α mRNA expression after stimulation with LPS in our experiments, was not reflected at the protein level and in TEER change. It seems that the weak pro-inflammatory stimulus by LPS is counterbalanced by the simultaneous activation of anti-inflammatory processes. This is not unexpected, as *Salmonella typhimurium* and *Escherichia coli* themselves have been described as nonpathogenic microbiotas with attenuated inflammatory response from epithelial cells. Instead the TLR recognition signal even helps the epithelium by protecting it from non-specific damages [66]. *In vivo*, additional various immune cells are present on the lamina propria side of epithelium and regulate the immunity towards external stimuli by secreting pro-inflammatory cytokines.

As LPS stimulation was not effective enough, a number of cytokines were evaluated as alternative inductors of inflammation. The potent cytokine IL-1 β had a strong effect, stimulating a 10-fold higher IL-8 release both at mRNA and protein level using only 1/10 of the concentration compared to LPS. The up-regulation of IL-8 mRNA production after IL-1 β stimulation was not as fast as after LPS stimulation peaking after 4 h instead of 2 h. While LPS is being recognized by TLR-4, IL-1 β is recognized by other receptor IL-1R on the cell surface which may give a delay in recognizing and the response in the subsequent downstream signaling pathway. Although both receptors are classified in one super family [67] and were suggested to share a common pathway in activation of inflammation, a

specific MyD88-independent pathway may exist for the LPS signaling cascade which leads to a difference in downstream signaling pathways [68],[69].

Interestingly, double stimulation of both IL-1 β and LPS from *S. typhimurium* showed a similar level of mRNA up-regulation as the single stimulation with IL-1 β , but showed a progression curve comparable to stimulation with LPS reaching its maximum after 2 hours and normalizing after 4 hours. This indicates a process where LPS may initialize the stimulation and increase the susceptibility of the signaling pathway for IL-1 β without actually increasing the signaling pathway activity. Similar to the effect on mRNA expression, double stimulation of the cells with IL-1 β and *S.typhimurium* LPS did not further increase the IL-8 production, which hints at a saturation effect of the inflammation machinery in Caco-2 cells. IL-1 β has been singled out to affect the pro-inflammatory cytokines excretion in Caco-2 cells predominantly compared to other factors [70], as a factor with wide-range of inflammatory activities [71] and markedly upregulated in IBD [72]. It has been hypothesized being one of the prominent pathogenic factor in IBD beside other genes such as IL-18 [73] and CD14 [74] due to the fact that the severity and the course of the inflammation was correlated to high occurrence rate of IL-1 β gene polymorphism in CD patients [75].

In contrast to LPS, IL-1 β was also proficient enough to decrease tight junction integrity and epithelial barrier function as seen in a drop of TEER values to about 80% of the non-stimulated control and transport data for the paracellular transported dye fluorescein sodium. A double stimulation by LPS and IL-1 β did not further increase the permeability than the stimulation with IL-1 β alone. This result is in line with the data on IL-8 production which also indicate saturation in the inflammatory signaling.

The activation of inflammation process through NF- κ B pathway has been shown to increase the tight junction permeability on those cells through phosphorylation of myosin L chain kinase (MLCK) which induces a contraction in actin-myosin filaments [76], a process that is thought to be central for loss of barrier function in inflammatory bowel disease [77]. Tight junction protein ZO-1 and adherens junction protein E-cadherin are directly coupled to the actin filaments and thus re-organize as a result of the contraction. This change in ZO-1 structure was visible in our immunofluorescent staining of the protein.: Looking at distribution of ZO-1 protein in stimulated Caco-2 cells, the tight junctional protein was still detectable but seemed to be thinner with the strands reaching down to the basolateral side of the monolayer. A similar observation has been reported by Clayburgh et al³⁸, which have shown a rearrangement of ZO1 to the tricellular junction. In contrast the organization of other tight junctions proteins such as Occludin and Claudin-1 not directly connected to the actin skeleton was unchanged in IL-1 β treated Caco-2 cells compared to non-stimulated cells. Overall expression of tight junction proteins including ZO-1 was unchanged as indicated by real time PCR results (data not shown). The structural change in the tight junctions serves as an explanation of the statistically significant but rather modest drop in TEER of 20-25%, Instead of a complete loss of tight junctional integrity and destruction of the intercellular contacts, the tight junctions simply become more leaky enabling easy and fast invasion of monocytes between the cell monolayer and to the apical side.

Studies with other pro-inflammatory compounds, such as IL-8, TNF- α alone or in combination with IFN- γ did not yield a decrease of TEER (data not shown). This is in contrast to previous reports on Caco-2 cells which showed a decrease of TEER value after stimulation with TNF- α [78] or in combination with IFN- γ [79]. The first study reported the drop of TEER value after 48 hours period stimulation with TNF- α to almost 40% reduction

while the second publication shows the drop only after stimulation of the cells with TNF in combination with IFN- γ , which in turn induced TNFR2 up-regulation and mediated the TNF-induced MLCK-dependent barrier dysfunction. It has not been clear if possibly different clones of Caco-2 cells have been utilized in both studies; however in this report we were using the C2Bbe1 Caco-2 clone which may have responded differently than the parental Caco-2 cells.

Increased monolayer permeability in state of inflammation was observed also in an increased level of transport of paracellular transported dye fluorescein sodium. In cells exposed to the highest tested concentration of 500ng/ml IL-1 β , the apical to basolateral transport was increased to about 15% while the basolateral to apical transport was significantly increased to 85%, each compared to the unstimulated control (Fig. 6).

The translocation of polystyrene model nanoparticles through cell monolayer was found not to be affected by the pathophysiological changes. Smaller nanoparticles ~50 nm size were taken up by the cells, while bigger nanoparticles (>200nm) only adhered to the cell surface but were not transported to the basolateral side. There were no observable differences in uptake or translocation between stimulated and unstimulated cells. However there seemed to be an increase in number of particles adhering to the inflamed tissue. This observation was further verified by the nanoparticle quantification using ImageJ calculation software. Significantly more 50 nm nanoparticles adhered to inflamed monolayer compared to the non-stimulated control. The distribution pattern of the particles in the confocal pictures hints at an association of particles to mucus patches on the cell monolayer. The mucoadhesive interaction of nanoparticles has been described in previous publications as depending on the structure of polymeric chain surface and its hydrophilicity [80]. However, the report did not observe dependence on particle size and molecular weight of molecules on the particle

surface. In contrast, our observations showed size dependence in transit rate of nanoparticles. Smaller particles may adhere to the mucus easier than bigger aggregates and therefore increase their transit rate in the intestinal tissue.

We quantified mucus production in stimulated and non-stimulated Caco-2 cells using alcian blue staining and mucin quantification by periodic acid/ Schiff reagent. Indeed mucus production in IL-1 β stimulated Caco-2 cells was statistically significantly increased, which is in line with reports on CD patients in which hypertrophy of goblet cells [46], leading to increased mucus formation was observed. Furthermore, IL-1 β has also been shown to cause a rapid increase of mucin in HT-29-CL.16E cells, reaching 200% higher amount of mucin. However, this was observed in HT-29 cell line, which is a model for goblet cells and Caco-2 cell as an enterocyte model is known to only produce very small amount mucus under normal condition. Our finding shows that even with low amount of mucus, its production is also affected after stimulation by pro-inflammatory cytokine IL-1 β in Caco-2 cells although to a lesser degree compared to the goblet cells.

Stimulation of inflammation in a co-culture model

Although we could stimulate an inflammatory reaction in Caco-2 cells which was accompanied by changes in the epithelial barrier properties and increased mucus production, the monoculture is not able to mimic the recognition of antigens by the intestinal innate immune system and the following interplay of cells. Therefore, a co-culture model was established which also contains dendritic cells and macrophages as the immunocompetent cells of the intestinal barrier.

Previously, different 3-dimensional *in vitro* models have been utilized to study healthy intestinal systems, mostly using various co-cultures of intestinal epithelial cells and

immune-competent cells. des Rieux et al [14] combined Caco-2 and Raji B cells to induce M-cell development. They found that Raji cells in co-culture with Caco-2 cells could drive their differentiation into M-cells, which are able to take up polystyrene nanoparticles >200nm by non-specific endocytosis. As a consequence, nanoparticle transport in this model was 50-fold higher in comparison to the monoculture. Other researchers have been working with various combinations of epithelial cells and either primary or macrophages cell lines, with some groups using fibroblast cells as feeder support. In most cases, the models were assembled on a polycarbonate filter inserts as they allow the mimicking of compartmental separation between lumen and lamina propria. Co-cultivation of HT-29 epithelial cell line with PBMC monocytes and primary intestinal fibroblasts led to aggregation of fibroblasts in the co-culture and phenotype change of the macrophages towards intestinal macrophages [15]. The intestinal epithelial cells co-cultured with PBMC-derived DC released exosomes that are capable to bind human serum albumin and interact preferentially with DCs [16]. Other co-culture studies with Caco-2 cells and activated monocyte cell line THP-1 showed apoptotic and necrotic effect to the Caco-2 cells besides damaging monolayer integrity. A similar model has also been established to construct the respiratory tract using epithelial cells and immunocompetent cells to study the particles distribution [23] and the 1 μm particles were found to be taken up into all three cell types used.

For specific inflammatory bowel disease model there has been a few approaches using primary blood cells from IBD patients and Caco-2 or primary colonic crypts cells. This model has shown that cells from IBD patients produced more IFN- γ than the healthy model but did not give any pathophysiological relevance because although cells were cultured together, they are not cultured to assembly the physiological arrangement in the intestine [81]. Besides, primary cell isolation is known to be arduous and problematic because of cells

origin from different individuals with various degrees of inflammation. Therefore, we propose this new model which consists of the relevant cells for the inflammation and antigen presenting signaling, allows controlled stimulation, and mimics major pathophysiological changes occurring in IBD

For our setup, the immunocompetent cells obtained from periphery blood mononuclear cells were analysed by FACS and macrophages and dendritic cells expressed CD14+/CD1a- and CD14-/CD1a+ respectively (data not shown). As macrophages and dendritic cells were to be co-cultured with Caco-2 cells, we also tested the pre-conditioning of these cells with medium from Caco-2 cultivation. Pre-conditioned macrophages showed a loss of CD14 expression (data not shown), in agreement with their differentiation into intestinal macrophage like state. A previous study showed that co-culturing macrophages with intestinal epithelial cell line HT-29 also drove the differentiation of the blood derived macrophages towards the phenotype of intestinal macrophages [15] and intestinal macrophages have been characterized as non-reactive with down-regulated expression of CD14, CD16 or CD80 [82].

Dendritic cells cultivated with Caco-2 secretion medium showed an increased CD1a expression (data not shown), which in turn showed a differentiation shift toward Th1 cells which are more responsive to stimulation from their environment and are responsible for antigen probing from the lumen and M-cells *in vivo* [15, 83-85]. DCs in IBD patients are also characterized by an upregulation of CD1a [86]. We therefore conclude that the co-cultivation of dendritic cells and macrophages together with the epithelial cells for three weeks is not only necessary for the monolayer formation in the co-culture model, but also allows the pre-conditioning which drives the differentiation of these cells towards a more intestine-like characteristic .

The co-culture itself showed the expected arrangement with Caco-2 building the monolayer on top of the culture while macrophages and dendritic cells were embedded in the collagen layer beneath the monolayer, though this condition seemed to be not static as in various areas we find immunocompetent cells mostly to be located directly under the epithelial layer and even reaching out to the apical side of the model (Fig. 13a). Some studies had reported the finding that antigen delivery across the intestinal barrier may either be conducted by specialized M-cells [87] or by direct probing by DCs from the lamina propria [88]. The mobility of immunocompetent cells in our model supports the latter theory and showed the viability of the immunocompetent cells in the co-culture. Caco-2 showed a similar development of tight junction in the presence of macrophages and dendritic cells as compared to the single cell culture. TEER reached a plateau after 20-21 days in culture at 600 -800 $\Omega \cdot \text{cm}^2$ and dropped to 80% compared to the non-stimulated control, in agreement with findings from the stimulated monoculture.

In contrast, IL-8 protein release into the medium in response to the pro-inflammatory cytokine IL-1 β was significantly higher in the co-culture in comparison to the Caco-2 monolayer model particularly to the basolateral compartment. Cytokine release in co-culture has been investigated by several groups previously, Haller et al. showed increased cytokine (TNF- α and IL-1 β) release in of co-culture of Caco-2 und PBMC also stimulated with IL-1 β [22]. Addition of PBMCs from healthy donors was shown to trigger the susceptibility of epithelial cells to non-pathogenic E. coli bacterial challenge [89], possibly by nitric oxid release that inhibit the gap junction of the enterocytes [14]. However, in these setups freshly isolated PBMCs were cultured with Caco-2 cells for one day before stimulation and the experiments were aimed to study the pathogenesis and the mechanistic undergoings after bacterial challenge in the inflamed intestine. Our setup is different in the objectives, cell

composition and structure, as our main aim is to mimic the pathophysiological changes and use the model for drug and drug formulation testing. We cultured macrophages and dendritic cells together with Caco-2 cells for 21 days to generate a tissue-like architecture with tight monolayer and active immune cells compartment which emulate the intestinal barrier.

The increased pro-inflammatory activity in the co-culture model is also reflected in the activity of the immunocompetent cells themselves. After stimulation with IL-1 β , we observed more immunocompetent cells mobilized to the apical side in inflamed model in comparison to healthy model. In particular, an increase in red signal at the surface of the Caco-2 monolayer is observed which might be ascribed to dendrites extending to the apical side of the monolayer or an increased invasion of immune cells.

Furthermore, these stimulated immune cells were highly active in sampling nanoparticles. Comparing nanoparticle disposition in the stimulated co-culture vs. the non-stimulated control, an increase in yellow signal, i.e. co-localization of red signal from the immune cells and green signal from the nanoparticles can be detected. In contrast, particle disposition in the non-inflamed control is dominated by particle endocytosis into the epithelial cells as indicated by the predominant green signal in the region of the epithelial nuclei.

Looking at the confocal images, we can identify two different populations of immunocompetent cells, one which embraced the particles and another population which tended to take less particles up. As both macrophages and dendritic cells were imaged using their auto fluorescence, we could not distinguish between them. Several attempts have been conducted to stain the immunocompetent cells with specific antibodies for their recognition. This approach has been unsuccessful so far since the immunocompetent cells in the co-

culture had undergone a differentiation and lost some of their markers, as discussed above. However, seen from their characteristic behavior, we assume that dendritic cells are more likely to take the particle up from the apical side. The particles may later be transferred to macrophages and be digested, or further processed to the T-cells.

This preferential uptake of nanoparticles by immunocompetent cells in the inflamed setup is in contrast to our observations in the stimulated Caco-2 single cell culture where polystyrene nanoparticles of the same size (50 nm) accumulated only in the intestinal epithelial cells and were internalized to a lesser degree. Thus studying particle interaction with the inflamed intestinal barrier in a single cell model would lead to potentially both underestimating as well as misjudging particle disposition.

In conclusion, this three-dimensional cell culture model will be an efficient tool for narrowing the gap between conventional cell culture system and animal testing, providing a pathophysiological relevance of inflamed tissue, while maintaining the convenience of cell culture.

3. Screening of budesonide nanoformulations for treatment of inflammatory bowel disease in an inflamed 3D cell-culture model

Parts of this chapter have been published in:

Fransisca Leonard, Hussain Ali, Eva-Maria Collnot, Bart J. Crielaard, Twan Lammers, Gert Storm, Claus-Michael Lehr. ALTEX. 2012;29(3):275-85.

3.1 Abstract

Drug formulation screenings for treatment of inflammatory bowel disease (IBD) are mostly conducted in chemically induced rodent models that represent the acute injury-caused inflammation instead of chronic condition. To accurately screen drug formulations for chronic IBD, there is an urgent need for a relevant model that mimics the chronic condition *in vitro*. In order to reduce and potentially replace this scientifically and ethically questionable animal testing for IBD drugs, our laboratory has developed an *in vitro* model for the inflamed intestinal mucosa observed in chronic IBD, which allows high-throughput screening of anti-inflammatory drugs and their formulations. The *in vitro* model consists of intestinal epithelial cells, human blood-derived macrophages and dendritic cells that are stimulated to inflammation via IL-1 β . In this study, the model was utilized for evaluation of the efficacy and deposition of budesonide, an anti-inflammatory drug, in three different pharmaceutical formulations: (1) a free drug solution, (2) encapsulated into PLGA nanoparticles, and (3) encapsulated into liposomes. The *in vitro* model of the inflamed intestinal mucosa demonstrated its ability to differentiate therapeutic efficacy among the formulations, while maintaining the convenience of conventional *in vitro* studies and adequately representing the complex pathophysiological changes *in vivo*.

3.2 Introduction

Inflammatory bowel diseases (IBD), encompassing among ulcerative colitis (UC) and Crohn's disease (CD), are a group of chronic, remitting inflammatory diseases affecting the gastrointestinal tract. Combination of genetic predisposition and environmental factors are the main causes to a de-regulated immune system resulting in aberrant mucosal inflammation [90]. Due to the impaired integrity of the epithelial barrier, both UC and CD are characterized by increased luminal antigen uptake [91, 92]. As an incurable disease, current therapies are directed towards induction of remission during acute episodes and prevention of relapses [93]. Treatment depends on the site of disease and its severity. While UC is restricted to the colon and rectum, CD is discontinuous and can affect any part of the gastro-intestinal tract. Common anti-inflammatory approaches include 5-aminosalicylates, antibiotics, corticosteroids, immunosuppressants, anti-TNF antibodies and other biological agents, such as cytokines [94-96]. These therapies are very promising but expensive. The standard treatment for moderate to mild cases consists of budesonide at a daily dose of 9 mg [97]. Although associated with less adverse effects compared to other corticosteroids, budesonide has demonstrated higher adverse effect compared to the placebo due to extensive first pass metabolism and low systemic bioavailability [98]. These adverse effects can be reduced by selectively delivering budesonide to its site of action.

The route of delivery for budesonide may be rectal, oral, or in some cases, intravenous. Rectal formulations are very effective for treatment in distal colonic areas and thus are mainly used in UC. For oral delivery, the drug compound has to resist or be protected from the acidic pH of the stomach and the metabolizing enzymes of the intestinal flora. Thus, orally applied anti-inflammatories, such as budesonide, tend to be administered at higher doses, increasing the risk of systemic adverse effects. Many drug delivery strategies have

been tried to circumvent this problem, e.g. pro-drugs, which are only activated in distal intestinal areas, and coated pellets or capsules. These approaches, however, show limited bioavailability at the sites of inflammation mainly due to rapid elimination as a result of diarrhea, which is a common symptom in IBD. Furthermore, budesonide is a hydrophobic compound and highly insoluble, demonstrating low local bioavailability.

A promising approach to increase the bioavailability and enhance the retention time of budesonide at the target site is via bioadhesion is through the use of nano-sized carriers. Nanocarriers can avoid the diarrhea symptom and passively accumulate in the inflamed intestinal tissue [99]. Although the exact mechanism of accumulation is not fully understood, similarities to the enhanced permeability and retention phenomenon observed in cancerous tissues are assumed. Additionally, nanocarriers can be taken up by intestinal macrophages and dendritic cells. Then, the encapsulated drugs are released upon the degradation of the nanocarrier in the desired areas [100]. This passive targeting to the inflamed intestinal tissue using nanocarriers was successfully applied with different kinds of drugs (e.g. tacrolimus, rolipram and 5-ASA) and different nanocarrier technologies by showing increased therapeutic efficacy and reduced adverse effects compared to free drug molecules [96, 97, 101]. Formulation development and testing in these studies was conducted in different rodent models of colitis based on the chemical induction of an acute inflammation by dextran sodium sulfate (DSS) or tri-nitrobenzene sulfonic acid (TNBS). [99, 102].

Although the DSS and TNBS rodent models are accounted to be the most widely used animal model for IBD, these models display several major disadvantages. Besides the obvious ethical issues, species differences and the methods of stimulation have lead to overestimated or false results: Chemically induced models focus on the damage to the

epithelial barrier and the subsequent immune reaction, but fail to take into account the dysregulation of the innate or adaptive immune system. [103] The dysregulation of the immune system can affect both the response of certain drugs and the interaction with nano- or microcarriers. In addition, the genetic background of the animals can influence the pathogenesis. TNBS colitis in BALB/c mice presented a more Th2 type response while a Th1 response was observed in SJL mice [104]. Thus, these models lack responsiveness to IBD drugs, such as corticosteroids and 5-ASA, and are not suitable to study the respective anti-inflammatory formulations [54].

Disease relevant *in vitro* cell culture models based on human tissues may present a promising alternative for drug formulation testing as they allow for higher throughput, reduction of animal testing, and may provide insight into mechanisms of action, uptake and deposition. Such an *in vitro* model of the intestinal mucosa in the state of inflammation was previously established in our lab. The three dimensional model is based on the co-culture of intestinal epithelial Caco-2 cells with primary, blood derived macrophages and dendritic cells as components of the intestinal innate immune system [105]. All cells in the model are of human origin, eliminating issues with species differences often associated with the different animal models. During 21 days of co-culture to allow tight barrier formation, immune cells assume an intestinal phenotype [15]. The incorporation of immunocompetent cells is crucial for the inflammation stimulation. They significantly enhance the inflammatory response after induction by cytokine IL-1 β addition, quantified via markers of inflammation such as increased IL-8 or TNF- α expression. As previously shown, the stimulated model reflects the pathophysiological changes observed at the intestinal barrier in IBD patients such as re-organization of tight junctions, reduced barrier properties, increase immune cell activity, release of pro-inflammatory markers and increased mucus

production, providing several parameters to monitor disease status and therapeutic activity of novel anti-inflammatory compounds and formulations.

In this study, two different nanocarriers were evaluated using the established *in vitro* model for their efficacy in inflammation treatment. One nanocarrier was generated from PLGA, an FDA approved polymer material. PLGA has been widely investigated as a scaffold for tissue regeneration and as a drug delivery vehicle in the form of implants and nano- or microsized carriers. It is prominently featured for the oral delivery route due to its biodegradability, biocompatibility, and its ability to accommodate a wide range of compounds. Although the hydrophobic nature of PLGA benefits small hydrophobic compounds, the carrier has demonstrated to be versatile by loading biomacromolecules, such as insulin, peptides, antigens, and nucleic acids [106]. Thus PLGA nanoparticles can improve oral bioavailability of poorly soluble and permeable drugs by increased translocation and transcytosis and target compounds to their site of action in the gastrointestinal tract for IBDs and potentially for colorectal tumors [107].

In contrast to the popularity of PLGA nanoparticles, there are only few studies that exploit liposomes for oral drug delivery applications. Instead, liposomes are commonly applied intravenously for a variety of treatments from antibiotics to vaccinations [108] and tumor therapies [109]. Typically, PEGylated stealth formulations are employed for liposomes, reducing recognition by the reticuloendothelial system and affording prolonged circulation time in blood. The prolonged circulation half-life together with high flexibility allows liposomes with sizes 100-200 nm to extravasate through the leaky vasculature in tumors and inflamed organs and thus passively target their site of action [109, 110]. The comparable passive targeting principle for malfunctioning endothelium and epithelium has not been extensively explored yet for liposomes in IBD treatment. Few groups have tried to approach

the inflamed intestinal mucosa via the endothelium “backside” after intravenous delivery [111, 112]. Due to rapid degradation in the harsh gastric environment, liposomes are rarely applied via the luminal side of the intestine, and so far, the Rubinstein lab has addressed the approach for IBD therapy after rectal application [113, 114].

With the current aims (1) to rationally develop novel nanomedicines for oral and rectal IBD treatment, (2) to better understand the mechanism of nanocarrier interaction with the inflamed barrier and (3) to evaluate the power of the *in vitro* model to differentiate between different treatments, we studied two different types of drug delivery vehicles (polymeric PLGA nanoparticles and liposomes) for glucocorticoid budesonide, comparing their anti-inflammatory activity and ability to recover epithelial barrier function in the novel 3D cell culture model of the inflamed intestinal mucosa. Budesonide loaded nanoformulations were prepared, characterized and applied to the *in vitro* model, using the free drug solution and blank nanocarriers as controls. IL-8 release was measured for inflammation monitoring. Transepithelial electrical resistance was monitored to observe recovery in epithelial barrier function. Furthermore, particle deposition was studied using confocal laser scanning microscopy.

3.3 Materials and methods

3.3.1 Materials

Poly(L-lactide-co-glycolide) (PLGA) (Resomer RG 503 H; inherent viscosity 0.31 dl/g) was bought from Boehringer Ingelheim (Ingelheim, Germany). Budesonide was also gifted kindly from Boehringer Ingelheim. Polyvinylalcohol Mowiol 4-88 (PVA) was purchased from Kuraray (Frankfurt am Main, Germany). Human colon adenocarcinoma cell line Caco-2 clone C2Bbe1 was obtained from American Type Culture Collection (Rockville, MD, USA). Dulbecco's modified Eagle's medium (DMEM), Fetal calf serum and non-essential amino acids were purchased from PAA (Pasching, Austria). Trypsin/EDTA was obtained from Lonza (Basel, Switzerland). Polycarbonate Transwell inserts with pore size 0.4 μm were purchased from Corning Incorporated (Acton, MA, USA). GM-CSF and IL-4 were obtained from R&D Systems (Minneapolis, USA) and IL-1 β from Promokine (Heidelberg, Germany). Ficoll Paque plus for PBMC isolation was obtained from GE Healthcare (Uppsala, Sweden) and human serum from Invitrogen (Wisconsin, USA). CBA human IL-8 Flex Set was purchased from BD Biosciences (Heidelberg, Germany). Purecol collagen was obtained from Advanced Biomatrix (Tucson, AZ, USA). 5-Fluoresceinamin (FA) and 1-ethyl-3-(3-Dimethylaminopropyl)-carbodiimide hydrochloride and all other chemicals were obtained from Sigma (St. Louis, MO, USA). All chemicals used in this study were of highest analytical grade.

3.3.2 Fabrication and characterization of budesonide loaded PLGA nanoparticles

Fluoresceinamine labeling of PLGA (FA-PLGA) was conducted as described previously [115]. From this modified polymer budesonide loaded FA-PLGA nanoparticles were

prepared using emulsion solvent evaporation method [116, 117]. Briefly, 45 mg of budesonide base was dissolved at room temperature in 15 ml of ethylacetate containing 300 mg of FA-PLGA. This organic phase was thereafter added via a gear pump (Gilson Minipuls, France) to an aqueous 2 % PVA solution under stirring. The emulsion was stirred for 2 hours at room temperature before homogenizing at 13,500 rpm for 10 minutes using an Ultra Turrax T-25 (Janke and Kunkle GmbH KG, Staufen, Germany). To this, emulsion water was added drop wise under stirring to a total volume of 80 ml. The organic solvent was evaporated overnight at room temperature and precipitated nanoparticles with encapsulated drug were then separated from free budesonide by tangential flow filtration using a Vivaflow 50 cassette (Sartorius, Goettingen, Germany) with a MW cut-off of 30k Da and a total washing volume of 500 ml. After freeze drying in the presence of 300 mg of sorbitol as a cryoprotectant, nanoparticle were stored at 4°C under light protection until further use.

FA-PLGA budesonide nanoparticles were characterized for their size, size distribution and surface charge after 1:10 dilution with purified water using Zetasizer Nano ZS (Malvern Instruments, Herrenberg, Germany).

Encapsulation efficiency of budesonide in FA-PLGA nanoparticles was determined by dissolving 10 mg of freeze dried particles in 10 ml of ethyl acetate under stirring for 4 to 5 hours. Then after complete evaporation of ethyl acetate the residue was dissolved in 5 ml of acetonitrile: phosphate buffer pH 3 (4:6) for 2 hours. The solution was then filtered through a disposable syringe filter paper (CHROMAFIL GF/PET 45/25) pore size 0.45 µm. 1ml of the clear filtrate was collected and analysed by HPLC.

The drug release was assessed by ultracentrifugation method. 5-10 mg of washed and freeze dried nanoparticles were dispersed in 5 ml PBS of pH 6.8 and 100 µl aliquots of this solution were added to 1.5 ml PBS in a ultracentrifugation vial, respectively and incubated at room temperature at a constant shaking speed of 500 rpm . At particular time intervals (1, 2, 4, 6, 24 and 48 hours) one sample tube was centrifuged at 244,000 g for 25 minutes at 25°C. 1 ml of supernatant was thereafter removed from the nanoparticle pellet and quantified by HPLC.

Budesonide content in the samples was quantified via HPLC (UltiMate® 3000, Dionex, Germany) using a reversed phase C18 Column (4.6 X 250 mm, pore size 5µm) (Merck KGaA, Germany). Mobile phase consisted of a mixture of phosphate buffer (pH 3) and acetonitrile (60:40) delivered at a flow rate of 1.900 ml/min. The injection volume was 80 µl and the retention time was 6.0 min for each sample with detection wave lengths of 214 and 254 nm. The method was linear ($r^2 = 0.9997$) over a range of 20 ng/ml to 500 µg/ml, with a limit of quantification of 347 ng/ml.

3.3.3 Liposome fabrication

DPPC, PEG2000-DSPE (Lipoid) and cholesterol were weighed in a 1.85:0.15:1 ratio in a 50 mL round bottom flask and dissolved in 5-10 mL ethanol (absolute) by heating at 50°C. The organic phase was evaporated using rotary evaporation resulting in a dry lipid film, which was dried further under nitrogen flow for 30 minutes. Due to better water solubility budesonide phosphate instead of the free base was used in the preparation of the liposomes. The drug was dissolved in reversed osmosis water at a concentration of 100 mg/ml. The lipid film and corticosteroid solution were heated to 50°C before adding the solution to the

film. The film was hydrated for 5-10 min using a rotary evaporator without applying vacuum. After hydration, the size and polydispersity was decreased by extruding the dispersion through two polycarbonate filters. Starting with two extrusions through a double 200 nm filter and two extrusions through 200 and 100 nm filter, the liposomes were extruded ten times through two 100 nm filters. Free corticosteroid not encapsulated into the liposomes was removed by means of dialysis (MWCO 30,000 Da) in PBS at 4-8 °C for 48 hours, where the PBS was refreshed regularly in order to remove all free corticosteroid. As for the PLGA particles size and polydispersity and of the liposome formulations were measured by size Dynamic Light Scattering using Zetasizer Nano ZS.

3.3.4 Setting up of co-culture

Co-culture was assembled and cultivated as described previously [105]. Briefly, dendritic cells and macrophages were isolated and differentiated from blood mononuclear cells for 7 days. 10^4 of each cell types were re-suspended in 80% collagen, 10 % 10x RPMI and 10% human serum and adjusted to pH 7.4. The collagen-cell mixture were seeded on a Transwell filter insert (1.13 cm², 0.4 μm pore size) and left for an hour before Caco-2 cells were seeded on the top of the layer at a seeding density of 60,000/well. The co-culture was cultivated for 21 days to allow intact Caco-2 monolayer formation. The barrier formation was monitored by Trans-Epithelial Electrical Resistance measurement (TEER) during the course of cultivation. After a tight monolayer was obtained, inflammation was induced by addition of IL-1β (10 ng/ml, diluted from a stock solution prepared with 1% BSA in demineralized water) for 48 hours.

3.3.5 Budesonide formulation testing

After 48 hours of stimulation, IL-1 β was removed from co-culture and 100 $\mu\text{g}/\text{ml}$ budesonide in free solution (prepared from a 100 mg/ml stock solution of budesonide in ethanol) as well as in PLGA and liposome formulations were added to the apical side of the co-culture for 4 hours, giving an effective budesonide concentration of 20 $\mu\text{g}/\text{well}$ (Fig. 16). At the end of incubation time budesonide formulations were removed and the co-culture were used either for Transepithelial Electrical Resistance (TEER) value tracking and IL-8 sampling or for confocal microscopy imaging.

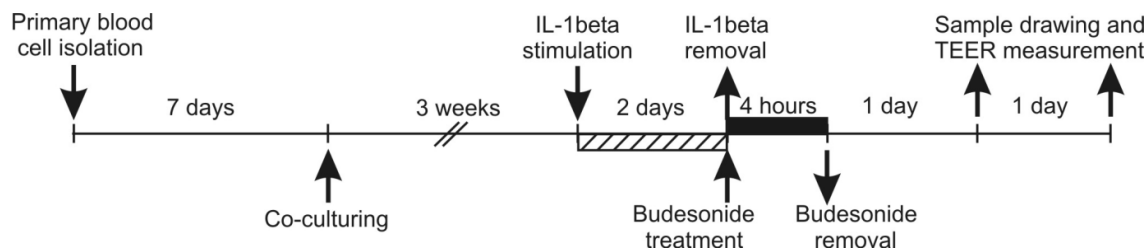


Figure 16. Experimental timeline of setting up the *in vitro* model of inflamed intestinal mucosa and subsequent budesonide formulation testing.

3.3.6 IL-8 cytokine measurement

Culture medium (50 μl) was removed after 24 and 48 hours and replaced with fresh medium. The IL-8 protein content measurement in the cell supernatant was conducted according to the manufacturer's protocol. The supernatant was mixed with 50 μl of CBA Flex beads and left for 1 hour before detection beads were added to the mixture and incubated for 2 hours without light exposure. The quantification was done via a fluorescent

activated cell sorter (FACS Calibur, BD Biosciences, Germany) using FCAP array v1.0.1 cytometric beat array analysis software.

3.3.7 Transepithelial Electrical Resistance (TEER) measurement

Transepithelial electrical resistance was measured with STX2 electrode using EVOM2 (World Precision Instruments, Sarasota, USA). For the measurement, the cells were placed on a pre-conditioned 37°C heating plate to avoid the temperature shock-related TEER value fluctuation. TEER value was obtained after subtracting the resulting value with the value of blank filter in the medium.

3.3.8 Confocal Laser Scanning Microscopy

Fluorescence images were captured by a Zeiss LSM 510 confocal microscope with the software LSM510 package. Z-stack dataset images were captured and reconstructed into three-dimensional image using Volocity (Improvisions, Lexington, MA, USA) imaging software.

3.3.9 Statistical analysis

All the experiments were conducted in triplicate and repeated twice for reproducibility. The mean values, standard deviations, stand errors and significant differences were calculated with ANOVA, Holm-Sidak test using SigmaStat 3.0 software.

3.4 Results

3.4.1 PLGA nanoparticle and liposome characterization

Both budesonide loaded nanocarrier systems were found to be monodisperse and in the same size range of 190 to 220 nm (Table 4). Budesonide encapsulation into FA-PLGA nanoparticles did not affect the size of the polymeric particles. Similar sizes were yielded for the blank nanocarrier control with a minor variance in polydispersity, which may be attributed to variations from batch to batch. A significantly smaller size was observed for drug-free liposomal formulation. In comparison with liposomal formulation, PLGA nanoparticles demonstrated 10-times higher encapsulation efficiency at 46% of 45 mg of drug employed in the particle preparation. The corresponding drug loading capacity for the PLGA particles was calculated at 0.07 mg budesonide per mg of FA-PLGA nanoparticles.

Table 4. Physicochemical properties of tested formulations and blank nanocarrier controls. PDI = Polydispersity index, EE = Encapsulation efficiency; mean \pm SD, n = 3

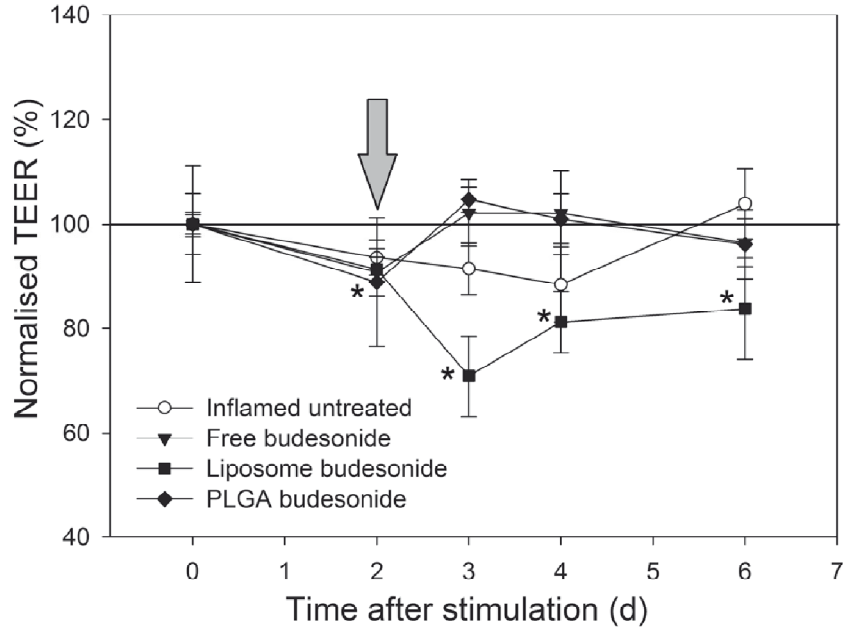
Formulation	Size (nm)	PDI	E.E. (%)
Budesonide solution	--	--	--
FA-PLGA-budesonide	220	0.1	46
FA-PLGA- drug free	220	0.06	--
Liposomal budesonide	190	0.05	4.2
Liposomes - drug free	120	0.02	--

3.4.2 TEER value monitoring

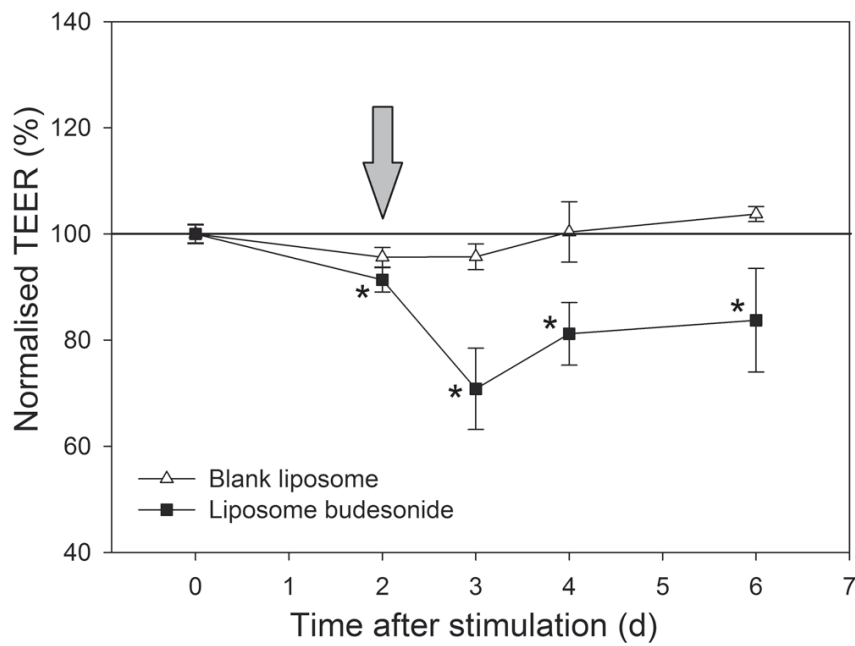
TEER value was monitored during the course of the experiment, starting at induction of inflammation up to day 4 of budesonide treatment. It was normalized with regards to the untreated non-inflamed control, which showed stable values with normal passage to passage variations of absolute TEER in the range of 650 to 800 $\Omega \cdot \text{cm}^2$ (data not shown) during the entire time course of the experiment. In response to stimulation with IL-1 β , a 10 to 20% drop in TEER was observed after 48 h, indicating successful induction of inflammation. IL-1 β was removed at day two and cells were treated immediately with the respective budesonide formulation (the time point of treatment being indicated with an arrow in figure 17a-c). As shown in figure 17a, the untreated inflamed control showed slow recovery after the inflammation, indicated by reduced TEER value of around 12% from day 2 to day 4 after stimulation. The barrier function was recovered 4 days after removal of IL-1 β . Budesonide treatment using the free drug solution acted rapidly and normalized the TEER value within the first 24 hours after treatment (Fig. 17a). A similar result for rapid recovery is also observed from the co-culture treated with PLGA-budesonide formulation, as the TEER value reached the level of control TEER value within 24 hours. Although budesonide seemed to work effectively in free solution and in PLGA particle formulation, budesonide in liposomal formulation worsened the inflammation and impaired the barrier function as indicated by the decrease of TEER level to 70% of the control value after the first 24 hours of treatment. TEER values then settled around 80% 4 days after treatment but did not completely recover. In comparison, blank liposomes did not have this impact on the barrier integrity (Fig. 17b) and led to a gradual recovery of the TEER value compared to the untreated inflamed control. The slow recovery of TEER value was also observed with blank PLGA nanocarriers (Fig. 17c). Treatment with both formulations without active compound

recovered barrier function 48 h days after treatment, which was slower than the formulations with budesonide, but earlier than the untreated inflamed control.

a)



b)



c)

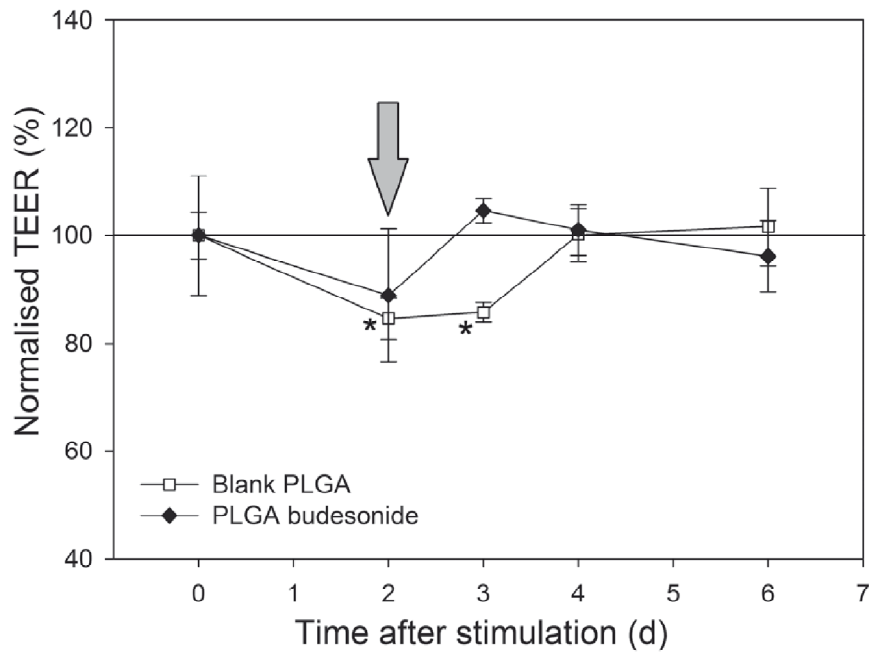


Figure 17. TEER values of triple co-culture model during the stimulation of inflammation and 4 days into treatment, normalized to healthy untreated control. Budesonide treatment was conducted 2 days after induction of inflammation (arrow). a.) TEER changes after treatment with budesonide in free solution, liposome and PLGA formulations, b.) comparison of blank liposomes and liposomal budesonide formulation c.) comparison blank and budesonide loaded FA-PLGA nanoparticles (mean \pm SD, n = 9, significant differences ($P < 0.05$) and very significant differences ($P < 0.01$) to non- inflamed control are indicated with * and ** respectively).

3.4.3 IL-8 release rate

As another marker of inflammation, the IL-8 release of the cells under budesonide treatment was measured. The healthy untreated control released around 8 pg/ml*hour IL-8 (data not shown). Upon stimulation of inflammation with IL-1 β , increased IL-8 release was observed in all experiments with release rates ranging between 20-25 pg/ml*hour 48 h after induction of inflammation (Fig. 18). The variance in IL-8 release can be attributed to normal variations among different triple culture isolations. At this point, IL-1 β was removed from the cell culture and cells were treated with the respective budesonide formulations at a budesonide concentration of 100 μ g/ml or blank carrier/medium control for 4 hours. Upon removal of IL-1 β the medium control showed slight self-healing effects as the IL-8 release dropped to around 40% from the initial inflammation level, but was twice as high as the healthy control (Fig. 18). Treatment with free budesonide reduced the IL-8 production to 13% of initial inflamed value during the course of the first day, which is similar to the levels of the healthy control. IL-8 production increased again in the following days, reaching back to 6% of initial inflamed value.

The two liposome formulations with or without budesonide showed the highest IL-8 release rate. In the cells treated with blank liposomes, IL-8 production was reduced to 38% of initial value after one day corresponding to the values from the non-treated medium control. However, the relapse over the next few days was stronger as IL-8 levels reached 75-80% of normalized value after 2-4 days. Budesonide loaded liposomes had increased production of IL-8 up to 124% to 156% of initial value after 24 and 48 hours, respectively, reaching 3 times higher IL-8 secretion rates than the starting values after 4 days. PLGA formulation seemed to be effective in reducing IL-8 release, as PLGA-budesonide particles led to 16% decrease of IL-8 during the first 2-days. This decrease indicates a prolonged effect of

budesonide compared to the free budesonide formulation, as IL-8 release remained at low levels of 19% compared to the healthy control after 4 days of treatment. The blank PLGA particles were also observed to reduce the IL-8 level to a fluctuating value of around 30 to 50% of initial value.

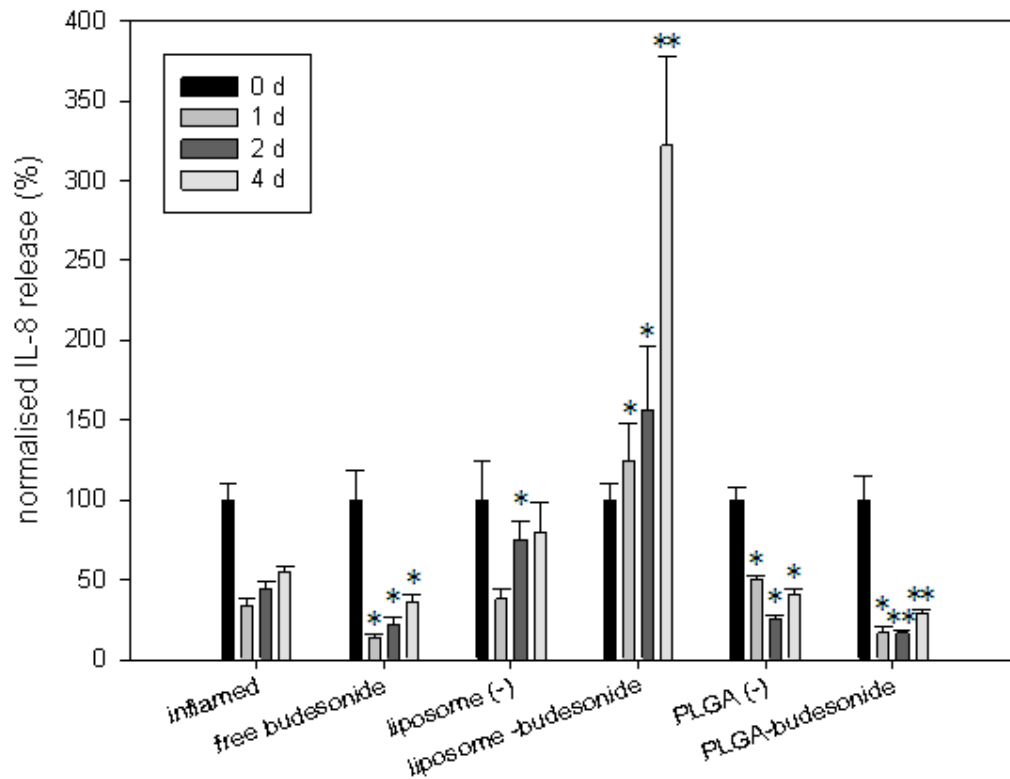


Figure 18. Normalized IL-8 release rate of triple co-culture model after induction of inflammation and treatment effects of various budesonide formulations and blank nanocarrier controls. (mean \pm SD, n = 9, * = significant difference to healthy untreated control ($P < 0.05$), ** = very significant difference to healthy untreated control ($P < 0.01$))

3.4.4 Deposition of drug carrier systems

For confocal laser scanning microscopy experiments, nanocarrier systems were fluorescently labeled by covalent coupling of fluorescein to PLGA [115] and by rhodamine to the liposomal lipid. For easier recognition, the red rhodamine signal was translated to green signal in the images displayed. The fluorescence microscopy pictures revealed the deposition of liposomes and PLGA budesonide particles throughout the healthy and inflamed *in vitro* model. In both the healthy and inflamed triple culture setup, only low amounts of PLGA budesonide particles were observed to adhere to the apical surface (Fig. 19a&c). Contrastingly, in the inflamed model, the particles were found in the junctional space of the monolayer and no co-localization with immunocompetent cells was observed (Fig. 19c). The liposomes were deposited on the surface and to some extent into the basolateral layer of the healthy model (Fig. 19b). A deeper penetration of the liposomes was observed in the inflamed model, in which the fluorescent signals were primarily found in the basolateral side of the model (Fig. 19d). In both healthy and inflamed models, some but not exclusively all rhodamine signals from the liposome was found in co-localization with auto-fluorescence signal of immunocompetent cells (Fig. 19b&d). Furthermore, the rhodamine signal appeared more diffuse and spread out, indicating at a break down or processing of the liposomes.

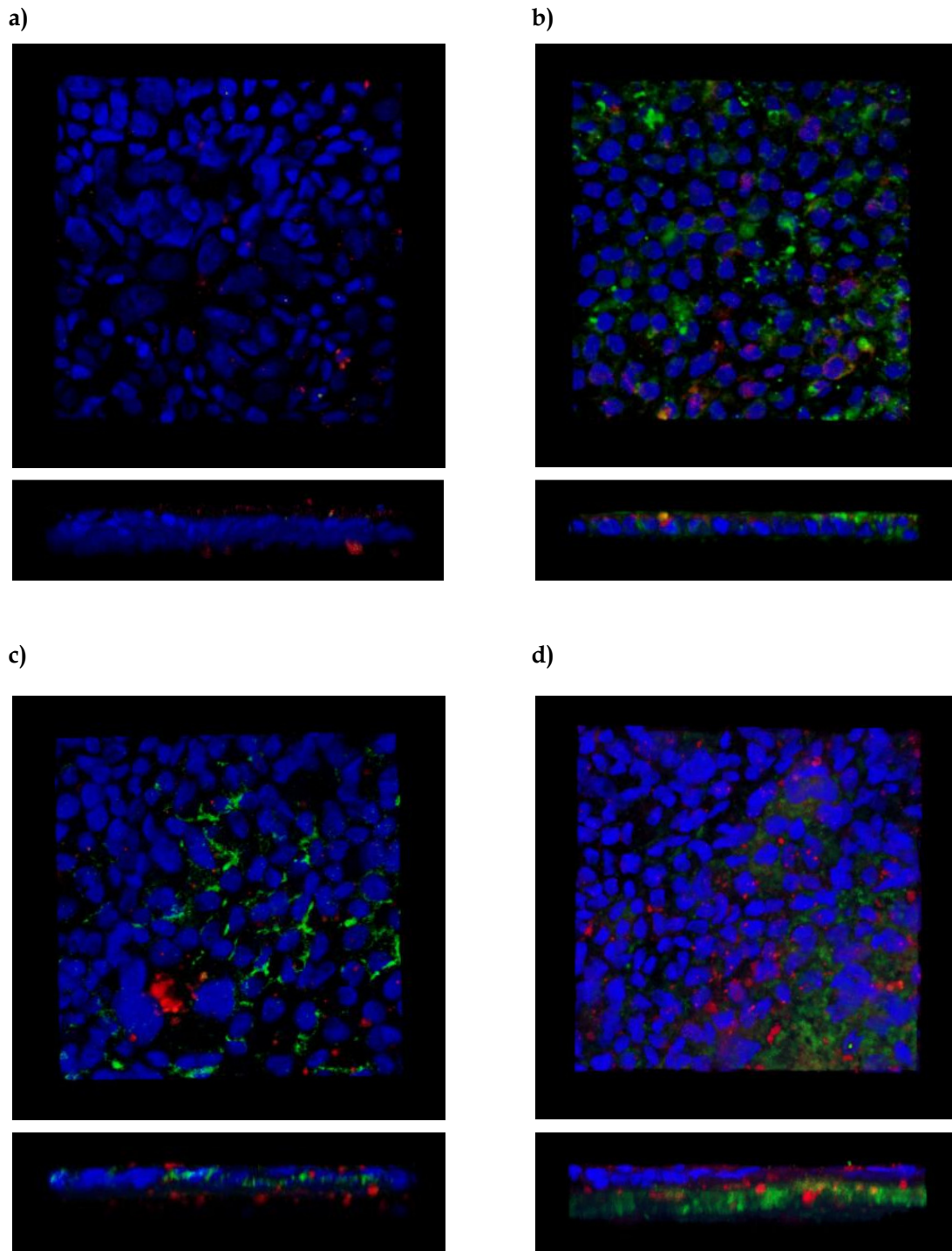


Figure 19. Deposition of budesonide loaded FA-PLGA nanoparticles (a.&c.) and liposomal budesonide (b.&d.)-in the triple co-culture model of the intestinal mucosa in non-inflamed state (a.&b.) and after successful induction of inflammation (c.&d.) as observed by confocal laser scanning microscopy; blue signal: Caco-2 cell nuclei stained with DAPI, red signal: autofluorescence of immunocompetent cells; green signal: fluorescence labeled nanoformulations (red).

3.5 Discussion

As reported previously, a novel *in vitro* model of the inflamed intestinal mucosa was established and characterized in our laboratory [105]. To further evaluate the power of the *in vitro* model in the context of pharmacology (formulation development and drug delivery research), two different carrier systems (a PLGA polymeric nanoparticle system and a liposomal system) loaded with the glucocorticoid budesonide were evaluated in the system. Both therapeutic efficacy and the mechanism of uptake and action for the two nanocarrier systems were tested in the *in vitro* model.

Nanocarrier systems have been extensively used in drug delivery applications due to their ability in controlled release and to actively or passively target the site of action. With regards to IBD treatments, nanocarriers were previously proven in different animal colitis models to accumulate passively in inflamed intestinal areas forming a drug depot for encapsulated compounds and thus improving anti-inflammatory therapy and reducing systemic adverse effects [118]. Both PLGA polymeric nanoparticles and liposomes are widely used in the field of nanomedicine for their easy-to-handle manner and their biodegradability. PLGA polymers are degraded in the body to their components through hydrolysis of the ester-bonds to lactic acid and glycolic acid. These molecules are further metabolized in the citric acid cycle, contributing to their biocompatibility and low toxicity. PLGA nanocarriers have previously been investigated for application in IBD as delivery systems for 5-aminosalicylic acid and tacrolimus and after chitosan surface modification for localized delivery of nuclear factor kappa decoy oligonucleotide [119]. To increase the stability in low pH and target the drug release to the distal ileum and colon, PLGA can also be blended with Eudragit S100 [116, 120].

Although some studies showed the potential of liposomes for oral drug delivery, their stability in the low pH and enzyme-rich environment of the gastrointestinal tract presents a significant issue. To target the inflamed intestinal mucosa from the luminal side, liposomes have to be applied rectally as enemas, avoiding the stressful gut passage and issues of stability and coalescence. The intravenous pathway is more common for liposome applications, in which they passively accumulate via endothelium fenestrations in inflamed areas. Stealth liposomal formulations as employed in this study are known to escape opsonization and uptake by reticuloendothelial system, and thereby increasing their circulation half-life and extravasation likelihood [121].

Both carrier systems are known to be “Trojan horses” for poorly soluble hydrophobic compounds, such as budesonide. In this study, budesonide was incorporated into the hydrophobic core of the PLGA nanoparticles and within the liposomes, thus increasing the apparent solubility and bioavailability. Encapsulation efficiency for budesonide in liposome was about 10-times lower compared to FA-PLGA nanoparticles which presented an ideal matrix for incorporation of small hydrophobic compounds with an encapsulation efficiency of 46% and a drug loading rate of 7%. It is to be noted that the fluorescence labeling of the polymer by covalent linking of fluorescein to the 50:50 PLGA polymer for detection in the confocal microscopy study led to a more hydrophilic derivative and reduced the drug loading capacity compared to the native polymer. The native polymer was found to accommodate up to 14% of budesonide drug in line with previous glucocorticoid PLGA formulations (data not shown). For the *in vitro* studies, the differences in drug loading between the two evaluated formulations were compensated by normalizing the amount of the respective formulation. The total budesonide dose was 100 µg/ml single application for each formulation to reach a comparable effect in the order of magnitude to the daily dosage

of Entocort® EC of 36µg/ml in intestinal fluid. The incubation time in the model was settled for 4 hours to approximate drug retention time in the intestine of IBD patients.

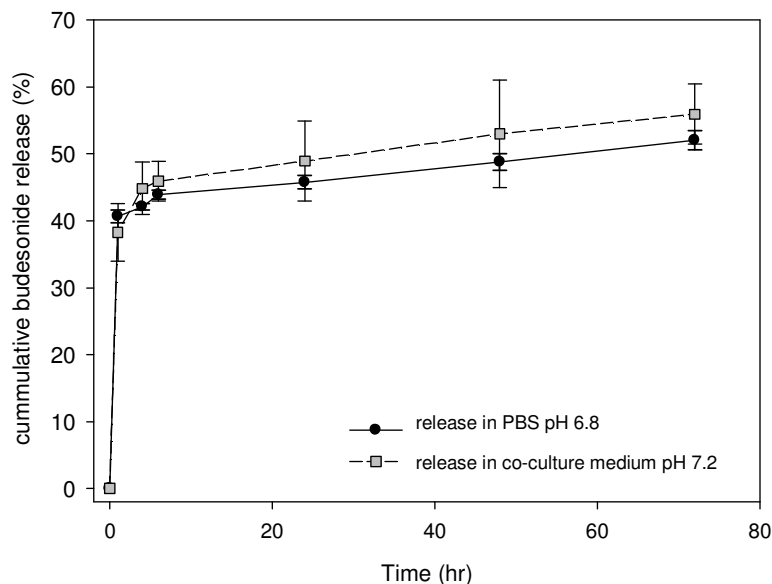


Figure 20. *In vitro* release of budesonide from PLGA nanoparticles in phosphate buffered saline pH 6.8 and co-culture apical medium (DMEM, 10%FCS, 1% nonessential amino acid, 1% Pen/Strep pH 7.2) (n=3).

At the site of action, drug release from non-coated PLGA nanoparticles is a two-step process with an initial burst release of drug adsorbed to the particle surface or bound in the outer layer of particle followed by a slower continuous release mediated by a combination of compound diffusion out nanopores and -channels and polymer degradation [122]. Under sink conditions, the budesonide burst release from FA-PLGA nanoparticles in this study was found to be 42% in the first 4 h, leaving almost 60% of encapsulated drug to form a drug depot at the target site (Fig. 20). Although previously known that stealth liposomes are able to escape from reticuloendothelial system when delivered from the blood side, the liposomes in our study seemed to be internalized and degraded by activated intestinal

immunocompetent cells, leading to an area-concentrated burst release after application from apical side of the intestinal model [117].

In our study, TEER values were decreased upon induction of inflammation in the co-culture model. Epithelial barrier integrity was disrupted due to tight junctional re-organization. Free budesonide showed a strong anti-inflammatory effect by immediately recovering the TEER value and reducing the IL-8 release in the model (Fig. 17a). PLGA-budesonide nanoparticles showed a similar anti-inflammatory effect. The results from IL-8 analysis, however, revealed the longevity of the PLGA treatment effect (Fig. 18). In the cells treated with free budesonide solution, we observed an immediate decrease of IL-8 production within the first 24 hours of treatment. The effect did not last long and the release rate rebounded and increased after the second day to 4th day, which fits with the *in vivo* dosing scheme of free budesonide that is renewed daily [97]. Meanwhile, PLGA-budesonide dispersion reduced the IL-8 release levels almost to the levels from the healthy control and maintained it throughout the experimental duration of 4 days (Fig. 18).

A slight carrier effect was observed in the control experiments as cells treated with drug free PLGA nanoparticles, as well as, blank liposomes showed a faster recovery of barrier properties compared to control (Fig. 17b&c). In addition, blank PLGA nanoparticles significantly reduced IL-8 inflammation marker levels after 24 h and 48 h of treatment (Fig. 18). This phenomenon may be related to blank particle interaction with immune cells in the triple culture leading to a pre-occupation of the immune system with this new stimulus. However, low probing and internalization of PLGA nanocarriers by immunocompetent cells were observed by confocal images. Alternatively, an adsorption of soluble signaling parameters in the inflammatory cascade of IL-8 to the particle surface might explain the findings.

The proposed hypothesis of a prolonged activity of PLGA-budesonide nanoparticles due to depot formation and prolonged budesonide release is supported by the findings from the confocal microscopy study. Epithelial barrier function was disrupted and slightly loosened up in the inflamed model, allowing the PLGA nanoparticles to accumulate in the space between the cells but not translocated to the basolateral side. This effect was not observed in the healthy model where almost no particles were adhering to the apical side or accumulated in the intercellular space. The PLGA nanoparticles at 220 nm size were retained in the upper region of the tight junctions since they are bigger than the tight junctional pore of 58 to 104 nm [123]. The inflammation of the cell model leads to a broadening of intercellular space where the nanoparticles are trapped, while not allowing to diffuse to the basolateral side. This differs from our previous observation with Fluoresbrite® nanoparticles, in which the particles were deposited on the top of the monolayer or internalized by activated immunocompetent cells [105]. Those particles were, however, rigid polystyrene particles and not biodegradable. Therefore, they were developed as model particles without concerns about drug delivery properties.

As reported in several publications, fluorescent dye in labeled nanocarriers may leak or be dissociated from the nanocarriers [124, 125], giving erroneous particle uptake and distribution data. The dissociation of fluorescein is unlikely in this study as the dye was covalently bound to the PLGA polymers and previously shown to not diffuse out of the PLGA nanoparticles [117].

In contrast to the PLGA nanoparticles, the liposomal formulation did worsen the inflammation by disrupting the barrier integrity and increasing the IL-8 release of the cells. (Fig. 17a&b, Fig. 18). The resulting epithelial defects are clearly detectable by confocal images of the liposome treated 3D model as irregular large areas with DAPI stained nuclei

(Fig. 19d). The loosening and rupture of the epithelial barrier resulted in transversing liposomes, which were then directly exposed to immunocompetent cells in the basolateral side (Fig. 19d). In our study, the rhodamine dye was incorporated into the liposome via covalent binding to the lipid (1,2-dipalmitoyl-sn-glycero-3-phosphoethanolamine-N-(Lissamine rhodamine B Sulfonyl). This coupling ensured that the fluorescence signal detected is mostly from the lipid. It does not, however, warrant the integrity of the liposomes. From the diffuse signal in the confocal images and the deposition of the fluorescence signal, it is observed that the lipids may have been dissociated and the liposome itself broken down. This effect is not associated to the liposome carrier itself but more to the specific liposomal budesonide formulation. The unloaded liposomes slightly increased the IL-8 release. In contrast, budesonide liposome formulation showed a significantly higher IL-8 release from the initial release in inflamed cells (Fig. 18). Therefore the toxicity is likely not associated to a formulation component or the liposome concentration (which is 10-fold higher compared to the PLGA nanoparticles to compensate for the lower loading capacity). The toxicity is caused by the sudden budesonide release in the basolateral side as a consequence of liposome uptake and disruption by phagocytic cells. The evaluated liposomal budesonide formulation at the concentration used in this study is thus not applicable for IBD treatment.

These results are in agreement with a previous study performed, in which a similar glucocorticoid (dexamethasone) in liposomal formulation seemed to aggravate the disease in a DSS mouse model of colitis. In contrast, the same dexamethasone formulation improved the condition in multiple sclerosis animal models [112]. The authors hypothesize that preferential uptake into tissue macrophages and shifting of macrophage may account for the differences observed. In the intestine, the M1 macrophage phenotype may be essential to

keep up innate immune answer preventing pathogen invasion across the barrier and in the same time tolerating commensal intestinal flora. However, direct uptake of glucocorticoid tends to shift the macrophage population to a more anti-inflammatory M2 characteristic, leading to more aberrant activation of immune system. Thus anti-inflammatory therapy in epithelial cells and dendritic cells may be beneficial for IBD treatment while interference with macrophage function should be avoided. For successful application in IBD treatment, liposomes do not only have to withstand diverse physiological condition found in GI tract but also have to be specifically directed to inflamed area of the intestine. Jubeh et al. reported the significance of charge properties for the liposome adhesion behavior [126]. Anionic liposomes were found augmented in inflamed area of rat intestine while cationic or neutral liposomes were accumulating in healthy tissue. The negative charge of the liposome used in this study may promote the adhesion to inflamed tissue, but the uptake by phagocytic macrophages seemed to particularly worsening the inflammation.

In summary, PLGA-budesonide formulation was found to be superior in this study, compared to both free budesonide solution and liposome formulation. As the first drug-loaded nanocarriers tested in the triple co-culture model, the particles showed an advantageous properties and good efficacy for recovery from inflammation as indicated by TEER value and pro-inflammatory protein release. This formulation also showed evidence of depot effect for budesonide release. Another advantage is the higher encapsulation efficiency of PLGA particles in comparison to the liposome. This avoids a higher loss of budesonide in the generation of the formulation. The PLGA particles did not adhere to the healthy model nor were they translocated to the basolateral side, showing their ability to avoid preemptive absorption in the upper non-affected parts of the gastro-intestinal tract and thus systemic exposure. Instead, they specifically adhere to the more mucus rich and

acidic inflamed model tissue also commonly found in IBD patients [127]. Furthermore, the loosening of tight junctional complexes increases their chance to reach and accumulate in the targeted inflammation area. Budesonide loaded liposomes at the concentration studied were proven to be toxic to the inflamed tissue, which was likely due to the instant release of budesonide after the uptake by immunocompetent cells. The effect of this dose dump is thought to be more pronounced for the liposomes compared to the free drug solution, as the majority of the budesonide dose is localized to the immune cells instead of being equally distributed among all three cell types in the triple culture. In conclusion, a smaller dosage of liposomes or lower budesonide loading might be more preferential for localized IBD treatment.

Several cell culture models have been developed incorporating immunocompetent cells, such as macrophages or B-cells, to simulate intestinal tissue [15, 20, 128]. In our model, inflammatory response is promoted by addition of pro-inflammatory cytokine to triple culture of epithelial and immunocompetent cells to mimic the inflammation in IBD. This model is able to reflect the long-term recovery process after controlled inflammation, while it can be used to study mechanism of carrier uptake in a complex system. Macrophages and dendritic cells were in direct contact with the epithelial cells, allowing the monitoring and tracking of carrier deposition and further processing in the inflamed intestinal tissue.

The superiority of the triple co-culture model compared to conventional cell culture models has been underlined in this study [105]. Different read out parameters could be used to evaluate the treatment efficacy and the experimental setup gives better representation of pathophysiological changes in IBD compared to Caco-2 cells alone. In particular, the involvement of immune cells for the inflammatory response is essential, giving significantly higher inflammatory marker release compared to the respective monocultures. This

interplay seems to exist between all three cell types in the co-culture model, as only the presence of both dendritic cells and macrophages synergistically enhanced the strength of the immune answer, as shown previously [105]. Also, a preferential uptake of nanoparticles and other foreign objects into immune cells was observed. As we are not able to differentiate between both immune cell types by direct antibody staining due to embedding in the collagen layer, it is not possible to state which immune cell type does the majority of nanoparticle or liposome processing. However, previous studies in a triple culture model of the alveolar mucosa found a preferential uptake by monocyte derived macrophages which then passed on the particulate cargo to the dendritic cells for further antigen processing and induction of immune answer [129].

In conclusion, testing in this advanced *in vitro* model should allow us to study the drug and formulation effect on the epithelial barrier as well as on the innate immune system. The model was found to be powerful for the screening of suitable anti-inflammatory formulations and drugs as a pre-stage for *in vivo* animal studies. Thereby the number of animal tests can be reduced, lessening the ethical burden and speeding up the screening process and the development of novel IBD therapies.

4. SIMPLI-Well: A novel cell culture system based on ultrathin silicon nitride (Si_3N_4) porous supports for transport and translocation studies

Article prepared for publication in Biomaterials:

Fransisca Leonard*, Sher Ahmed*, Julia Susewind, Nadia Ucciferi, Silvia Angeloni, Martha

Liley, Marta Giazzon, Claus-Michael Lehr, Eva-Maria Collnot

**These authors contributed equally to this work*

4.1 Abstract

Nanoparticles are being intensively investigated for their toxicity as well as their use as drug delivery vehicles. In this context, a tool for studying particle translocation across different biological barriers is crucial. Conventional polyester/polycarbonate-based filter inserts have been reliably used for transport studies of drug-like compounds and other small molecules as they present only a negligible barrier for low molecular-weight substances.

However, the filters pose a significant hindrance to the translocation of macromolecules and nanoparticles due to the thickness of the permeable substrate (typically 10 μm), which leads to an underestimation of particle translocation. Therefore we propose a novel SIMPLI (Silicon Microporous Permeable Insert)-Well system as an alternative two compartment setup. The SIMPLI-Well accommodates a porous support made in silicon nitride with greatly reduced thickness (500 nm) and higher pore density (15 or 20%) compared to commercial inserts. These physical features essentially remove the hindrance to (nano)particle translocation. Here, the SIMPLI-Well system was characterized with regards to proliferation, differentiation and functionality of the intestinal epithelial cell line, Caco-2. The formation of tight junctions was studied as well as the transport behaviour of the high permeability marker propranolol and low permeability marker sodium fluorescein. The transport of 50 nm polystyrene nanoparticles was also investigated to validate the system as suitable for the study of Caco-2/nanoparticle interactions. Results were compared with those of cells grown on conventional polymer based filter inserts. The SIMPLI-Well was found to be a good growth support for Caco-2 cells, allowing the cells to form confluent monolayers with appropriate transepithelial electrical resistance (TEER) values. The overall transport across the SIMPLI-Well was increased compared to commercial inserts and the system was able to differentiate between paracellularly and transcellularly transported compounds. In addition, the reduced thickness of the porous support in the novel device

allowed 50 nm polystyrene particles to translocate, thus demonstrating the potential of the system for nanotoxicology studies and pharmacokinetic testing of nanomedicines.

4.2 Introduction

Predicting the permeability of a molecule and thus its ability to be absorbed into the body is crucial for the pharmaceutical development of drug candidates. Permeability studies have been mostly conducted using epithelial cell monolayers grown to confluence on porous poly-ester/-carbonate filter inserts. These inserts are suspended in a standard multi-well plate where they form distinct apical and basolateral compartments separated by the permeable polymer filter.

Absorption and permeability can be studied in this setup, as it is assumed that diffusion across a monolayer of epithelial cells is the rate limiting step in the transport process with the permeable polymer filter providing only growth support and mechanical stability. This correlates to the fact that the monolayer of enterocytes is the principal barrier for drug absorption after oral application *in vivo* [1].

Caco-2 is the most relevant model for the intestinal mucosa. Data obtained from drug transport behavior across confluent Caco-2 cell monolayers has been found to correlate directly to data from oral drug absorption in humans [130]. Thus the Caco-2 *in vitro* model has become the most widely spread permeability model and has been validated for the use in the BCS (Biopharmaceutics Classification System) of active pharmaceutical substances (API), directly affecting drug regulatory processes via the so called biowaiver[11].

Various other immortalized or human cancer originated cell lines have been used as models for other epithelial barriers e.g. Calu-3 [131] or 16HBE14o- [132] for the bronchial mucosa. As a general feature, all of these cell lines differentiate to monolayers after confluence and form tight junctions to build a more or less tight barrier regulating absorption and secretion. They quite adequately mimic the *in vivo* situation also with regards to phenotypic expression of drug transporters and metabolizing enzymes. Thus it is possible to distinguish

between different compounds with regards to their preferred transport pathway across a certain epithelium - for example, transcellular transport of small hydrophobic molecules and paracellular transport of hydrophilic solutes - and to investigate drug- transporter interactions [133].

Apart from investigations on drug compounds alone, the interaction of more complex formulations of drugs and excipients with the respective epithelial barrier is also of interest. Formulations may range from simple physical mixtures of different compounds to complex and smart drug carriers [134, 135]. Excipients can modulate barrier properties, the activity of drug transporters and metabolizing enzymes and the transport pathways of a compound [136]. Nanoscaled drug carrier systems such as polymeric particles or liposomal formulations are of particular interest in pharmaceutical technology as they can selectively target their cargo molecules to their site of action [137].

On the other hand, novel nanotechnology based approaches also present risks to patients and consumers. Non-biodegradable, engineered nanoparticles such as metal and metal oxide particles are employed in paints, surface coatings and various high tech products [138]. *In vivo* findings of translocation of the ultrafine particles from environmental pollution across the lung barrier [139] into human systemic circulation and across the blood-brain barrier into the brain [140] have raised awareness of these particles and associated risks. Thus the hazard, risk and toxicology of particulate air pollutants and industrially fabricated nanoparticles have been and continue to be intensively studied [141].

Increasing evidence is emerging that the conventional polymer-based commercial inserts may not be suitable for the study of particle translocation. For example, particles have been reported to be able to breach the *in vivo* barrier of the gastrointestinal tract [142] or the lungs and nanoparticles have been found in the liver, lungs, heart, kidney, spleen, brain [143]. However, *in vitro* translocation studies of these particles using standard setups have shown

tremendously low rate of transport and led to underestimated values of translocation compared to *in vivo* situation [144, 145].

The main reason for the low permeability of nanoparticles across polyester/-carbonate inserts is the filter thickness which is typically over 10 μm . The thickness contributes to low permeability in three ways. Firstly, the reduction of the thickness of the filters by a factor of 20 will reduce the time needed to cross the filter by a factor of 20. Secondly, adsorption of the species under study may take place on the internal surfaces of the filter i.e. in the pores. This surface area increases linearly with the thickness of the filter. Finally, adsorption of large species to the internal (pore) surfaces of the filter may not only remove the species from the experiment but also block the pores. A new porous support for the study of nanoparticle transport should therefore be as thin as is feasible

Silicon nitride (Si_3N_4) is a hard ceramic with exceptional toughness (for a ceramic) and chemical resistance. It is used in biomedical implants because of its robustness, and biocompatibility [146] Silicon nitride surfaces have served successfully as cell growth supports [147-149]. Using standard silicon microfabrication techniques it is possible to produce free-standing ultrathin ($\sim 500\text{nm}$) microporous membranes of low-stress silicon nitride in a silicon 'frame'. A similar porous membrane support has been reported before for observation of cell-cell contacts in a blood-brain barrier model [150]. In this paper we expand the use of these ultrathin silicon nitride supports (in combination with a dedicated holder) to nanoparticle and macromolecule transport studies. When fitted in the holder, the porous support can be suspended in a multiwell plate to form a two-compartment system in which apical and basolateral compartments are separated by a porous support that is only 500nm thick. We have named this the Silicon Microporous Permeable Insert) or SIMPLI-Well system.

This paper describes a characterisation of the SIMPLI-well system as a cell growth support, particularly focussing on cell differentiation and the formation of tight junctions on the example of the Caco-2 cell line. The system's molecular transport properties were investigated using classical transcellular and paracellular markers. Finally we studied its use in nanoparticle translocation experiments using 50 nm sized polystyrene beads as model particles.

4.3 Material and Methods

4.3.1 Materials

Fluoresbrite® carboxylated nanoparticles 50 nm in diameter were purchased from Polysciences (Warrington, PA, USA). The human colon adenocarcinoma cell line Caco-2 clone C2Bbe1 was obtained from the American Type Culture Collection (Rockville, MD). Dulbecco's modified Eagle's medium (DMEM), foetal calf serum, non-essential amino acids and Phosphate buffered saline (PBS) were purchased from PAA (Pasching, Austria). Trypsin/EDTA was obtained from Sigma (Steinheim, Germany). Plastic dishes and plates were obtained from Greiner Bio-One, Transwell inserts with pore sizes 0.4 µm and 3 µm were purchased from Corning Incorporated (Acton, MA, USA), and with pore sizes of 0.4, 1 and 3 µm were obtained from BD Biosciences (Heidelberg, Germany). 4, 6-Diamidino-2-phenylindol, Fluorescein sodium salt (FluNa) and organic solvents were acquired from Sigma (Steinheim, Germany). Rabbit anti-ZO-1 antibody was obtained from Zymed Laboratories Inc (San Francisco, CA, USA) and Alexa Fluor 568 labelled goat-anti rabbit secondary antibody was purchased from BD (Heidelberg, Germany). Fluorsafe™ for sample mounting was obtained from Calbiochem (San Diego, USA). Polyaryl ether ether ketone (Ketron ® PEEK-1000) was purchased from Angst & Pfister (Zurich, Switzerland)

4.3.2 Design and fabrication of the Silicon Microporous Permeable Insert (SIMPLI) - Well system

The SIMPLI-Well holder was machined in Polyether ether ketone (PEEK) due to its excellent mechanical and chemical resistance even at high temperatures, which allows sterilisation by autoclaving. The porous supports for cell culture are fabricated using a standard microfabrication process [151, 152]. Briefly, 500 nm of low stress (non-stoichiometric) silicon

nitride (Si_3N_4) is deposited on both sides of a 380 μm thick silicon wafer by low pressure chemical vapour deposition (LPCVD). Photolithography defines structures on both sides of the wafer that are etched into the silicon nitride by reactive ion etching (RIE). The structures on the top side define the pore size, shape, and period in the porous support. On the other side of the wafer, square openings in the silicon nitride are used as a mask for a wet KOH etch that removes the exposed silicon and releases the porous silicon nitride supports as microporous membranes 1 x 1 mm in size. The silicon wafer was then diced into 14 x 14 mm chips each of which had 23 porous membranes.

The combination of the PEEK holder with the 14 x 14 mm silicon nitride chips allowed the use of the porous supports in a standard 6-well cell culture plate.

4.3.3 Pre-treatment and regeneration of silicon nitride porous supports

After fabrication, the porous supports were cleaned with Piranha Solution (H_2SO_4 98% and H_2O_2 30%, in a 4:1 ratio) at 110°C, extensively rinsed with water and dried at room temperature. They could then be stored in Milli-Q water for a few days till use. Alternatively they were dried and cleaned with SC1 solution (NH_4OH 24%, H_2O_2 30% and deionized water H_2O_2 , in 1:1:5 ratio) at 70°C followed by extensive rinsing with water and drying at room temperature just prior to use. The porous supports were immersed in cell culture medium for at least 30 minutes before cell seeding. After cell growth the supports were cleaned using Piranha solution and re-used.

4.3.4 Cell culture

Caco-2 clone C2Bbe1 (passage 65-78) were passaged and cultured with a seeding density of 6×10^4 cells/cm² in the 6 well inserts from Corning and BD and the SIMPLI-Well system. For the geometrical characteristics of the supports used in this study see table 5. The cells were fed with culture medium composed of DMEM, 10% FCS and 1% non-essential amino acid and maintained at 37°C in a 5% CO₂ and 95% humidity environment. TEER was measured every other day with Epithelial Voltohmmeter (World Precision Instruments, Sarasota, US) and the medium was changed directly afterwards.

Table 5. Geometrical characteristics of membranes used in the study

	Pore diameter (μm)	Pore density (* 10^6 cm^{-2})	Filter area (cm^2)	Total pore area/filter (* $10^6 \mu\text{m}^2$)	Pore area /filter (%)
Corning	0.4	4.0	1.12	0.45	0.4
	3	2.0	1.12	15.83	14.1
BD Falcon	0.4	2.0	0.90	0.23	0.3
	1	1.6	0.90	1.13	1.3
	3	0.8	0.90	5.09	5.7
Si ₃ N ₄ - SIMPLI-Well	2	6.5	0.23	4.60	20.0
	1	19.1	0.23	3.45	15.0

4.3.5 Permeability of fluorescein, propranolol and nanoparticles on blank and cell grown filter

Either 10 mg/ml sodium fluorescein or propranolol was dissolved in Krebs-Ringer buffer (KRB) and added to the apical side of the insert. For nanoparticle translocation experiments, 0.1% (1.5×10^{13} particles/ml) of 50 nm Fluoresbrite® carboxylated nanoparticles were suspended in 1% BSA in KRB buffer to prevent aggregation and added to the apical compartment. Transport buffer was added to the basolateral compartment and the setup was put on an orbital shaker at 150 rpm in the incubator. For the cell-free set up, samples were taken every 2 minutes for the first 10 minutes and at 10 minutes intervals up to 1 hour. Samples of translocated compounds and nanoparticles in cell-covered system were taken every 30 minutes up to 4 hours. In case of the polystyrene beads the duration of the transport experiment was extended to 24 h. Transported sodium fluorescein and fluoresbrite particle was measured with a Tecan Infinite 200 Reader at an excitation wavelength of 488 nm and emission wavelength of 530 nm. Propranolol concentration was measured with an Ultimate 3000 HPLC (Dionex) and analysed with Chromeleon software.

Apparent permeabilities (P_{app}) were calculated according to the equation:

$$P_{app} = (dQ/dt) \cdot (1/A) \cdot (1/C_0) \quad (\text{eq 2})$$

Where dQ/dt is the amount of drug transported per time, A is the surface area of the monolayer and C_0 is initial concentration.

4.3.6 Immunohistological staining and Confocal Laser Scanning Microscopy

Caco-2 cells were fixed with ice-cold ethanol for 30 minutes and stained for ZO-1 expression. Samples were incubated with 2.5 µg/ml rabbit-anti human ZO-1 antibody dissolved in 1.5% Bovin Serum Albumin (BSA) in phosphate buffered saline (PBS) solution for 1 hour at 37°C and later washed with PBS before 1 hour incubation with a second goat rhodamine-anti rabbit antibody at the same temperature. Cell nuclei were stained by incubation with DAPI for 15 minutes at room temperature. Confocal images were captured with a Zeiss LSM 510 microscope with LSM510 software package.

4.3.7 Scanning Electron Microscopy

Cells were fixed in a 2.5% glutaraldehyde in 0.2M cacodylate buffer (pH 7.4) overnight. Following this the cells were dehydrated in a series of ethanol/water mixtures: 20%, 30%, 40%, 50%, 60%, 70%, 80%, 90%, 100% (5 minutes each incubation), followed by critical point drying. The sample was then sputtered with 20nm of gold on both sides twice.

4.3.8 Transmission Electron Microscopy

Cells were fixed in 2.5% glutaraldehyde in 0.2M cacodylate buffer (pH 7.4) overnight. The samples were then rinsed in PBS and treated with 1% Osmium tetroxide in 0.1M sodium cacodylate buffer (pH7.4) adjusted to 350mosm with NaCl for 2 hour at 4°C. Samples were then rinsed with 0.05M sodium maleate buffer (0.05M Maleic acid adjusted to pH5 with concentrated NaOH) 3 times for 5 minutes each time. Following this the samples were blockstained with 0.5 uranyl acetate in the sodium maleate buffer for 2 hours at 4°C and

rinsed with the sodium maleate buffer again (3x5mins). Samples were dehydrated in a series of ethanol/water mixtures: 70%, 80%, 90% for 15 minutes per dilution and then in 100% ethanol 3 times for ten minutes each step. Finally samples were left in a propylene oxide: EPON 1:1 mixture for embedding and left for 5 days at 60 degrees C and then the samples were cut

4.3.9 Statistical analysis

All the experiments were conducted in triplicate for reproducibility. The mean values, standard deviations, stand errors and significant differences were calculated with ANOVA, Holm-Sidak test using SigmaStat 3.0 software.

4.4 Results

4.4.1 SIMPLI-Well

The SIMPLI-Well is a clamping system which allows extremely thin microfabricated porous supports to be used in the same way as regular polymer inserts (Fig. 21a&b). When the SIMPLI-Well is placed in a 6 well plate, the porous support is approximately 1.5 mm from the bottom of the well plate to allow for observation by light microscopy. The system has been designed in order to have two distinct compartments. This allows for the *in vitro* characterisation of biological barriers, for the investigation of transport properties and for TEER measurements to be taken. To ensure that upon cell confluency molecule and/or particle transport takes place exclusively through the porous area, it is essential that the mechanical tightness of the SIMPLI-well is ensured. This is achieved by clamping the porous support via a bayonet system that allows the inner and outer cylinder to slide into each other (Fig. 21a). In order to lessen the wear generated by the bayonet movement, a thin Teflon O-ring is placed between the chip and the outer cylinder. A silicon O-ring is inserted into the bottom of the inner cylinder. This comes into contact with the silicon nitride porous support to form a watertight seal and create the apical chamber of the SIMPLI-well. A groove has been included in the inner cylinder. This is used for addition and removal of cell culture media and for inserting STX2 electrodes for TEER measurements without touching the delicate silicon nitride porous support. All the components of the SIMPLI-well can be sterilised using a standard laboratory autoclave. The silicon nitride porous support can be re-used after cleaning with piranha water. The remaining components can be cleaned in an ultrasound bath. The final result is an insert with a distinct apical and basolateral compartment that accommodates a rigid ultra-thin silicon nitride porous support whilst still allowing for the use of routine laboratory practices.

4.4.2 Silicon nitride chip

Each porous support chip has an area of about 2cm^2 and has 23 porous pads each with an area of 1mm^2 to give a total porous area of 23mm^2 (Fig. 22a). The silicon nitride porous areas are $0.5\mu\text{m}$ thick and are ideal for light microscopy studies due to its high transparency (Fig. 22a). They are also suitable for Scanning Electron Microscopy (SEM), Transmission Electron Microscopy (TEM) and fluorescence microscopy.

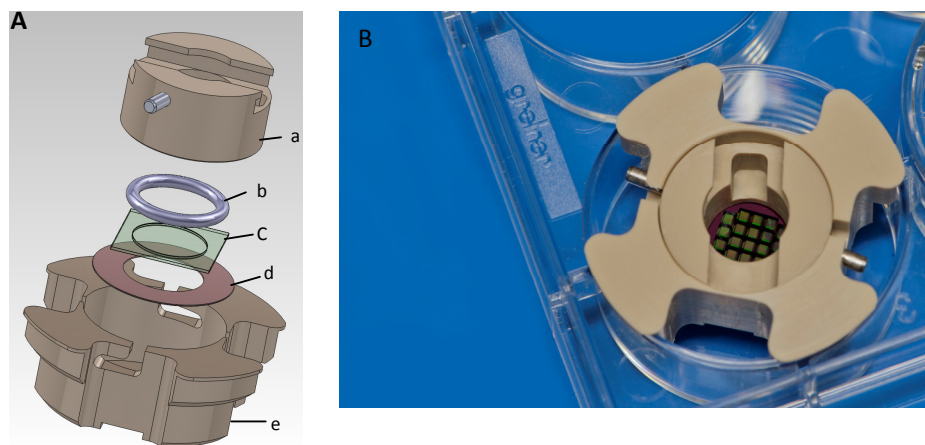


Figure 21. **A** An exploded view of the SIMPLI-Well showing all the components that make it up; (a) the upper cylinder which clamps into the lower support (e) to create the apical well; (b) a rubber o-ring to ensure a watertight seal, (c) the silicon nitride porous support, (d) a Teflon o-ring to minimize frictional forces generated by the bayonet movement; (e) the lower support which sits suspended in the well plate. **B** A photo of the SIMPLI-Well.

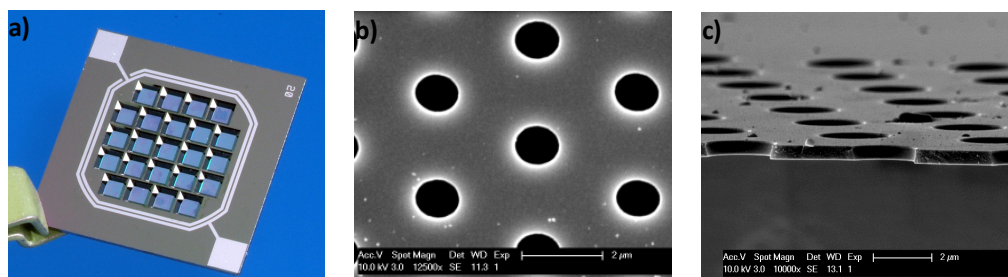


Figure 22. **a)** Image of the SIMPLI-Well silicon nitride porous support; **b)** SEM image of the $1\mu\text{m}$ pores in a hexagonal arrangement; **c)** SEM image of the 500nm thick silicon nitride porous support cross section.

4.4.3 Epithelial cell growth and differentiation

Caco-2 cells were seeded on 1 and 2 μm SIMPLI-Well membranes and cell proliferation and differentiation was monitored via light microscopy and TEER measurement over 28 days. Polyester cell culture inserts from Corning (0.4 μm pore size) and BD (1 μm pore size) were used for comparison. A seeding density of 6×10^4 cells/ cm^2 was used for all setups.

Cells grown on silicon nitride porous supports showed slightly slower cell proliferation but were able to reach confluency after 14 days, compared to the 8-10 days' time span needed for cells grown on conventional supports. The slower development on SIMPLI-Well is mirrored in the TEER values which reached a plateau after 25 days compared to 16-18 days for cells grown on polyester insert. The absolute resistance values measured for Caco-2 monolayers in the SIMPLI-Well was $\sim 2000 \Omega$ (Fig. 23a). This value has to be adjusted for TEER by subtracting the background resistance and multiplying by the filter area. The TEER was lowest for the Caco-2 cells on 1 μm pore size SIMPLI-Well, followed by the 2 μm pore size SIMPLI-Well which peaked at $\sim 300 \Omega \cdot \text{cm}^2$. The TEER values measured in the SIMPLI-well were significantly lower than for cells grown on Corning or BD inserts which displayed values of 450 to 500 $\Omega \cdot \text{cm}^2$.

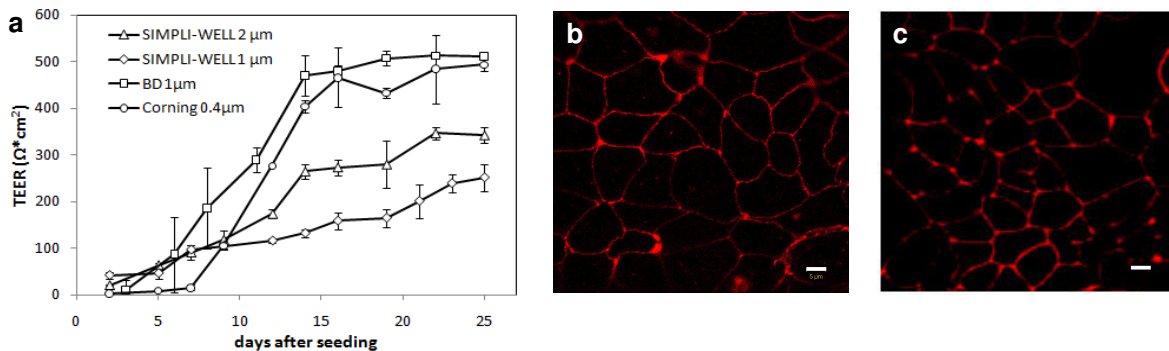


Figure 23. a) Normalized TEER measurements of Caco-2 cells grown on SIMPLI-Well and polyester inserts. Mean \pm SD; n = 6-9 b) Expression of tight junction protein ZO-1 in Caco-2 cells grown on silicon nitride inserts c) Expression of ZO-1 on polyester inserts- Scale bars are 5 μm .

4.4.4 Confocal and SEM analysis

Cells were characterised by electron microscopy and immunostaining of the tight junction protein ZO-1 after maximum TEER values were observed.

Confocal laser microscopy showed continuous ZO-1 expression at the cell junctions for cells grown on 1 μm pore SIMPLI-Well and on commercial inserts (Fig. 23b&c). The ZO-1 signal in cells on 2 μm pore SIMPLI-Well was discontinuous (data not shown). A higher fluorescence signal intensity was observed on cells grown on polyester inserts than on cells grown on 1 μm SIMPLI-wells.

However, mRNA quantification of ZO-1 expression by real time PCR did not identify any statistically significant differences between the different supports (data not shown).

Observing a mature monolayer of Caco-2 cells by SEM and TEM showed that a differentiated monolayer of cells could be seen with functional microvilli regardless of the type of support used (Fig. 24a&b). Cells grown on 2 μm SIMPLI-Wells formed a secondary layer of cells on the basolateral side, while for 1 μm pore size only parts of cell cytoplasm reached across the porous support. No nuclei were found on the basolateral side showing that cell migration did not occur (Fig. 24c).

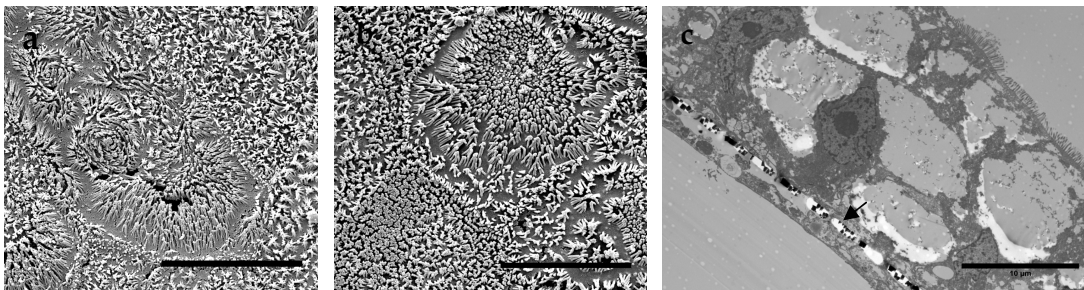


Figure 24. **a+b** show scanning electron microscope images of Caco-2 cells grown for 21 days on 1 μm SIMPLI-Well and 0.4 μm commercial polyester inserts respectively. Microvilli can be seen on both surfaces. **c** Transmission Electron Microscope image of Caco-2 cells grown for 21 days on 1 μm SIMPLI-Wells. The silicon nitride support fractured during sample preparation. The remains of the support are visible as dark cubic fragments, indicated by an arrow. All scale bars are 10 μm

4.4.5 Translocation of small molecules and polystyrene beads in the absence of cells

To assess the barrier properties of the blank filter inserts, translocation studies with sodium fluorescein, propranolol and 50 nm polystyrene beads were conducted in the absence of cells. Apparent permeability values were calculated over a period of 20 min until sink conditions could no longer be maintained. Commercially available inserts with varying pore size were used as a reference.

Due to the slow speed of 50nm polystyrene particle translocation across conventional polyester inserts, the incubation time was increased and the amount of translocated polystyrene beads was determined after 1, 4 and 24 hours

The 50 nm polystyrene beads were greatly hindered in their translocation across the conventional polyester filter inserts. Even after 24 hours of incubation, only filters with 3 μm pore size reached an equilibrated state. The 0.4 μm Corning and 0.4 and 1 μm BD filters did not reach equilibrium after 24h. At this time they still retained more than 70% of the initial dose applied to the apical side.

4.4.6 Translocation of small molecules and polystyrene beads in the presence of cells

Fluorescein sodium (paracellularly transported) and propranolol (transcellularly transported) were translocated in the presence of fully differentiated Caco-2 cells in order to assess the functionality of tight junctions in the various cell culture systems.

50 nm polystyrene beads were evaluated as a model nanoparticle formulation.

The lipophilic propranolol with its rapid transcellular diffusion showed high permeability across the Caco-2 cells grown on polyester filter inserts. Transport of the more hydrophilic

fluorescein was statistically significantly slower (Fig. 25b). Almost no nanoparticles translocated to the basolateral compartment during the 4 h duration of the experiment, resulting in an extremely low Papp value of 10^{-7} cm/s. Results were comparable in ranking and order of magnitude for both polyester filter inserts tested (0.4 μm pore size, Corning and 1 μm pore size, BD).

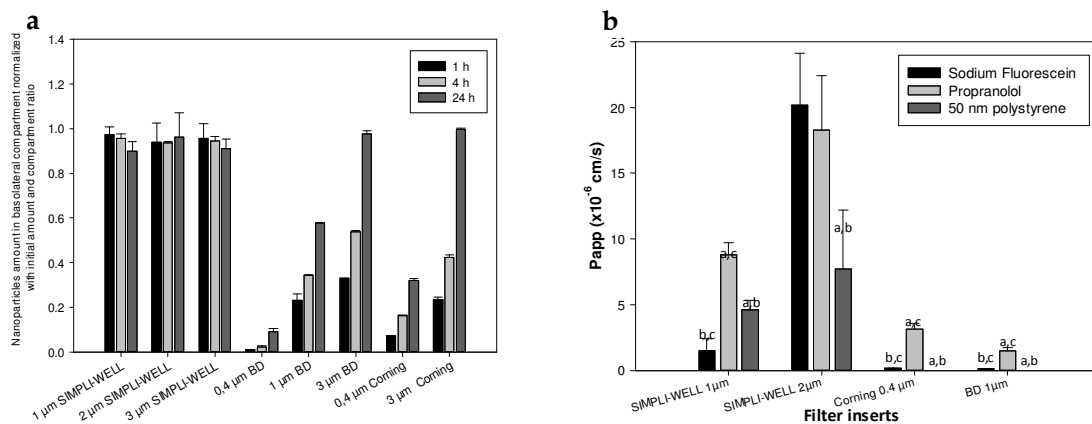


Figure 25. **a)** Translocation of 50 nm Fluoresbrite beads across varying pore sizes of SIMPLI-Wells and commercially available polyester membranes. **b)** Apparent permeability (Papp) values of sodium fluorescein, 50 nm polystyrene beads and propranolol through Caco-2 cells grown on SIMPLI-Well membranes and commercial polyester membranes with various pore sizes. a: highly significant difference $P < 0.001$ to sodium fluorescein Papp value, b: highly significant difference to propranolol Papp value, c: highly significant difference to 50 nm polystyrene beads Papp value (mean \pm SD, $n=6$).

Significantly increased transport rates were observed for all three tested substances with SIMPLI-Wells. The apparent permeability of propranolol and sodium fluorescein across the SIMPLI-Well system was higher than across a polyester insert with the same pore size (Fig. 25b). However, using the 2 μm pore SIMPLI-Well, no difference between transport of the low permeability substance (sodium fluorescein) and the high permeability substance

(propranolol) could be observed. Utilizing 1 μm pore SIMPLI-Well, we observed that the system was able to discriminate between the different permeability markers giving approximately 5 times faster transport of propranolol compared to fluorescein sodium, the effect being statistically significant ($p < 0.05$) (Fig. 25b).

In contrast to the polymer-based commercial systems, the SIMPLI-Well also allowed translocation of 50 nm polystyrene beads in the presence of the cells (Fig. 25b). Transport was higher for 2 μm sized pores but was still faster than the diffusion of fluorescein sodium for cells grown on 1 μm pore size SIMPLI-Well.

4.5 Discussion

In vitro systems are needed to assess nanomaterial translocation across an epithelium, to screen and predict *in vivo* absorption of nanoparticles and nanomedicines. Testing of epithelial permeability is generally conducted using permeable cell culture inserts with porous polyester or polycarbonate filters. These systems are available from a number of suppliers with different filter pore sizes and insert diameters. The polyester and polycarbonate membranes provide excellent growth support and allow a multidirectional supply with nutrients, leading the epithelial cells not only to proliferate but also differentiate with 3D cell growth and morphology similar to that found *in vivo*. Furthermore, numerous studies of the kinetics of absorption and secretion of hydrophilic to moderately lipophilic small molecular compounds have been carried out. In this context the polyester and polycarbonate systems have been accepted as *in vitro* testing setup by the regulatory authorities and provide good *in vitro* and *in vivo* correlations.

Permeability testing in these systems is based on the assumption that the effect of the filter support on the overall transport is negligible and that the limiting factor for translocation is the epithelial cell monolayer. As shown in equation 2, the total resistance to translocation of a compound ($1/P_e$) can be described as a series of individual resistances put in a row, where P_m is the permeability coefficient of the cell monolayer, P_f is the permeability coefficient of the filter and P_{abl} is the permeability of the aqueous boundary layer.

$$\frac{1}{P_e} = \frac{1}{P_{abl}} + \frac{1}{P_f} + \frac{1}{P_m} \quad (\text{eq 3}) [153]$$

(eq 3) [153]

The permeability coefficient of the filter is proportional to the filter porosity (ϵf), aqueous diffusion coefficient of the molecule (D), function of the molecule size (r) to pore size ratio (R_f) and reciprocally proportional to membrane thickness (δf) (eq 3).

$$Pf = \frac{\epsilon \cdot D \cdot F\left(\frac{r}{R_f}\right)}{\delta f} \quad (\text{eq 4}) [153]$$

Our studies of the transport of test compounds across a cell-free filter insert identified problems when nanoparticle translocation was investigated: although the filter insert should not present a barrier to diffusion, equilibrium in the system was not reached when using the commercial insert even after 24 h of incubation (Fig. 25a). Compared to small molecules the transport of biomacromolecules and nanoparticles across a filter is reduced due to a higher molecule size to pore size ratio. Increasing the pore size reduces the issue, as transport is faster. However, even with a 3 μm pore size no equilibrium was reached when using polyester inserts. Thus the issue is not only related to the larger hydrodynamic diameter but a large fraction of the particles seem to adsorb to the filter and clog the pores. Our results are in line with previous findings of Geys et al. who showed that polystyrene nanoparticles of 46 nm size were not adequately translocated across the 0.4 μm membrane setup [154]. Only in 3 μm polyester filter system 50 - 70% of the total amount was translocated.

Unfortunately, pore size cannot be increased ad libitum, as epithelial cell growth is dependent on the porosity parameters of the cell culture support. A bigger pore diameter can negatively affect cell differentiation and epithelial functionality giving cell monolayers with low physiological relevance. In addition, with large pore sizes, Caco-2 cells may grow through the porous substrate and form a second layer of cells on the basolateral side of the same. As a consequence, polarization of transport is lost and the model is no longer valid to

study active uptake and secretion processes. TEER as an indicator of barrier tightness is also reduced [154]. In spite of the observed not optimal conditions, in absence of easily accessible alternative tools, several translocation studies with Calu-3 and Caco-2 cells conducted on 3 μm polyester filter have been reported [144, 145].

A number of different approaches have been taken to address this problem. Changing the geometry of the cell culture support to a mesh/trench allows increasing the pore size in Caco-2 cell culture as shown by the Gabor work group who utilized a trench construction with 10-20 μm width and 35 μm depth [148] but did not further characterize their system with regards to epithelial barrier function. Other alternative cell culture supports such as ThinCert™ also failed to resolve the problem, although having pore size ranging from 0.4 to 8 μm . The overall thickness of 15 to 22.6 μm drastically reduces the permeability properties of the system. Another interesting approach for cell growth supports is microporous alumina with pore sizes from 50 to 250 nm, which has been utilized in hepatocyte engineering [155]. Unfortunately alumina has been shown to affect the proliferation and viability of cells [156] and cells grown on this surface were found to have increased distinct focal adhesion sites and actin stress fibers compared to cells grown on tissue culture plastics [155]. Another system that also addresses the permeability issue is CytoVu® from SiMPore Inc. This porous support has a thickness of 100 nm to enable faster diffusion of molecules between the two compartments, and to allow studies of cell-cell interactions and migration. Available with pore sizes of 3 and 8 μm , and with an optional Nanobarrier™ addition of 50 nm pore size, the system has been tested for the separation of molecules and nanoparticles [157, 158]. The system however, does not allow for TEER measurements and to the best of our knowledge no cell-related work has been published to date. This could be due to the fact that the overall surface available for cell growth is very small making the investigation of

translocation challenging especially if low concentrations are used. Given the unsatisfying results of these systems in nanoparticle studies, a new system is clearly needed in which reduced thickness and/increased pore density of the cell culture support improve transport properties.

The SIMPLI-Well system was designed to fulfil these criteria. Photolithography and microfabrication allow the production of silicon chips with porous support areas that are only 500 nm thick, enhancing permeability by a theoretical factor of 20 (Table 5). Pore size can be varied from 1 μm up to 3 μm as can the pore density. Studying nanoparticle translocation in the absence of cells in this system, equilibrium was reached within the first hour for both 1 μm and 2 μm pore sized porous supports. Thereby, the transport across the porous support itself is no longer a limiting factor when studying *in vitro* absorption across cells.

The SIMPLI-Well has been shown to be a suitable culture support for Caco-2 cells. Fully differentiated and polarized Caco-2 cells developed on the silicon nitride porous supports with microvilli structures on the apical side (Fig. 24a&b). Cell proliferation was only minimally delayed: TEER, as a marker of cell proliferation and especially differentiation, reached a plateau after 25 days instead of 18 days in standard cell culture inserts. On supports with 2 μm pores, cell nuclei and microvilli were seen on both the apical and basolateral compartment indicating the formation of a non-polarized double layer of cells. In contrast, although Fig. 24c shows that although cells were observed on both sides of a support with 1 μm pores, cell nuclei and functional microvilli were not seen on the basolateral side (data not shown). This indicates that the cell layer is polarised and suitable for transport studies.

Further tests also indicated that SIMPLI-Wells with 1 μm pores were optimal for CaCo-2 cells. The double cell layer formed on the 2 μm SIMPLI-Wells led to higher TEER values but negatively affected tight junction functionality as seen in the immunostaining for ZO-1 and in the transport data for fluorescein and propranolol. Fluorescein sodium as a small hydrophilic molecule is transported by paracellular diffusion across aqueous pores in the tight junctions, a process which is significantly slower than the transcellular passive diffusion of small lipophilic molecules such as propranolol. Both compounds used in this study for characterizing the barrier function of Caco-2 cells are recommended by the regulatory authorities in the evaluation of transport models. For 2 μm SIMPLI-Wells no statistically significant difference between low and high permeability marker was found (Fig. 25b) indicating poor barrier function. In contrast Caco-2 cells grown on 1 μm pore sized silicon nitride supports were able to differentiate between the two compounds with a 5-6 times higher transport of propranolol compared to fluorescein.

Barrier function for Caco-2 cells grown on commercial polyester or polycarbonate filter membranes was better than on the SIMPLI-Wells, as indicated by an even larger difference in the transport rates of propranolol and fluorescein (Fig. 25b). However, a number of studies have suggested that the Caco-2 model in the commercial cell culture systems tends to overpredict the differences between transcellularly and paracellularly transported compounds [159]. The cell monolayer was deemed to have tighter tight junctions and higher TEER value than in *in vivo* values of small intestine [10]. Therefore the cells grown on 1 μm pore sized silicon nitride membranes giving lower TEER values of 250-300 $\text{ohm}\cdot\text{cm}^2$ and significant but not overly pronounced barrier function may be closer to the actual *in vivo* situation and better simulate intestinal epithelial function.

A theoretical “cell permeability value” was calculated from the transport data in the absence and presence of cells using equation 2. In turn the relative contribution of intrinsic mechanical substrate resistance and cell resistance to the overall transport process could be calculated (Table 6). For all types of substrate and pore sizes investigated the intrinsic resistance of the substrate for sodium fluorescein was less than 0.2% of the total resistance. However, the intrinsic resistance of the substrate towards propranolol was slightly higher, 0.6-1.4% of the total resistance. Corning 0.4 μm inserts initially presented a relatively high resistance to propranolol transport at 13.1% contributed resistance (data not shown). However, this high value may be an artefact related to an unspecific binding of propranolol to the polyester surface in the absence of cells reducing the free concentration of propranolol available for transport. Indeed repeat experiments with buffer supplemented with 1% BSA showed increased propranolol transport across the blank polyester membrane, reducing the membrane resistance factor to merely 3.1%.

Table 6. The percentage ratio calculated from total resistance attributed to the cells and to the filter.

	SIMPLI-WELL 1 μm % Ratio	SIMPLI-WELL 2 μm % Ratio	Corning 0.4 μm % Ratio	BD 1 μm % Ratio
Sodium fluorescein cells	99.97	99.83	99.85	99.97
filter	0.03	0.17	0.15	0.03
Propranolol cells	99.32	99.28	96.89	99.49
filter	0.68	0.72	3.11	0.51
Propranolol cells	98.78	98.98	60.73	90.99
filter	1.21	1.02	39.27	9.01

Transport experiments with fully differentiated Caco-2 cells in the SIMPLI-Well system gave significantly enhanced transport not only for the small molecular drugs but also for the 50 nm nanoparticles. For nanoparticle transport, the relative resistances of both 1 μm and 2 μm pore sized SIMPLI-Well were very low at 1-1.2% while 1 μm BD filter inserts contributed 9% to the total resistance and Corning 0.4 μm filter inserts accounted for 39.3% of the total resistance to transport (Table 6). The low transport resistance of the membranes in SIMPLI system allows the cell monolayer to be the determining factor in translocation and transport study. For the first time, sufficient amount of particles were translocated through the cell monolayer and its membrane support to the acceptor compartment to linearly integrate particle translocation over a longer period of time thus allowing a calculation of valid permeability values. In contrast, the transport of nanoparticles is severely underestimated when using the commercial filter inserts and only the SIMPLI-Well allows an evaluation of nanoparticle/cell interactions and barrier function.

Surprisingly, the transport rate of 50 nm polystyrene particles observed in this study was higher than the fluorescein transport, which may hint at a fast transcellular transport pathway. So far, using conventional polyester or polycarbonate-based cell culture inserts, nanoparticle translocation across the epithelial barriers of the body has been underestimated. *In vitro* results showing little or no nanoparticle uptake are in strong contrast to *in vivo* data showing nanoparticles to be absorbed after intragastric or intrapulmonary [160]. Thus, it may be necessary to revisit previous *in vitro* studies which reported negative results for nanoparticle uptake across epithelia.

In conclusion, we found the SIMPLI-Well to be a good compromise between the need for a suitable mechanical support for the cells and a minimal influence on the transport process itself. The transport of nanoparticles was found to be significantly improved. Essentially,

this was achieved by reducing the thickness of the porous support from 10 μm to 0.5 μm in the SIMPLI-Well. This new insert system should allow, for the first time, a systematic *in vitro* screening of nanoparticles of different sizes and surface properties to determine qualitative and quantitative parameters predicting extent and speed of uptake across epithelia

In this study characterizing the novel cell culture system we only focussed on 50 nm polystyrene latex beads as an easily detectable model nanoparticle. It remains to be seen if the surprisingly fast transcellular transport of the nanospheres observed here is mirrored in other nanomaterials.

5. Summary

Inflammatory bowel disease is one of the five most prevalent gastrointestinal diseases in the United States and has recently increasing incidence number in developed countries and, along with the industrialization, also in developing countries. As incurable disease, the treatment for IBD are mostly includes immunosuppressant to treat the symptoms and prolong the remission state to increase the quality of life of the patients.

The drugs used in the treatment are mostly highly potent and may cause severe side effects from nausea and vomiting to hemorrhoids and intestinal obstruction. A highly promising approach for better treatment and reduced side effects is the utilization of nanocarriers for specific drug targeting. The nanocarriers have been shown previously to have extended circulation time and may accumulate in the diseased area via active or passive targeting. The passive targeting takes advantage of one of the feature in cancer or inflamed cells, the EPR-effect.

Although the interest in nano research has generated huge numbers of new formulation strategies, there is still lack of testing tool for screening purposes. The available screening tools are not yet adapted to the needs in specific diseases and specific drug formulations. Therefore we developed the *in vitro* model that has the complexity and physiological state of inflamed colonic mucosa for the testing of specific drug and its formulations.

The inflamed model of colonic mucosa described in this thesis showed that *in vitro* models are not out of date and can be developed to a more complex system, reaching a better approximation of *in vivo* condition. Although simple with only three cell components, the *in vitro* model enables characterization of each of its component and therefore builds a tightly controlled microenvironment of diseased tissues. The development of the model has

revealed the stimulation by LPS was able to increase the cytokine level, but not to disrupt the barrier function. IL-1 β in the other hand was able to reduce the TEER value and to inflame the model reversibly. The addition of immune cells as expected also enhances the immune response in the model and also allows the first insight in the mechanistic study of particle uptake. The resulting inflamed model were found to have similar characteristics as inflamed tissue, having increased pro-inflammatory cytokine level, reduced TEER value and increased mucus production. The inflammation state retained for about 5 days, giving sufficient timeframe for drug testing.

The first drug formulations tested in the system were of budesonide encapsulation. This drug is a well known potent drug for IBD, though still has low availability in the site of action due to its hydrophobic properties. PLGA nanoparticles and liposomes were designed to encapsulated budesonide and the efficacy in the treatment was evaluated by the inflamed model of colonic mucosa.

The results from the evaluation showed that the PLGA nanoparticles are suitable for IBD treatment as they seemed to be accumulated in the leaky area of epithelial barrier and acted as a depot that may release the budesonide slowly over the time, as hinted by the extended low inflammation level of the model treated with this formulation. Liposomal budesonide in our study worsen the inflammation state of the model, presumably due to its toxicity. We speculate that the liposomes were taken up by the immune cells compound in the model and get a peak in immune response over the threshold to the level of high toxicity to the epithelial cells. The problem may be solved by modulating the concentration of budesonide and liposome used to reach the optimal formulation concentration without toxicity to be used in further animal study.

In our approach of developing the *in vitro* model for drug evaluation we have previously not addressed a very important factor: the study of nanocarriers transport across the epithelial barrier. With all the advantages, the developed model is not suitable for the transport study due to the collagen layer in the model, and most importantly due to the filter support used in the model being thick and small in pore size. As part of the project we tried to overcome this issue by testing a novel silicon nitride membrane support system with increased pore size and number as well as reduced membrane thickness. The resulting membranes are biocompatible and robust for cell culture handling. One of the vital factors in drug permeability study is the monolayer state of the cells, simulating the monolayer in epithelial or endothelial barrier. This novel membrane system has small enough pore size to not allow the cells to slip through the membrane and form a double layer beneath the membrane, but big enough for nanocarrier translocation. The cells grown on the membrane filters were shown to have characteristics of differentiated monolayer, with increased TEER value and microvilli formation. With differentiated monolayer grown on the alternative silicon support membrane, the transport properties were significantly increased in most of the substance tested, especially for nanoparticles, when previously only very low detectable amount was found to be transported in the conventional Transwell filter system. The cells grown on these membranes were also able to discriminate different compounds transported paracellularly or transcellularly. To our best knowledge, this is the first study to report the suitable transport study set up for nanoparticles tested for intestinal absorption study.

In conclusion, we have successfully developed a working *in vitro* model for inflamed colonic condition which can be utilized for drug and formulation testing. Although with its limitation, the model can predict the drug formulation efficacy, length of action and accumulation in inflamed tissue. The novel silicon membrane system developed in this

study has been proven as a useful and promising tool for nanoparticles transport study. The membrane support may as well be combined with the *in vitro* model in the future to overcome the transport limitation of the model. The thinness of the silicon membrane may enable the model without collagen layer and immune cell seeding on the basolateral side, allowing a close contact to the epithelial cells on the apical side of the system.

6. Outlook

The *in vitro* model of inflamed mucosa, although was developed as inflammatory model, has potential to be utilized for other applications. Well equipped for evaluation of inflammatory response, the non-inflamed model can be used to test various food allergens and food toxicity. The main critic, which could also be one of the main advantages of this model, is the simplicity of the model. By including only the three cell types important to the immune response with a certain ratio of cells, the controlling over the three variables are easier than *in vivo* condition. This enables the tight control over the parameters and monitoring of their changes upon the drug formulation testing, delivering the mechanistic information of drug formulation and their effects in the intestinal barrier. Although very superior in mimicking the inflammation, the model still missed some important factors and may be enhanced in the future direction to improve the prediction for clinical success, depending on its application. In UC, the mucus thickness was found to be decreased compared to healthy tissue and therefore our *in vitro* model gives very close approximation to the *in vivo* condition. However, the mucus barrier has been reported to be increased in CD. Therefore the addition of mucus layer, by adding the mucus producing goblet cells for example, is important to simulate the additional barrier for drug delivery and to study the adhesion of drug formulations in the healthy or CD-affected intestine. The culture length of 21 days before maturation, although necessary for enterocytes differentiation, might have influence the phenotype and viability of the primary immune cells. Primary macrophages and dendritic cells, being isolated directly from human blood, have the variability of immune response and viability of each isolation. Another approach for standardization of the inflamed model is to incorporate stimulated monocytic cell lines to replace the primary immune cells.

Another valid point that was not addressed in this model is the flow condition in the intestine. The shear stress of the flow may affect drug formulation adhesion and accumulation in the lumen. Addition of flow in the model will add more accurate prediction of drug accumulation and absorption in non-static condition.

So far we have used conventional filter membrane system to simulate the dual compartment in *in vivo* intestinal tissue. The thickness of the membrane did not allow the cells on the basolateral compartment of the membrane to interact freely with the cells on the apical side, and therefore the immune cells were added in the same compartment in the inflamed colonic mucosa model. Our findings with the silicon nitride membrane revealed that the membranes are much thinner and not only give better transport properties to the cells grown on the membranes, but also will allow cells from both compartments to interact directly. Thus, the novel SIMPLI-Well can be utilized to improve the *in vitro* model. Addition of immune cells can be conducted after the maturation of epithelial monolayer, therefore increasing the viability and inflammatory potential. This will also add the value of the model for transport study of drug formulations by removing the collagen component, which hinders the transport study in the previous model.

7. References

1. Jackson, M.J., ed. *Drug transport across gastrointestinal epithelial*. Physiology of the Gastrointestinal Tract (2nd ed.), ed. L.R. Johnson. 1987, Raven Press: New York. 1597.
2. Aktories, K. and J.T. Barbieri, *Bacterial cytotoxins: Targeting eukaryotic switches*. Nature Reviews Microbiology, 2005. 3(5): p. 397-410.
3. Ulluwishewa, D., et al., *Regulation of Tight Junction Permeability by Intestinal Bacteria and Dietary Components*. The Journal of Nutrition, 2011. 141(5): p. 769-776.
4. Artursson, P., A.L. Ungell, and J.E. Lofroth, *Selective paracellular permeability in two models of intestinal absorption: Cultured monolayers of human intestinal epithelial cells and rat intestinal segments*. Pharmaceutical Research, 1993. 10(8): p. 1123-1129.
5. Lipinski, C.A., et al., *Experimental and computational approaches to estimate solubility and permeability in drug discovery and development settings*. Advanced Drug Delivery Reviews, 1997. 23(1-3): p. 3-25.
6. Voigt, R., *Pharmazeutische Technologie*. 10th ed. 2006: Deutscher Apotheker Verlag.
7. Al-Sadi, R., M. Boivin, and T. Ma, *Mechanism of cytokine modulation of epithelial tight junction barrier*. Frontiers in Bioscience, 2009. 14(7): p. 2765-2778.
8. Balimane, P.V., Y.H. Han, and S. Chong, *Current industrial practices of assessing permeability and P-glycoprotein interaction*. AAPS Journal, 2006. 8(1).
9. Chantret, I., et al., *Epithelial Polarity, Villin Expression, and Enterocytic Differentiation of Cultured Human Colon Carcinoma Cells: A Survey of Twenty Cell Lines*. Cancer Research, 1988. 48(7): p. 1936-1942.
10. Deferme, S., P. Annaert, and P. Augustijns, eds. *In vitro Screening Models to Assess Intestinal Drug Absorption and Metabolism*. Drug Absorption Studies: In Situ, In vitro and In Silico Models. Vol. Volume VII 2008. 182-215.
11. Smetanová, L., et al., *Caco-2 cells, biopharmaceutics classification system (BCS) and biowaiver*. Acta medica (Hradec Králové) / Universitas Carolina, Facultas Medica Hradec Králové, 2011. 54(1): p. 3-8.
12. Andrews, G.P., T.P. Lavery, and D.S. Jones, *Mucoadhesive polymeric platforms for controlled drug delivery*. European Journal of Pharmaceutics and Biopharmaceutics, 2009. 71(3): p. 505-518.
13. Park, J.H., et al., *Targeted delivery of low molecular drugs using chitosan and its derivatives*. Advanced Drug Delivery Reviews, 2010. 62(1): p. 28-41.

14. des Rieux, A., et al., *An improved in vitro model of human intestinal follicle-associated epithelium to study nanoparticle transport by M cells*. *European Journal of Pharmaceutical Sciences*, 2007. 30(5): p. 380-391.
15. Spottl, T., et al., *A new organotypic model to study cell interactions in the intestinal mucosa*. *European Journal of Gastroenterology and Hepatology*, 2006. 18(8): p. 901-909.
16. Mallegol, J., et al., *T84-Intestinal Epithelial Exosomes Bear MHC Class II/Peptide Complexes Potentiating Antigen Presentation by Dendritic Cells*. *Gastroenterology*, 2007. 132(5): p. 1866-1876.
17. Holland-Cunz, S., et al., *Three-dimensional co-culture model of enterocytes and primary enteric neuronal tissue*. *Pediatric Surgery International*, 2004. 20(4): p. 233-237.
18. Toumi, F., et al., *Human submucosal neurones regulate intestinal epithelial cell proliferation: Evidence from a novel co-culture model*. *Neurogastroenterology and Motility*, 2003. 15(3): p. 239-242.
19. Forest, V., et al., *Apc+/Min colonic epithelial cells express TNF receptors and ICAM-1 when they are co-cultured with large intestine intra-epithelial lymphocytes*. *Cellular Immunology*, 2003. 223(1): p. 70-76.
20. Tanoue, T., et al., *In vitro model to estimate gut inflammation using co-cultured Caco-2 and RAW264.7 cells*. *Biochemical and Biophysical Research Communications*, 2008. 374(3): p. 565-569.
21. Pontier, C., et al., *HT29-MTX and Caco-2/TC7 monolayers as predictive models for human intestinal absorption: Role of the mucus layer*. *Journal of Pharmaceutical Sciences*, 2001. 90(10): p. 1608-1619.
22. Haller, D., et al., *Non-pathogenic bacteria elicit a differential cytokine response by intestinal epithelial cell/leucocyte co-cultures*. *Gut*, 2000. 47(1): p. 79-87.
23. Rothen-Rutishauser, B.M., S.C. Kiama, and P. Gehr, *A three-dimensional cellular model of the human respiratory tract to study the interaction with particles*. *American Journal of Respiratory Cell and Molecular Biology*, 2005. 32(4): p. 281-289.
24. Perrière, N., et al., *A functional in vitro model of rat blood-brain barrier for molecular analysis of efflux transporters*. *Brain Research*, 2007. 1150(1): p. 1-13.
25. Gaillard, P.J., et al., *Establishment and functional characterization of an in vitro model of the blood-brain barrier, comprising a co-culture of brain capillary endothelial cells and astrocytes*. *European Journal of Pharmaceutical Sciences*, 2000. 12(3): p. 215-222.
26. Gutiérrez, G., et al., *Dehydroepiandrosterone inhibits the TNF-alpha-induced inflammatory response in human umbilical vein endothelial cells*. *Atherosclerosis*, 2007. 190(1): p. 90-99.

27. Bodet, C., F. Chandad, and D. Grenier, *Modulation of cytokine production by Porphyromonas gingivalis in a macrophage and epithelial cell co-culture model*. *Microbes and Infection*, 2005. 7(3): p. 448-456.
28. Gretzer, C., et al., *Co-culture of human monocytes and thyrocytes in bicameral chamber: Monocyte-derived IL-1 β impairs the thyroid epithelial barrier*. *Cytokine*, 2000. 12(1): p. 32-40.
29. Nickerson, C.A., E.G. Richter, and C.M. Ott, *Studying host-pathogen interactions in 3-D: Organotypic models for infectious disease and drug development*. *Journal of Neuroimmune Pharmacology*, 2007. 2(1): p. 26-31.
30. Reichl, S., J. Bednarz, and C.C. Müller-Goymann, *Human corneal equivalent as cell culture model for in vitro drug permeation studies*. *British Journal of Ophthalmology*, 2004. 88(4): p. 560-565.
31. Bisping, G., et al., *Patients with inflammatory bowel disease (IBD) reveal increased induction capacity of intracellular interferon-gamma (IFN- γ) in peripheral CD8+ lymphocytes co-cultured with intestinal epithelial cells*. *Clinical and Experimental Immunology*, 2001. 123(1): p. 15-22.
32. Satsu, H., et al., *Induction by activated macrophage-like THP-1 cells of apoptotic and necrotic cell death in intestinal epithelial Caco-2 monolayers via tumor necrosis factor-alpha*. *Experimental Cell Research*, 2006. 312(19): p. 3909-3919.
33. Haller, D., et al., *Differential effect of immune cells on non-pathogenic Gram-negative bacteria-induced nuclear factor- κ B activation and pro-inflammatory gene expression in intestinal epithelial cells*. *Immunology*, 2004. 112(2): p. 310-320.
34. Willemsen, L.E.M., et al., *A coculture model mimicking the intestinal mucosa reveals a regulatory role for myofibroblasts in immune-mediated barrier disruption*. *Digestive Diseases and Sciences*, 2002. 47(10): p. 2316-2324.
35. Pichavant, M., et al., *Asthmatic bronchial epithelium activated by the proteolytic allergen Der p 1 increases selective dendritic cell recruitment*. *Journal of Allergy and Clinical Immunology*, 2005. 115(4): p. 771-778.
36. Chen, V., et al., *Co-culture of synovial fibroblasts and differentiated U937 cells is sufficient for high interleukin-6 but not interleukin-1 β or tumour necrosis factor- α release*. *British Journal of Rheumatology*, 1998. 37(2): p. 148-156.
37. Pretzel, D., et al., *In vitro model for the analysis of synovial fibroblast-mediated degradation of intact cartilage*. *Arthritis Research and Therapy*, 2009. 11(1).
38. Mehta, P.K., et al., *Entry and intracellular replication of Mycobacterium tuberculosis in cultured human microvascular endothelial cells*. *Microbial Pathogenesis*, 2006. 41(2-3): p. 119-124.

39. Hino, M., et al., *Establishment of an in vitro model using NR8383 cells and mycobacterium bovis calmette-guérin that mimics a chronic infection of Mycobacterium tuberculosis. In vivo*, 2005. 19(5): p. 821-830.
40. Daxecker, H., et al., *Endothelial adhesion molecule expression in an in vitro model of inflammation. Clinica Chimica Acta*, 2002. 325(1-2): p. 171-175.
41. Head, K.A. and J.S. Jurenka, *Inflammatory bowel disease Part 1: ulcerative colitis--pathophysiology and conventional and alternative treatment options. Altern Med Rev*, 2003. 8(3): p. 247-83.
42. Gramlich, T. and R.E. Petras, *Pathology of inflammatory bowel disease. Semin Pediatr Surg*, 2007. 16(3): p. 154-63.
43. Lamprecht, A., U. Schaefer, and C.M. Lehr, *Size-dependent bioadhesion of micro- and nanoparticulate carriers to the inflamed colonic mucosa. Pharmaceutical Research*, 2001. 18(6): p. 788-793.
44. Sands, B.E., *Inflammatory bowel disease: Past, present, and future. Journal of Gastroenterology*, 2007. 42(1): p. 16-25.
45. Munkholm, P., *Review article: The incidence and prevalence of colorectal cancer in inflammatory bowel disease. Alimentary Pharmacology and Therapeutics, Supplement*, 2003. 18(2): p. 1-5.
46. Nagel, E., M. Bartels, and R. Pichlmayr, *Scanning electron-microscopic lesions in Crohn's disease: Relevance for the interpretation of postoperative recurrence. Gastroenterology*, 1995. 108(2): p. 376-382.
47. Meissner, Y. and A. Lamprecht, *Alternative drug delivery approaches for the therapy of inflammatory bowel disease. Journal of Pharmaceutical Sciences*, 2008. 97(8): p. 2878-2891.
48. Schulzke, J.D., et al., *Epithelial tight junctions in intestinal inflammation, in Annals of the New York Academy of Sciences* 2009. p. 294-300.
49. Lamprecht, A., et al., *Nanoparticles enhance therapeutic efficiency by selectively increased local drug dose in experimental colitis in rats. Journal of Pharmacology and Experimental Therapeutics*, 2005. 315(1): p. 196-202.
50. Nakase, H., et al., *An oral drug delivery system targeting immune-regulating cells ameliorates mucosal injury in trinitrobenzene sulfonic acid-induced colitis. Journal of Pharmacology and Experimental Therapeutics*, 2001. 297(3): p. 1122-1128.
51. Hoffmann, J.C., et al., *Animal models of inflammatory bowel disease: An overview. Pathobiology*, 2003. 70(3): p. 121-130.

52. Dahlhoff, M., et al., *Betacellulin stimulates growth of the mouse intestinal epithelium and increases adenoma multiplicity in Apc+/Min mice*. FEBS Letters, 2008. 582(19): p. 2911-2915.
53. Mutschler, E., H.-G. Schaible, and P. Vaupel, *Anatomie, Physiologie, Pathophysiologie des Menschen*. 6. ed. 2007, Stuttgart: Wissenschaftliche Verlagsgesellschaft mbH. 981.
54. Murthy, S. and A. Flanigan, *Animal Model of inflammatory bowel disease*, in *In vivo Models of Inflammation* D.W. Morgan and L.A. Marshall, Editors. 1999, Birkhauser Verlag AG.
55. Mullin, J.M., et al., *Keynote review: Epithelial and endothelial barriers in human disease*. Drug Discovery Today, 2005. 10(6): p. 395-408.
56. van Deventer, S.J.H., *Taming the mucosal immune response in Crohn's disease*. Bailliere's Best Practice and Research in Clinical Gastroenterology, 2002. 16(6): p. 1035-1043.
57. Mantle, M. and A. Allen, *A colorimetric assay for glycoproteins based on the periodic acid/Schiff stain*. Biochemical Society Transactions, 1978. 6(3): p. 607-609.
58. Elphick, D., S. Liddell, and Y.R. Mahida, *Impaired luminal processing of human defensin-5 in Crohn's disease: Persistence in a complex with chymotrypsinogen and trypsin*. American Journal of Pathology, 2008. 172(3): p. 702-713.
59. Edelblum, K.L. and J.R. Turner, *The tight junction in inflammatory disease: communication breakdown*. Current Opinion in Pharmacology, 2009. 9(6): p. 715-720.
60. Hyun Chae, J., et al., *A distinct array of proinflammatory cytokines is expressed in human colon epithelial cells in response to bacterial invasion*. Journal of Clinical Investigation, 1995. 95(1): p. 55-65.
61. Ou, G., et al., *Contribution of intestinal epithelial cells to innate immunity of the human gut - Studies on polarized monolayers of colon carcinoma cells*. Scandinavian Journal of Immunology, 2009. 69(2): p. 150-161.
62. Jobin, C. and R. Balfour Sartor, *The IKB/NF-KB system: A key determinant of mucosal inflammation and protection*. American Journal of Physiology - Cell Physiology, 2000. 278(3 47-3): p. C451-C462.
63. Liboni, K., N. Li, and J. Neu, *Mechanism of glutamine-mediated amelioration of lipopolysaccharide-induced IL-8 production in Caco-2 cells*. Cytokine, 2004. 26(2): p. 57-65.
64. Abreu, M.T., et al., *Decreased expression of Toll-like receptor-4 and MD-2 correlates with intestinal epithelial cell protection against dysregulated proinflammatory gene expression in response to bacterial lipopolysaccharide*. Journal of Immunology, 2001. 167(3): p. 1609-1616.
65. Suzuki, M., T. Hisamatsu, and D.K. Podolsky, *Gamma interferon augments the intracellular pathway for lipopolysaccharide (LPS) recognition in human intestinal epithelial cells*

- through coordinated up-regulation of LPS uptake and expression of the intracellular Toll-like receptor 4-MD-2 complex. *Infection and Immunity*, 2003. 71(6): p. 3503-3511.
66. MacDonald, T.T. and G. Monteleone, *Immunity, inflammation, and allergy in the gut*. *Science*, 2005. 307(5717): p. 1920-1925.
67. O'Neill, L.A.J. and C.A. Dinarello, *The IL-1 receptor/toll-like receptor superfamily: Crucial receptors for inflammation and host defense*. *Immunology Today*, 2000. 21(5): p. 206-209.
68. Kawai, T., et al., *Unresponsiveness of MyD88-deficient mice to endotoxin*. *Immunity*, 1999. 11(1): p. 115-122.
69. Adachi, O., et al., *Targeted disruption of the MyD88 gene results in loss of IL-1- and IL- 18-mediated function*. *Immunity*, 1998. 9(1): p. 143-150.
70. Schuerer-Maly, C.C., et al., *Colonic epithelial cell lines as a source of interleukin-8: Stimulation by inflammatory cytokines and bacterial lipopolysaccharide*. *Immunology*, 1994. 81(1): p. 85-91.
71. Dunne, A. and L.A. O'Neill, *The interleukin-1 receptor/Toll-like receptor superfamily: signal transduction during inflammation and host defense*. *Science's STKE [electronic resource] : signal transduction knowledge environment*, 2003. 2003(171).
72. Reinecker, H.C., et al., *Enhanced secretion of tumour necrosis factor-alpha, IL-6, and IL-1 β by isolated lamina propria mononuclear cells from patients with ulcerative colitis and Crohn's disease*. *Clinical and Experimental Immunology*, 1993. 94(1): p. 174-181.
73. Tamura, K., et al., *IL18 polymorphism is associated with an increased risk of crohn's disease*. *Journal of Gastroenterology*, 2002. 37(SUPPL. 14): p. 111-116.
74. Klein, W., et al., *A polymorphism in the CD14 gene is associated with crohn disease*. *Scandinavian Journal of Gastroenterology*, 2002. 37(2): p. 189-191.
75. Nemetz, A., et al., *IL1B gene polymorphisms influence the course and severity of inflammatory bowel disease*. *Immunogenetics*, 1999. 49(6): p. 527-531.
76. Ma, T.Y., et al., *Mechanism of TNF- α modulation of Caco-2 intestinal epithelial tight junction barrier: Role of myosin light-chain kinase protein expression*. *American Journal of Physiology - Gastrointestinal and Liver Physiology*, 2005. 288(3 51-3): p. G422-G430.
77. Blair, S.A., et al., *Epithelial myosin light chain kinase expression and activity are upregulated in inflammatory bowel disease*. *Laboratory Investigation*, 2006. 86(2): p. 191-201.
78. Ye, D., I. Ma, and T.Y. Ma, *Molecular mechanism of tumor necrosis factor-a modulation of intestinal epithelial tight junction barrier*. *American Journal of Physiology - Gastrointestinal and Liver Physiology*, 2006. 290(3): p. G496-G504.

79. Wang, F., et al., *IFN- γ Induced TNFR2 Expression Is Required for TNF-Dependent Intestinal Epithelial Barrier Dysfunction*. *Gastroenterology*, 2006. 131(4): p. 1153-1163.
80. Sakuma, S., et al., *Mucoadhesion of polystyrene nanoparticles having surface hydrophilic polymeric chains in the gastrointestinal tract*. *International Journal of Pharmaceutics*, 1999. 177(2): p. 161-172.
81. Bisping, G., et al., *Patients with inflammatory bowel disease (IBD) reveal increased induction capacity of intracellular interferon-gamma (IFN- γ) in peripheral CD8+ lymphocytes co-cultured with intestinal epithelial cells*. *Clinical and Experimental Immunology*, 2001. 123(1): p. 15-22.
82. Rogler, G., et al., *Isolation and phenotypic characterization of colonic macrophages*. *Clinical and Experimental Immunology*, 1998. 112(2): p. 205-215.
83. Rimoldi, M., et al., *Intestinal immune homeostasis is regulated by the crosstalk between epithelial cells and dendritic cells*. *Nature Immunology*, 2005. 6(5): p. 507-514.
84. Shale, M. and S. Ghosh, *How intestinal epithelial cells tolerise dendritic cells and its relevance to inflammatory bowel disease*. *Gut*, 2009. 58(9): p. 1291-1299.
85. Zaph, C., et al., *Epithelial-cell-intrinsic IKK- β expression regulates intestinal immune homeostasis*. *Nature*, 2007. 446(7135): p. 552-556.
86. Cernadas, M., et al., *CD1a expression defines an interleukin-12 producing population of human dendritic cells*. *Clinical and Experimental Immunology*, 2009. 155(3): p. 523-533.
87. Iwasaki, A., *Mucosal dendritic cells*, in *Annual Review of Immunology* 2007. p. 381-418.
88. Rescigno, M., et al., *Dendritic cells shuttle microbes across gut epithelial monolayers*. *Immunobiology*, 2001. 204(5): p. 572-581.
89. Haller, D., et al., *Differential effect of immune cells on non-pathogenic Gram-negative bacteria-induced nuclear factor- κ B activation and pro-inflammatory gene expression in intestinal epithelial cells*. *Immunology*, 2004. 112(2): p. 310-320.
90. Baumgart, D.C. and S.R. Carding, *Inflammatory bowel disease: cause and immunobiology*. *Lancet*, 2007. 369(9573): p. 1627-1640.
91. Hering, N.A. and J.D. Schulzke, *Therapeutic options to modulate barrier defects in inflammatory bowel disease*. *Digestive Diseases*, 2009. 27(4): p. 450-454.
92. McGuckin, M.A., et al., *Intestinal barrier dysfunction in inflammatory bowel diseases*. *Inflammatory Bowel Diseases*, 2009. 15(1): p. 100-113.
93. Siegel, C.A., *What options do we have for induction therapy for Crohn's disease?* *Digestive Diseases*, 2010. 28(3): p. 543-547.

94. Akobeng, A.K., *Crohn's disease: Current treatment options*. Archives of Disease in Childhood, 2008. 93(9): p. 787-792.
95. Ghosh, S. and R. Panaccione, *Review: Anti-adhesion molecule therapy for inflammatory bowel disease*. Therapeutic Advances in Gastroenterology, 2010. 3(4): p. 239-258.
96. Rutgeerts, P., S. Vermeire, and G. Van Assche, *Biological Therapies for Inflammatory Bowel Diseases*. Gastroenterology, 2009. 136(4): p. 1182-1197.
97. Greenberg, G.R., et al., *Oral budesonide for active Crohn's disease*. New England Journal of Medicine, 1994. 331(13): p. 836-841.
98. Löfberg, R., et al., *Budesonide prolongs time to relapse in ileal and ileocaecal Crohn's disease. A placebo controlled one year study*. Gut, 1996. 39(1): p. 82-86.
99. Hasani, S., Y. Pellequer, and A. Lamprecht, *Selective adhesion of nanoparticles to inflamed tissue in gastric ulcers*. Pharmaceutical Research, 2009. 26(5): p. 1149-1154.
100. Tabata, Y., Y. Inoue, and Y. Ikada, *Size effect on systemic and mucosal immune responses induced by oral administration of biodegradable microspheres*. Vaccine, 1996. 14(17-18): p. 1677-1685.
101. Lamprecht, A., et al., *Biodegradable nanoparticles for targeted drug delivery in treatment of inflammatory bowel disease*. Journal of Pharmacology and Experimental Therapeutics, 2001. 299(2): p. 775-781.
102. Lamprecht, A., U. Schafer, and C.M. Lehr, *Size-dependent bioadhesion of micro- and nanoparticulate carriers to the inflamed colonic mucosa*. Pharmaceutical Research, 2001. 18(6): p. 788-793.
103. Wirtz, S. and M.F. Neurath, *Mouse models of inflammatory bowel disease*. Adv Drug Deliv Rev, 2007. 59(11): p. 1073-83.
104. Strober, W., I.J. Fuss, and R.S. Blumberg, *The immunology of mucosal models of inflammation*, 2002. p. 495-549.
105. Leonard, F., E.M. Collnot, and C.M. Lehr, *A three-dimensional coculture of enterocytes, monocytes and dendritic cells to model inflamed intestinal mucosa in vitro*. Molecular Pharmaceutics, 2010. 7(6): p. 2103-2119.
106. Mundargi, R.C., et al., *Nano/micro technologies for delivering macromolecular therapeutics using poly(D,L-lactide-co-glycolide) and its derivatives*. Journal of Controlled Release, 2008. 125(3): p. 193-209.
107. Dinarvand, R., et al., *Polylactide-co-glycolide nanoparticles for controlled delivery of anticancer agents*. International Journal of Nanomedicine, 2011. 6: p. 877-895.

108. Henriksen-Lacey, M., et al., *Liposomal vaccine delivery systems*. *Expert Opinion on Drug Delivery*, 2011. 8(4): p. 505-519.
109. Maruyama, K., *Intracellular targeting delivery of liposomal drugs to solid tumors based on EPR effects*. *Advanced Drug Delivery Reviews*, 2011. 63(3): p. 161-169.
110. Maeda, H., et al., *Tumor vascular permeability and the EPR effect in macromolecular therapeutics: A review*. *Journal of Controlled Release*, 2000. 65(1-2): p. 271-284.
111. Awasthi, V.D., et al., *Accumulation of PEG-liposomes in the inflamed colon of rats: Potential for therapeutic and diagnostic targeting of inflammatory bowel diseases*. *Journal of Drug Targeting*, 2002. 10(5): p. 419-427.
112. Crielaard, B.J., et al., *Macrophages and liposomes in inflammatory disease: Friends or foes?* *International Journal of Pharmaceutics*, 2011.
113. Jubeh, T.T., et al., *Local treatment of experimental colitis in the rat by negatively charged liposomes of catalase, TMN and SOD*. *Journal of Drug Targeting*, 2006. 14(3): p. 155-163.
114. Tirosh, B., et al., *Transferrin as a luminal target for negatively charged liposomes in the inflamed colonic mucosa*. *Molecular Pharmaceutics*, 2009. 6(4): p. 1083-1091.
115. Weiss, B., et al., *Nanoparticles made of fluorescence-labelled Poly(L-lactide-co-glycolide): preparation, stability, and biocompatibility*. *J Nanosci Nanotechnol*, 2006. 6(9-10): p. 3048-56.
116. Gurny, R., et al., *Development of biodegradable and injectable latices for controlled release of potent drugs*. *Drug Development and Industrial Pharmacy*, 1981. 7(1): p. 1-25.
117. Metselaar, J.M. and G. Storm, *Liposomes in the treatment of inflammatory disorders*. *Expert Opinion on Drug Delivery*, 2005. 2(3): p. 465-476.
118. Lamprecht, A., U. Schafer, and C.M. Lehr, *Size dependency of microparticle deposition to the inflamed colon in inflammatory bowel disease: in-vivo results from rat*. *Journal of Controlled Release*, 2001. 72(1-3): p. 235-237.
119. Tahara, K., et al., *Oral nuclear factor- κ B decoy oligonucleotides delivery system with chitosan modified poly(d,l-lactide-co-glycolide) nanospheres for inflammatory bowel disease*. *Biomaterials*, 2011. 32(3): p. 870-878.
120. Makhlof, A., Y. Tozuka, and H. Takeuchi, *pH-Sensitive nanospheres for colon-specific drug delivery in experimentally induced colitis rat model*. *European Journal of Pharmaceutics and Biopharmaceutics*, 2009. 72(1): p. 1-8.
121. Immordino, M.L., F. Dosio, and L. Cattel, *Stealth liposomes: review of the basic science, rationale, and clinical applications, existing and potential*. *International Journal of Nanomedicine*, 2006. 1(3): p. 297-315.

122. Allison, S.D., *Analysis of initial burst in PLGA microparticles*. Expert Opinion on Drug Delivery, 2008. 5(6): p. 615-628.
123. Linnankoski, J., et al., *Paracellular porosity and pore size of the human intestinal epithelium in tissue and cell culture models*. Journal of Pharmaceutical Sciences, 2010. 99(4): p. 2166-2175.
124. Suh, H., et al., *Cellular uptake study of biodegradable nanoparticles in vascular smooth muscle cells*. Pharmaceutical Research, 1998. 15(9): p. 1495-1498.
125. Pietzonka, P., et al., *Transfer of lipophilic markers from PLGA and polystyrene nanoparticles to Caco-2 monolayers mimics particle uptake*. Pharmaceutical Research, 2002. 19(5): p. 595-601.
126. Jubeh, T.T., Y. Barenholz, and A. Rubinstein, *Differential adhesion of normal and inflamed rat colonic mucosa by charged liposomes*. Pharmaceutical Research, 2004. 21(3): p. 447-453.
127. Press, A.G., et al., *Gastrointestinal pH profiles in patients with inflammatory bowel disease*. Alimentary Pharmacology and Therapeutics, 1998. 12(7): p. 673-678.
128. des Rieux, A., et al., *An improved in vitro model of human intestinal follicle-associated epithelium to study nanoparticle transport by M cells*. European Journal of Pharmaceutical Sciences, 2007. 30(5): p. 380-391.
129. Blank, F., et al., *Macrophages and dendritic cells express tight junction proteins and exchange particles in an in vitro model of the human airway wall*. Immunobiology, 2011. 216(1-2): p. 86-95.
130. Artursson, P. and J. Karlsson, *Correlation between oral drug absorption in humans and apparent drug permeability coefficients in human intestinal epithelial (CACO-2) cells*. Biochemical and Biophysical Research Communications, 1991. 175(3): p. 880-885.
131. Foster, K.A., et al., *Characterization of the Calu-3 cell line as a tool to screen pulmonary drug delivery*. International Journal of Pharmaceutics, 2000. 208(1-2): p. 1-11.
132. Forbes, B., et al., *The human bronchial epithelial cell line 16HBE14o- as a model system of the airways for studying drug transport*. International Journal of Pharmaceutics, 2003. 257(1-2): p. 161-167.
133. Taipalensuu, J., et al., *Correlation of gene expression of ten drug efflux proteins of the atp-binding cassette transporter family in normal human jejunum and in human intestinal epithelial Caco-2 cell monolayers*. Journal of Pharmacology and Experimental Therapeutics, 2001. 299(1): p. 164-170.
134. Kim, S., et al., *Engineered polymers for advanced drug delivery*. European Journal of Pharmaceutics and Biopharmaceutics, 2009. 71(3): p. 420-430.

135. Stuart, M.A.C., et al., *Emerging applications of stimuli-responsive polymer materials*. *Nature Materials*, 2010. 9(2): p. 101-113.
136. Chen, M.L., *Lipid excipients and delivery systems for pharmaceutical development: A regulatory perspective*. *Advanced Drug Delivery Reviews*, 2008. 60(6): p. 768-777.
137. Devalapally, H., A. Chakilam, and M.M. Amiji, *Role of nanotechnology in pharmaceutical product development*. *Journal of Pharmaceutical Sciences*, 2007. 96(10): p. 2547-2565.
138. Maynard, A.D., et al., *Safe handling of nanotechnology*. *Nature*, 2006. 444(7117): p. 267-9.
139. Nemmar, A., et al., *Passage of inhaled particles into the blood circulation in humans*. *Circulation*, 2002. 105(4): p. 411-414.
140. Oberdoerster, G., et al., *Translocation of inhaled ultrafine particles to the brain*. *Inhalation Toxicology*, 2004. 16(6-7): p. 437-445.
141. Terzano, C., et al., *Air pollution ultrafine particles: Toxicity beyond the lung*. *European Review for Medical and Pharmacological Sciences*, 2010. 14(10): p. 809-821.
142. Florence, A.T., *The oral absorption of micro- and nanoparticulates: Neither exceptional nor unusual*. *Pharmaceutical Research*, 1997. 14(3): p. 259-266.
143. Elder, A. and G. Oberdörster, *Translocation and Effects of Ultrafine Particles Outside of the Lung*. *Clinics in Occupational and Environmental Medicine*, 2005. 5(4): p. 785-796.
144. Van Der Lubben, I.M., et al., *Transport of chitosan microparticles for mucosal vaccine delivery in a human intestinal m-cell model*. *Journal of Drug Targeting*, 2002. 10(6): p. 449-456.
145. Gullberg, E., et al., *Expression of specific markers and particle transport in a new human intestinal M-cell model*. *Biochemical and Biophysical Research Communications*, 2000. 279(3): p. 808-813.
146. Voskerician, G., et al., *Biocompatibility and biofouling of MEMS drug delivery devices*. *Biomaterials*, 2003. 24(11): p. 1959-1967.
147. Carter, E.A., et al., *Silicon nitride as a versatile growth substrate for microspectroscopic imaging and mapping of individual cells*. *Molecular BioSystems*. 6(7): p. 1316-1322.
148. Guell, I., et al., *Influence of structured wafer surfaces on the characteristics of Caco-2 cells*. *Acta Biomaterialia*, 2009. 5(1): p. 288-297.
149. Hui, E.E. and S.N. Bhatia, *Silicon microchips for manipulating cell-cell interaction*. *Journal of Visualized Experiments*, 2007(7).
150. Ma, S.H., et al., *An endothelial and astrocyte co-culture model of the blood-brain barrier utilizing an ultra-thin, nanofabricated silicon nitride membrane*. *Lab on a Chip - Miniaturisation for Chemistry and Biology*, 2005. 5(1): p. 74-85.

151. Madou, M.J., *Fundamental of microfabrication: the science of miniaturization*. 2002, Boca Raton, FL: CRC Press.
152. Halamoda, K.B., et al., *Direct transfer of ultrasmall iron oxide nanoparticles from human brain-derived endothelial cells to human glioblastoma cells*. submitted, 2012.
153. Adson, A., et al., *Quantitative approaches to delineate paracellular diffusion in cultured epithelial cell monolayers*. *Journal of Pharmaceutical Sciences*, 1994. 83(11): p. 1529-1536.
154. Geys, J., et al., *In vitro study of the pulmonary translocation of nanoparticles: A preliminary study*. *Toxicology Letters*, 2006. 160(3): p. 218-226.
155. Hoess, A., et al., *Self-supporting nanoporous alumina membranes as substrates for hepatic cell cultures*. *Journal of Biomedical Materials Research - Part A*, 2012.
156. Campbell, A., D. Hamai, and S.C. Bondy, *Differential toxicity of aluminum salts in human cell lines of neural origin: Implications for neurodegeneration*. *NeuroToxicology*, 2001. 22(1): p. 63-71.
157. Striemer, C.C., et al., *Charge- and size-based separation of macromolecules using ultrathin silicon membranes*. *Nature*, 2007. 445(7129): p. 749-753.
158. Gaborski, T.R., et al., *High-performance separation of nanoparticles with ultrathin porous nanocrystalline silicon membranes*. *ACS Nano*, 2010. 4(11): p. 6973-6981.
159. Kerns, E.H. and L. Di, eds. *In vitro Permeability Methods*. *Drug-like Properties: Concepts, Structure Design and Methods: From ADME to Toxicity Optimization*, ed. E.H. Kerns and L. Di. 2008, Academic Press.
160. Schleh, C., et al., *Size and surface charge of gold nanoparticles determine absorption across intestinal barriers and accumulation in secondary target organs after oral administration*. *Nanotoxicology*, 2012. 6(1): p. 36-46.

8. Abbreviations

ADME	absorption, distribution, metabolism, and excretion
ANOVA	analysis of variance
API	active pharmaceutical ingredient
BCRP	breast cancer resistance protein
BCS	Biopharmaceutical Classification System
CBA	Cytometric Bead Array
CD	Crohn's disease
cDNA	Complimentary Deoxyribonecleotide acid
CFU	Colony-forming unit
CLSM	Confocal Laser Scanning Microscopy
CYP3A4	Cytochrome P450 3A
DC	dendritic cells
DMEM	Dulbecco's modified Eagle's medium
DPPC	Dipalmitoyl Phosphatidylcholine
DSPE	Distearoyl-Phosphatidylethanolamine
DSS	dextran sulfate sodium
EDTA	ethylenediaminetetraacetic acid
EPR	Enhanced Permeability and Retention
FACS	Fluorescence-activated cell sorting

FCS	Fetal Calf Serum
FDA	Food and Drug Administration
FITC	fluorescein isothiocyanate
FluNa	fluorescein sodium salt
GM-CSF	granulocyte-macrophage colony-stimulating factor
HPLC	high-performance liquid chromatography
IBD	Inflammatory bowel disease
IFN- γ	interferon gamma
I- κ B	inhibitor of κ B
IL-x	Interleukin
KRB	Krebs ringer buffer
LPCVD	low-pressure chemical vapor deposition
LPS	Lipopolysaccharide
MLCK	myosin light-chain kinase
MRP	multidrug resistance associated protein
NF- κ B	nuclear factor kappa-light-chain-enhancer of activated B cells
NOD2	nucleotide-binding oligomerization domain-containing protein 2
Papp	apparent permeability
PBMC	peripheral blood mononuclear cell
PBS	phosphate buffered saline

PCR	polymerase chain reaction
PEEK	Polyether ether ketone
PepT1	peptide transporter 1
PLGA	poly(lactic-co-glycolic acid)
PMA	Phorbol 12-myristate 13-acetate
PVA	Polyvinyl alcohol
RIE	reactive-ion etching
RNA	ribonucleic acid
R-PE	R - Phycoerythrin
RPMI	Roswell Park Memorial Institute medium
SIMPLI	Silicon Microporous Permeable Insert
TEER	transepithelial electrical resistance
TNBS	trinitrobenzene sulfonate
TNF- α	Tumor Necrosis Factor alpha
TLR \times	Toll-like receptor
UC	Ulcerative colitis
ZO-1	Zona occludens-1

9. Curriculum vitae

Personal information

Name Fransisca Leonard
Address 7107 Harmony Cove
Houston, TX 77036
Date of birth 24th April 1981
Nationality Indonesian

School

1987-1993 Santa Maria Fatima elementary school
1993-1996 Marsudirini I middle school
1996-1999 Fons Vitae high school

Undergraduate studies

1999-2000 Foundation course Berlin Institute of Technology (TU Berlin), Germany
2000-2007 Biotechnology, Berlin Institute of Technology (TU Berlin), Germany
2003-2004 Biotechnology, Dongseo University, Busan, South Korea

Master and study thesis

2004 Chemical-technical analysis Institute, Biotechnology Department,
Dongseo University, Busan, South Korea
"Purification of synthetic fimbrolide and beckerelide with semi-
preparative normal phase HPLC"

2006 Cell Differentiation and Tumorigenesis Department, Max-
Delbrück-Center for Molecular Medicine, Berlin, Germany
"Regulation of the Ubiquitin-Conjugating Enzyme E2H (UBE2H)
Gene by the Hematopoietic Transcription Factor Tal1 (SCL)"

PhD thesis

08/2007-07/2011 Department of Biopharmaceutics and Pharmaceutical Technology
Saarland University, Saarbrücken, Germany
"Novel cell based *in vitro* models to study nanoparticle interaction
with the inflamed intestinal mucosa"

Awards and honors

- 2003-2004 Scholarship of Dongseo University in Busan, South Korea under the dual-degree program in biotechnology between Berlin Institute of Technology and Dongseo University, Busan, South Korea
- 2010 German Rhineland-Palatinate Ministry of Environment, Forestry and Consumer Protection Research Award for the investigation on alternative and supplementary methods for animal testing
- 2011 30th Animal Protection Research Prize of the German Federal Ministry of Food, Agriculture and Consumer Protection on "Development and establishment of an *in vitro* model of the inflamed human intestinal mucosa" for replacement of animal experiments in biomedical and pharmaceutical research and development.
- 2011-2012 Research Fellowship for Euro-PhD Program from Helmholtz Centre for Infection Research (HZI), Braunschweig, Germany

Scientific publications

- Impidjati; **Leonard, F.**; and Thielecke, H. Evaluation of capillary measuring system for characterisation of small tissue samples by impedance spectroscopy at higher frequencies. *IEEE Eng Med Bio*, 2005, 645:1-4.
- Leclerc, C.; Brose, C.; Nouzé, C.; **Leonard, F.**; Majlessi, L.; Becker, S.; Von Briesen, H.; Lo-Man, R. Immobilized cytokines as biomaterials for manufacturing immune cell based vaccines. *Journal of Biomedical Materials Research - Part A*, 2008, 86 (4), pp. 1033-1040
- Lausen, J.; Pless, O.; **Leonard, F.**; Kuvardina, O.N.; Koch, B.; Leutz, A. Targets of the Tal1 transcription factor in erythrocytes: E2 ubiquitin conjugase regulation by Tal1. *Journal of Biological Chemistry*, 2010, 285 (8), pp. 5338-5346
- Leonard, F.**; Collnot, E.M.; Lehr, C.M. A 3-dimensional co-culture of enterocytes, monocytes and dendritic cells to model the inflamed intestinal mucosa *in vitro*. *Molecular Pharmaceutics*, 2010, 7 (6), pp. 2103-2119
- Leonard, F.**; Hussein, A.; Collnot, E. M.; Crielaard, B.; Lammers, T.; Storm, G.; Lehr, C.-M.. Screening of various vehicle for budesonide drug delivery to treat IBD with an improved 3D *in vitro* model. *ALTEX*. 2012;29(3):275-85

Leonard, F*; Ahmed, S*; Susewind, J; Ucciferi, N; Angeloni, S; Liley, M; Giazzon, M; Lehr, C.M.; Collnot, E.M. SIMPLI-Well: A novel cell culture system based on ultrathin silicon nitride (Si_3N_4) porous supports for transport and translocation studies. *Biomaterials*, prepared

Posters and Podium Presentations

Leonard, F; Collnot, E.-M.; Lehr, C.-M. Development of a novel 3D inflamed intestinal mucosa model: Initiation of inflammation in Caco-2 cells. 7th conference and workshop on biological barriers and nanomedicine, 20-29 February 2008, Saarbrücken, Germany (Poster)

Leonard, F; Collnot, E.-M.; Lehr, C.-M. Development of a novel Caco-2 based 3D model of the inflamed intestinal mucosa: Initiation of inflammation. 35th Controlled Release Society Annual Meeting & Exposition, 12-16 July 2008, New York, USA (Lecture)

Leonard, F; Collnot, E.-M.; Lehr, C.-M. The intestinal 'enhanced permeability and retention effect': a passive targeting principle for PLGA nanocarriers in the treatment of inflammatory bowel disease. 2nd European Conference for Clinical Nanomedicine, 27-29 April 2009, Basel, Switzerland (Lecture)

Collnot, E.-M.; Bur, M; **Leonard, F**; Schmidt, C.; Stallmach, A.; Lehr, C.-M. Nanoparticle in men against inflammatory bowel diseases - a promising approach for the therapy of diarrhea. 2nd European Conference for Clinical Nanomedicine, 27-29 April 2009, Basel, Switzerland (Lecture)

Leonard, F; Collnot, E.-M.; Lehr, C.-M.; . Development of a 3D Model of Inflamed Intestinal Mucosa. 7th World Congress on Alternative & Animal Use in the Life Sciences, Rome, 30 August - 3 September 2009, Rome, Italy (Poster). Also in *Altex*, Vol 26, Spec. Issue, p. 327 (2009)

Leonard, F; Collnot, E.-M.; Lehr, C.-M.;. The intestinal 'enhanced permeability and retention effect': passive targeting of PLGA nanocarriers in the treatment of Crohn's disease. EuroNanoMed, 28-30 September 2009, Bled, Slovenia (Lecture)

Leonard, F; Collnot, E.-M.; Lehr, C.-M.;. Development of a 3 D *in vitro* model of the inflamed colonic mucosa. Young Researchers' Technical Workshop, 28 September 2009, Bled, Slovenia (Lecture)

Leonard, F; Vajda, V.; Collnot, E.-M.; Lehr, C.-M.;. *In vitro* model of the intestinal mucosa in state of inflammation - adaption to high throughput applications. 8th conference and workshop on biological barriers and nanomedicine, 20-29 February 2008, Saarbrücken, Germany (Poster)

Leonard, F; Vajda, V.; Collnot, E.-M.; Lehr, C.-M.. *In vitro* model of the intestinal mucosa in state of inflammation - adaption to high throughput applications. Nanotoxicology, 2-4 June 2010, Edinburgh, Scotland (Poster)

Leonard, F; Collnot, E.-M.; Lehr, C.-M. Size dependent accumulation of nano- and microparticulate carriers in the inflamed intestinal tissue—A novel targeting strategy for the treatment of inflammatory bowel diseases. 37th Controlled Release Society Annual Meeting & Exposition, 10-14 July, 2010 Portland, USA (Poster)

Leonard, F; Collnot E.M.; Crielaard, B.J.; Lammers, T; Storm, G; Lehr, C. M. *In vitro* Model of Inflammatory Bowel Disease for Screening of Drug Formulations. Globalization of Pharmaceutics Education Network: Eighth Meeting, 10-12 November 2010, UNC, Chapel Hill, USA (Lecture)

Leonard, F; Collnot E.M.; Crielaard, B.J.; Lammers, T; Storm, G; Lehr, C. M. Screening of Budesonide Formulations in *In vitro* Model of Inflammatory Bowel Disease. FIP Pharmaceutical Sciences World Congress in Verbindung zu AAPS (American Association of Pharmaceutical Science) Annual Meeting 14-18 November 2010, New Orleans, USA (Poster)

Leonard, F; Collnot, E; Lehr, C. M; Ferarri, M; Godin B. Engineered systems for tumor-site specific oral delivery of chemotherapeutics and immunosuppressants. Physical Science in Oncology (NCI) Annual Network Investigators Meeting, Tampa, FL, April 2012 (Poster).

10. Acknowledgements

I would like to use this opportunity to thank Prof. Dr. Claus-Michael Lehr for giving me the chance to join the group, to work under your supervision and not only provided me with excellent scientific ideas, facilities and financial support but also giving me the opportunity to broaden my knowledge and challenge my skills further. You have helped me way extending the thesis in paving my own future and I am really grateful for that.

My deepest gratitude to my supervisor Dr. Eva-Maria Collnot, an extraordinary supervisor who was never tired to support me right from the beginning till the end. Thanks for the excellent mentoring, you always have great ideas and always spend the time to take good care of your students. It was not only your scientific competence, but also your kindness and care, you know how to motivate me and you were always there when I needed you. I still remember your moral support when I got the first contamination in the cell culture. You are the awesomest supervisor ever!

I would like to thank Prof. Dr. Ulrich Schaefer, for his guidance and valuable suggestions. The institute would never be the same without you. I would also like to thank my scientific companion Jun. prof. Dr. Marc Schneider for his support and his ideas and suggestions regarding the confocal microscopy.

This work would never be completed without the cooperation from the CSEM team: Martha Liley, Silvia Angeloni, Sher Ahmed, and Marta Giazzon. I really enjoy the hospitality during my stay in the Switzerland (remember, triple kiss!) and I am really thankful for giving us the chance to be one of the first to work on the SIMPLI-Well, and thank you for all the suggestions and spending the time to Skype call for scientific discussion

I have to thank the “Darm Team”, although the timing has never been natural for me, our meetings have always been hilarious but also fruitful in resolving scientific problems. I will never forget the line in front of the coffee machine every morning before the meeting ☺. Thanks to all the people that have shared the office with me, to bear my crazyness and tolerated the late hours with me. Special thanks goes to my friend Claudia Philippi, thanks for the days we shared together, the ups and downs of working in the lab and in the office, You always made me smile with your witty comments. Hiroe Yamada, I cannot thank you enough for all your help during my move and during finishing the thesis. I am also very thankful for the time we have spent together. Thanks to Christine Schulze for your “inheritance” of the legendary birdcage and being an awesome officemate.

Thanks to our expert technicians Petra König and Leon Muijs for their generous help with cell culture handling, flow cytometry, confocal microscopy and processing histological cuts.

To all my colleagues in the Biopharmacy & Pharmaceutical Technology Institute, Saarland University, thanks for all your cooperation, the help and support. You all made me feel welcomed in a new environment in a new state right from the beginning, thanks for the various activities we shared together, the sport activities, Friday cooking club, cinema nights, and institute’s own nights of diverse countries; it has never been boring in our little corner of Saarland.

I would also like to give a special thanks to my host for the Euro-PhD program, Prof. Dr. Mauro Ferrari, who has kindly welcomed me in his prestigious institute. You gave me the freedom to do the research and always give the motivation in your speech to not only think about the laboratory part of the research but also to think about the patients whose life we tried to change. Special thank goes to Dr. Biana Godin-Vilentchouk, my supervisor in the

Methodist Hospital Research Institute. I would like to thank you for all the opportunity you have given me, you always supported me and give me the right idea for solving problems, but also stimulate me to think outside-the-box and gave me all the freedom in my research work. Also all the girls in our group, thanks for all the time we shared together in the lab and our lunchtime. Thanks to Srimeenakshi Srinivasan for the scientific discussion and all the long nights spent together trying to write the thesis and book chapter.

I would like to thank all the people in my personal life. Impidjati, not only you helped me with the getting the job and the move to Saarland, you always gave me the support, tolerated me during my cranky days, but also broaden my scientific knowledge and kick me in the back when I needed it. Hestining Hasan for welcoming me and showed me all the “survival skills” I needed here in my new home, Houston; thanks for being an awesome friend. Yenni Tjandra, thanks for being my best friend, no matter how far we are apart, we have always connected, thanks for always be there for me and keep my feet on the ground.

Last but not least I would like to thank my parents, they always inspire me to reach for the stars but keep my feet on the ground. Thank you for nurturing me, all the tireless support and all the love. All of this wouldn't be possible without you.